DETERMINATION OF TRACE METALS IN MICROSAMPLES USING A CAPACITIVELY COUPLED MICROWAVE PLASMA

By

ANDREA MARA PLESS

A DISSERTATION PRESENTED TO THE GRADUATE SCHOOL
OF THE UNIVERSITY OF FLORIDA IN PARTIAL FULFILLMENT
OF THE REQUIREMENTS FOR THE DEGREE OF
DOCTOR OF PHILOSOPHY

UNIVERSITY OF FLORIDA

1996

Dedicated to my parents for all the love and encouragement they gave me

ACKNOWLEDGEMENTS

During my time here at the University of Florida, I have encountered many people who have helped me in countless ways both professionally and personally. Therefore it is of the utmost importance that I express my sincere and deepest gratitude to each and every one of them. First, I would like to thank my research advisor, Dr. Jim Winefordner, for giving me the opportunity to become a part of his group, as well as his constant guidance and support. These past 5 years have provided me with valuable experiences that I never could have learned from a textbook. I would also like to thank Dr. Ben Smith for his willingness to provide his creative and expert advice to the situations at hand. I would like to express my appreciation to Drs. Mikhail Bolshov, Bill Spencer, and Anil Raghani for their enlightening and most helpful discussions throughout the course of this work. Of course, it is also necessary to thank Mary Jane Gordon, an undergraduate who assisted me for the past year and a half. I am especially grateful to Andrea Croslyn, a fellow graduate student, for all her thought provoking questions and ideas, not to mention her enthusiasm, her laughter, and most of all her support. I am also indebted to Jeanne Karably for all of our discussions, her wealth of knowledge about anything and everything, her great advice, and her encouraging "pep talks". I will always treasure her words of wisdom. I would like to acknowledge the financial support of the Engineering Research Center (ERC) for Particle Science and Technology at the University

of Florida, The National Science Foundation (NSF) grant #EEC-94-02989, and the Industrial Partners of the ERC.

I would like to extend a special thank you to Thermo Jarrell Ash, particularly Bob Krupa and Dick Belmore, for giving me the opportunity to visit their research laboratory in Massachusetts as well as the funding they provided for that endeavor. In addition, I am thankful to Bryan Castle for all of his invaluable help with the computer work involved in this research.

As for the friendships that I have made along the way, words cannot express how grateful I am for the support, encouragement, and advice they each provided me. I would like to thank Lauren Cordell, Maria Lackey-Hancock, Nikki Schultz, MaryAnn Gunshefski, Monica Escobar, Sue Ohorodnik, Cindy Baker, Robin Russell, Susan Rasmussen, Leslie Anthony, Wendy Clevenger, Rob Guenard, and Eugene Wagner for their friendship both in and out of the lab and all the experiences we shared during my "term" here. I am very lucky to have known them and wish them all the best in the future. An extra special thank you is extended to Lisa Spurlock for helping me to endure the bad times, to enjoy the good times, and to remind me I was not alone.

Finally, I would like to sincerely express my love and gratitude to my family for their love, encouragement, and guidance. They never stopped believing in me, even when I would lose faith in myself. If it were not for their endless support and continuous interest in my success, I would not have been able to see this through to the very end. For whether or not they know this, they made all the difference.

TABLE OF CONTENTS

page

ACKNOWLEDGEMENTS iii

LIST OF FIGURES vii

LIST OF ACRONYMS xi

ABSTRACT xiv

CHAPTERS

1 INTRODUCTION TO PLASMAS 1

- Plasmas in Elemental Analysis 1
- Microwave Plasmas 3

2 CAPACITIVELY COUPLED MICROWAVE PLASMAS 15

- History 15
- Recent Developments 17
- Diagnostics 20
- Interferences 23
- Microwave Radiation 25
- Sample Introduction 26

3 INSTRUMENTATION 34

- Introduction 34
- Instrumental Design 34
- Microwave Generators 37
- Waveguides 38
- Electrodes 45
- Plasma Composition 48
- Detector 51

4 DETERMINATION OF TRACE ELEMENTS IN SOLUTION . . . 53

Introduction 53
Experimental 54
Results and Discussion 56
Conclusions 103

5 DIRECT DETERMINATION OF CADMIUM IN SOLIDS 106

Introduction 106
Experimental 108
Results and Discussion 111
Conclusions 129

6 SIMULTANEOUS MULTIELEMENT ANALYSIS 130

Introduction 130
Instrumentation 133
Experimental 141
Results and Discussion 143
Conclusions 155

7 CONCLUSIONS AND FUTURE WORK 158

REFERENCE LIST 163

BIOGRAPHICAL SKETCH 174

LIST OF FIGURES

Figure | Page

1-1 Beenakker cavity (a) top and (b) side views. Components are as indicated: (1) cylindrical wall, (2) fixed bottom wall, (3) removable lid, (4) discharge tube, (5) discharge tube holder, (6) coupling loop, (7) connector, (8) vacuum seal, (9, 10) tuning screws, (11) holes for viewing or for air cooling, (12) mount. 5

1-2 Schematic diagram of a capacitively coupled microwave plasma. 8

1-3 Schematic diagram of a surfatron. 11

3-1 Schematic diagram of the experimental design. 35

3-2 Illustration of the boundary conditions required in a waveguide. E is the electric field, B is the magnetic field, and Z is the direction of propagation. 41

3-3 Field distributions inside a waveguide. 42

3-4 Exaggerated view of W cup electrode designs. 47

3-5 Stability diagram for a He-CMP. 50

4-1 Effect of drying power on Cd, Mg, and Zn signals. 57

4-2 Effect of drying power on Pb and Na signals. 58

4-3 Temporal profile of 0.5 ng of Cd at 228.802 nm. 59

4-4 Temporal profile of 1 ng of Cd at 228.802 nm using a cylindrical plasma. 61

4-5 Temporal profile of 2 ng of Zn at 213.856 nm using a spherical plasma. 62

4-6 Temporal profile for a 0.5 ng sample of Mg at 285.213 nm in each of the thick and thin bottom cups. 63

4-7 Temporal profile of the effect of matrix on 7 ng of Pb at 405.78 nm. . . . 64

4-8 Temporal profile of 2 ng of Na at 588.995 nm. 66

4-9 Vertical distribution of Cd and Mg signals and backgrounds. 67

4-10 Vertical distribution of Pb signal and background. 68

4-11 Background emission spectrum at 589.0 nm. 70

4-12 Horizontal distribution of Mg signal and background using a spherical plasma. 71

4-13 Horizontal distribution of Cd signal and background using a cylindrical plasma. 73

4-14 Effect of atomization power on Zn signal and background (cylindrical plasma). 74

4-15 Effect of atomization power on Pb signal and background. 75

4-16 Effect of atomization power on Cd and Mg signals and backgrounds. . . . 76

4-17 Effect of atomization power on Ca signal. 78

4-18 Effect of atomization power on K signal. 79

4-19 Effect of atomization power on Na signal. 80

4-20 Effect of He gas flow rate on Cd, Mg, and Zn signals and backgrounds. . 81

4-21 Effect of He gas flow rate on Pb signal and background. 82

4-22 Effect of He gas flow rate on Na signal. 83

4-23 Effect of H_2 gas flow rate on Cd, Mg, and Zn signals and backgrounds. . 85

4-24 Effect of H_2 gas flow rate on Pb signal and background. 86

4-25 Effect of H_2 gas flow rate on Na signal. 87

4-26 Log-log calibration curve for Cd (spherical plasma). 90

4-27 Log-log calibration curve for Zn (spherical plasma). 91

4-28 Log-log calibration curve for Mg (spherical plasma). 92

4-29 Log-log calibration curve for Pb (cylindrical plasma). 93

4-30 Spectrum of a 5 ng sample of Pb. 95

4-31 Log-log calibration curve for Na. 96

4-32 Log-log calibration curve for Ca. 97

4-33 Log-log calibration curve for K. 98

5-1 Effect of preatomization power on solid Cd signal. 112

5-2 Effect of preatomization time on solid Cd signal. 113

5-3 Temporal profile of 180 pg of Cd in graphite powder at 228.802 nm. . . . 115

5-4 Vertical distribution of solid Cd signal and background. 116

5-5 Horizontal distribution of solid Cd signal. 117

5-6 Effect of atomization power on solid Cd signal. 119

5-7 Effect of He gas flow rate on solid Cd signal. 120

5-8 Effect of H_2 gas flow rate on solid Cd signal. 121

5-9 Log-log calibration curve for solid Cd. 124

5-10 Comparison of Cd calibration curves in a solid and an aqueous matrix. . . 126

6-1 Cross sectional view of a MOS capacitor structure in a pixel. 136

6-2 Design of a TJA CID/echelle spectrometer. 140

6-3 Representative peak of 10 mg/L Cd. 148

6-4 Representative peak of 10 mg/L Mg. 149

6-5 Representative peak of 10 mg/L Pb. 150

6-6 Representative peak of 10 mg/L Zn. 151

6-7 Preliminary calibration curve for Mg using the TJA spectrometer. 152

6-8 CID image of a Au chip. 154

6-9 CID image of a 29 element aqueous standard. 156

LIST OF ACRONYMS

The following is a list of the acronyms used throughout this dissertation. On occasion, a lower case "s" is added to the acronym to indicate the plural form. In addition, two or more of the acronyms can be hyphenated to form a new acronym. In this list, only the simple acronyms are given.

AAS	atomic absorption spectrometry
AES	atomic emission spectrometry
ANSI	American National Standards Institute
CID	charge-injection device
CMP	capacitively coupled microwave plasma
DSI	direct sample insertion
EIE	easily ionizable element
ETV	electrothermal vaporization
GC	gas chromatography
GFAAS	graphite furnace atomic absorption spectrometry
ICP	inductively coupled plasma
KiP-MIP	kilowatt-plus microwave induced plasma
LOD	limit of detection
MDMI	monodisperse dried microparticulate injector

MIP	microwave induced plasma
MOS	metal oxide semiconductor
MPT	microwave plasma torch
n_e	electron number density
NIST	National Institute of Standards and Technology
OES	optical emission spectrometry
PDA	photodiode array
PMT	photomultiplier tube
ppb	parts per billion
ppm	parts per million
RAI	random access integration
RF	radio frequency
RSD	relative standard deviation
SFC	supercritical fluid chromatography
SIMAAC	simultaneous multielement atomic absorption continuum source
SMA	simultaneous multielement analysis
SRM	standard reference material
TE	transverse electric
T_{exc}	excitation temperature
TJA	Thermo Jarrell Ash
TM	transverse magnetic
T_{rot}	rotational temperature

TV	thermal vaporization
UHF	ultra high frequency

Abstract of Dissertation Presented to the Graduate School
of the University of Florida in Partial Fulfillment of the
Requirements for the Degree of Doctor of Philosophy

DETERMINATION OF TRACE METALS IN MICROSAMPLES USING A CAPACITIVELY COUPLED MICROWAVE PLASMA

By

Andrea Mara Pless

May 1996

Chairperson: James D. Winefordner
Major Department: Chemistry

Microwave plasmas, generally operated at 2450 MHz, have become a powerful excitation and atomization source for the determination of trace metals and nonmetals. A capacitively coupled microwave plasma (CMP), is characterized by the propagation of microwaves through a waveguide with the plasma forming at the top of an electrode. This plasma enables thermal vaporization (TV) sample introduction to be accomplished *in situ* as the plasma forms directly around the sample. Thus, the need for sample preparation, procedural steps, and sample transport is eliminated. This technique is readily employed for discrete sampling without any resultant sample dilution or losses.

This dissertation examines a CMP operating at 450 to 1000 W for the trace detection of metals in solids and solutions by atomic emission spectroscopy (AES). The laboratory-constructed system contains a tungsten cup electrode capable of holding a volume of up to 30 μL. Microwaves are used to dry the sample, while at higher powers the plasma is ignited for sample vaporization and excitation. The entire analysis is carried out in less than 5 minutes. A mixture of helium and hydrogen is used as the plasma gas. A spherical or cylindrical shaped plasma is formed depending upon the gas flow rate and microwave power selected. The effects of experimental parameters, such as gas flow rate, atomization power, electrode position, and plasma shape, are examined. Either plasma shape is effective for the sensitive detection of various elements in aqueous and solid samples. Both plasma types produce similar trends for most of the experimental parameters studied. The electrode design is a critical factor in this technique due to its potential for influencing atomization and thus temporal behavior of the analytes. The determination of trace metals in microsamples by TV-CMP-AES compares favorably with other atomic methods and produces detection limits for Ca, Cd (aqueous and solid), K, Mg, Na, Pb, and Zn in the picogram range with less than 10 % relative standard deviation (RSD). The accuracy and precision of this method are investigated by measuring Cd in standard reference materials. This technique is also well suited for simultaneous multielement analysis.

CHAPTER 1
AN INTRODUCTION TO PLASMAS

Plasmas in Elemental Analysis

Elemental analysis is commonly performed using atomic spectroscopy techniques which are capable of providing both qualitative and quantitative information. Atomic spectroscopy can be divided into absorption, emission, and fluorescence methods. Atomic emission spectroscopy (AES) has evolved into an attractive means for routine elemental analysis. This is in direct response to the increasing need of determining many elements at all concentration levels in a large number of samples [1]. In fact, emission techniques have approached many of the ideal requirements for methods of elemental analysis. These include applicability to all elements; simultaneous or rapid sequential multielement determination capability at the major, minor, trace, and ultratrace levels without changing the operating conditions; few inter-element interference effects; applicability to the analysis of microsamples; solid, liquid, and gaseous analysis capabilities with minimal sample preparation; rapid analysis capability and acceptable accuracy and precision [2].

Also contributing to the popularity of AES, is the emergence of an excitation source capable of effectively vaporizing, dissociating, and exciting the analyte of interest [3]. This emission source should be capable of exciting lines of a large number of elements, have a high sensitivity, possess good stability, be free from interferences, provide for the reproducible introduction of samples, and be convenient to operate [4]. Therefore, the nature of the emission source is a critical factor. Typically, flames have been an excellent emission source for the alkali and alkaline earth metals [5]. However, flames do not provide the required energy to excite many other elements. Thus, plasmas have emerged as an atomic emission source during the past several decades [1]. This is due to its advantages of high temperature, low chemical reactivity, relative freedom from interference effects, and the capability of multielement determinations [6]. A plasma is a partially ionized gas in which a portion of the atomic or molecular species are present as ions. Some common examples include interstellar space, neon lamps, and argon welding arcs [5].

There are several different types of plasmas. They may be classified according to the frequency of electromagnetic radiation used to sustain the plasma, radio (RF) or microwave. The most popular type of plasma used in the field of analytical chemistry, especially for elemental analyses, is the inductively coupled plasma (ICP). The ICP is produced using radio frequency to generate a fluctuating magnetic field in which both ions and electrons can interact. A thorough review of ICP, including fundamental properties, instrumentation, and applications, may be found in Montaser and Golightly [7]. The reader is also referred to several other reviews concerning ICP as an emission source for atomic spectroscopy [8-11]. Therefore, the ICP will not be discussed in detail here except for comparison purposes.

Plasmas may also be generated using microwave radiation. Microwave plasmas operate at frequencies greater than 10^9 Hz or 1 GHz. Microwave plasmas, commonly operated at 2450 MHz, have become a powerful atomization and excitation source for the determination of both metals and nonmetals. In comparison to the ICP, microwave plasmas offer several important advantages. Microwave plasmas generally have lower initial costs than the ICP. This is due to the development and popularity of commercial microwave ovens which allow for magnetron power sources that are inexpensive and widely available. Also, microwave plasmas have lower operational costs as they use lower gas flow rates than those employed in typical ICP work.

Microwave Plasmas

Microwave plasmas may be divided into categories depending on the way in which the energy is transferred from the generator to the plasma. The microwave induced plasma (MIP) is formed inside a quartz discharge tube which is contained inside a resonant cavity. The microwave energy is transferred from the generator to the cavity through a coaxial cable [12,13]. A capacitively coupled microwave plasma (CMP) is characterized by the propagation of microwaves through a waveguide with the plasma forming at the top of an electrode. A surface-wave induced plasma is generated from the propagation of surface waves within a quartz tube which lies along the axis of a coaxial structure.

Microwave Induced Plasmas

The MIP has received considerable attention as an emission source in analytical chemistry. It possesses a high degree of flexibility in both its design and usage. In general, the MIP consists of a quartz discharge tube which is filled with the gas used to sustain the plasma. This tube is contained in a resonant cavity parallel to the electric field. Ideally, the discharge tube is placed at the position where the electric field is at a maximum [14]. The microwave energy is then transferred to the cavity via a coaxial cable. However, efficient energy transfer depends on the impedance match of all the components of the system [15]. If impedances are not matched, the coupling efficiency is reduced and the power reaching the plasma is decreased. Therefore, impedance matching is usually performed with the aid of tuning stubs.

There are many types of resonant cavities that can be used to generate MIPs. The earlier cavities, which have been reviewed by Fehsenfeld *et al.* [16] and Goode and Baughman [14], were usually operated at low pressures. Beenakker [12] significantly improved the resonant cavity design which could easily be operated at atmospheric pressure. The Beenakker cavity is illustrated in Figure 1-1 [12]. Further modifications on the coupling mechanism were made by van Dalen *et al.* [17]. The role of the resonant cavity is to support a standing wave and, thus, concentrate the microwave energy within the vicinity of the plasma. The cavities are commonly cylindrical in shape with a diameter that ranges from 86 to 93 mm for 2450 MHz frequency of radiation [18]. The cavity design allows emission to be viewed either axially or end-on, as well as from the side.

There are several comprehensive reviews concerning MIPs [13,18-22]. The MIP, in general, has a lower background than its microwave plasma counterpart, the CMP. The MIP is normally operated at low powers. This is due to the limitation imposed by the

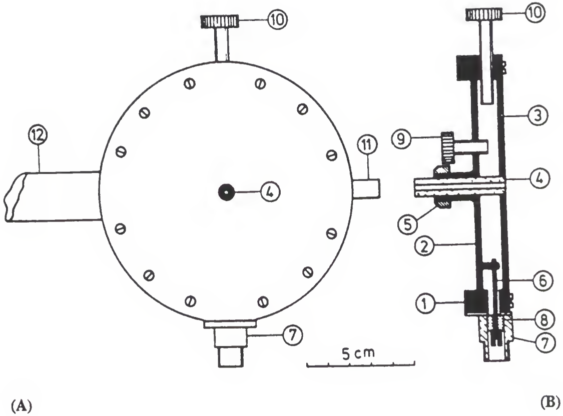

Figure 1-1. Beenakker cavity (A) top and (B) side views [12]. Components are as indicated: (1) cylindrical wall, (2) fixed bottom wall, (3) removable lid, (4) discharge tube, (5) discharge tube holder, (6) coupling loop, (7) connector, (8) vacuum seal, (9, 10) tuning screws, (11) holes for viewing or for air cooling, (12) mount.

use of coaxial cables. These cables tend to become hot and radiate heat at high power levels (> 150 W), thereby causing power losses [15]. Also, the plasma produced is very small in size with a diameter less than 4 mm and a length of 10 to 30 mm [23]. Because of its small size and low power of operation, solution introduction into the MIP is difficult. The MIP has insufficient plasma enthalpy to effectively desolvate and atomize samples that have been directly introduced [6,24,25]. Thus, the plasma is easily perturbed or extinguished with high sample loading [13]. Solids analysis is plagued with problems as well, due to the low power of operation and the difficulty with sample introduction. Thus, work with the MIP has been largely restricted to gaseous samples [6].

Regardless of the inherent problems associated with MIPs, research in this area is still active. Trace analysis of both metals and nonmetals [26-31] has been achieved with the MIP. Analysis with the MIP has also been extended to biological samples [32,33]. Improved system designs are being investigated as well [34-36]. However, because of its small sample loading, the MIP has been primarily used as a detector for gas chromatography (GC) [37-41] and supercritical fluid chromatography (SFC) [42]. Since its development in 1965 by McCormack and coworkers [43] for the detection of organic compounds, the GC-MIP technique has evolved considerably in terms of its design and application [44]. In fact, a commercial gas chromatograph with an MIP-AES detector is currently available from Hewlett Packard. Recently, the MIP has also served as a source for a mass spectrometer [45-47].

Capacitively Coupled Microwave Plasmas

The operation of the CMP is rather distinct from that of the MIP. These plasmas require an electrode to transfer the microwave radiation to the plasma gas. In the CMP, a magnetron is used to generate the microwave energy. The energy is then transferred from the magnetron probe into a rectangular waveguide which is short-circuited at both ends. The microwave radiation is transported through the waveguide as a standing wave. It is coupled to the coaxial waveguide whose central conductor is the electrode. The plasma forms at the surface of this electrode which is contained inside the center tube of a two concentric tube quartz torch. Emission can then be viewed from the side. A schematic diagram of a typical CMP design is shown in Figure 1-2 [48].

The CMP has been used considerably less than the low powered MIP. It suffers from a higher background than the MIP due to its high power of operation [49]. The CMP is also plagued with interferences from electrode contamination and with the frequent replacement of this electrode due to erosion [50]. Even so, the CMP does offer several advantages over the MIP. Higher power levels may be used with the CMP. This is due to the high power handling capabilities of the waveguide compared to coaxial cables which are employed in MIP operation. The CMP is also larger in size, having a diameter that ranges from 8 to 25 mm and a length of approximately 25-70 mm [51]. Due to their larger size and higher power of operation, these plasmas are fairly robust, allowing for the efficient introduction of solutions without disrupting or extinguishing the plasma. Also, they are more tolerant to molecular species [49], and therefore CMPs have

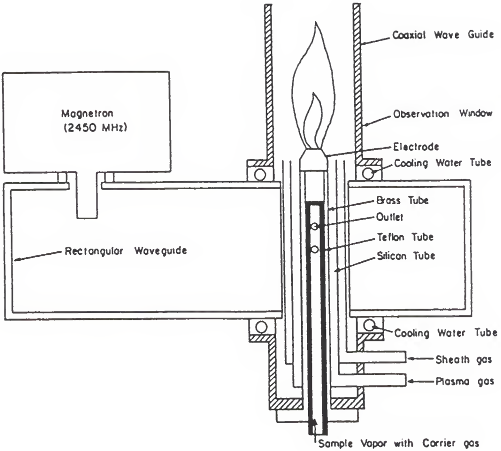

Figure 1-2. Schematic diagram of a capacitively coupled microwave plasma [48].

an increased ability over MIP sources to desolvate, atomize, and excite species that have been introduced.

The performance of the CMP has also been compared to the ICP [52,53]. Boumans *et al.* [54] compared the ICP and the CMP for differences in analytical performance on the analysis of solutions. In this case, the two plasmas were evaluated in terms of detection limits, sensitivity, precision, and matrix effects. The results of 14 spectral lines from 12 representative elements were corrected for dissimilarities in sample introduction and measuring equipment. On all accounts, it was suggested that the ICP was superior to the CMP as an excitation source for trace elemental analyses.

Regardless of this conclusion, the CMP has still been examined as an alternative emission source for elemental analysis. Since 1981, Dahmen has published yearly reviews concerning the advances of the CMP [55]. The CMP has found use for the determination of trace elements in both gaseous [56] and solid [57,58] samples. Routine elemental analysis of silicate rocks and minerals [59] has also been achieved with the CMP. Uchida *et al.* interfaced the CMP with a GC in order to speciate and detect organotin compounds [60], as well as several nonmetals [61]. The CMP has even been coupled with hydride generation [62,63] where it was applied to the determination of arsenic. Recently, the CMP has been extended to the detection of trace elements in complicated matrices, such as whole blood [64,65]. Consequently, this research also focuses on the further development of the CMP as a potential emission source for elemental analysis. Its application to microsamples of both solutions and solids will be evaluated, as well as its suitability for simultaneous multielement analysis (SMA).

Surface-wave Induced Plasmas

The surface-wave induced plasma is unique. It is generated without the use of a resonant cavity which is required for MIP formation. Instead, the surface-wave induced plasma incorporates a surface wave launcher, or surfatron [66], which is a localized device for producing surface waves, in order to generate a plasma. Surface waves propagate along the interface of two media without any resulting energy loss by radiation. These waves can be characterized by the exponential decay of the electromagnetic field in the direction perpendicular to the boundary sustaining the propagation. If the surface waves are intense, they are capable of breaking down a gaseous medium, and thus producing a plasma. As a result, a resonant cavity is not necessary as the plasma acts as the sole propagating medium for the surface wave. Therefore, the propagation of the waves is independent of the surfatron configuration [67]. The surface waves that are formed by the surfatron are dependent only on the plasma frequency being used. The electric field present within the surfatron is distinct from that within a resonant cavity. In a cylindrical resonant cavity, the electric field has a central maximum, whereas in a surfatron, the electric field has a minimum along a central axis.

A schematic diagram of a surfatron is presented in Figure 1-3 [67]. It consists of two main parts: a coupler and a coaxial structure. The coupler transfers the energy from the generator to the surfatron with the aid of a standard coaxial cable. The coupler can be vertically adjusted in order to match the impedance of the surfatron with that of the generator. The air-filled coaxial structure serves to shape and orient the electric field. It is terminated by an adjustable short-circuit at one end and by a capacitative gap at the

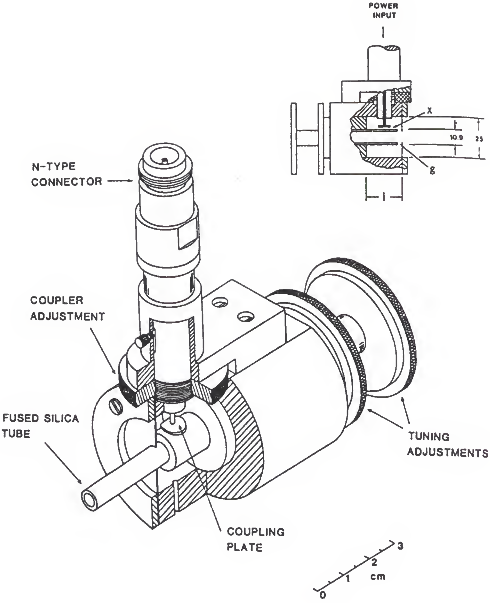

Figure 1-3. Schematic diagram of a surfatron [67].

other end. The surface waves are launched from the gap along a fused silica tube which is positioned through the axis of the device. The plasma is sustained inside this tube. These plasma columns increase linearly with power and have reached lengths of 1 m or more [68]. Surfatrons, usually fabricated from brass, have been investigated as to their performance and design by Selby and Hieftje [67] and Moisan *et al.* [66].

Surface waves can also be launched within a rectangular waveguide structure, or surfaguide [68]. In this device, the microwave energy is supplied to one end of a rectangular waveguide section that is terminated at the other end by a movable short-circuited plunger. The discharge tube is placed perpendicular to the symmetrically tapered center of the waveguide. The plasma that is formed extends evenly on both sides of the launcher. Tuning is achieved by adjusting the plunger. The surfaguide also possesses excellent tuning capabilities like its counterpart, the surfatron. In addition, the surfaguide has a higher power handling capability than the surfatron, as well as the ability to operate at higher frequencies [68].

Surface-wave induced plasmas have found application in laser systems, spectral lamps, plasma-jet welding, and thin film creation devices [67]. The surfatron, in particular, has readily been applied to spectrochemical analysis [15]. The long plasma columns can be produced in both argon and helium gases. They are more easily tuned than other microwave plasma devices and are more resistant than the MIP to detuning by solvent and solute loading [67]. Plasmas generated from surfatrons are stable and reproducible [69]. However, surfatrons are expensive since they require precise machining and major modifications in order to be adapted for other uses [15]. Even so, the surfatron has been used with ultrasonic nebulization for the determination of Hg, achieving a detection limit of 0.9 ppb [70]. Richts *et al.* [71] compared thermal vaporization sample introduction into both the surfatron and the Beenakker cavity. They found that the surfatron performed better than the Beenakker cavity under similar operating conditions for the detection of Cd and Cu and obtained detection limits in the ppb range.

Other Microwave Plasmas

Other novel microwave plasma systems have been developed in order to overcome the problem of sample introduction into the MIP. One of these such refinements is the microwave plasma torch (MPT) developed by Jin and coworkers [72]. The MPT allows for the sample to be introduced directly into the plasma, thereby improving the sample-plasma interaction and enhancing the overall analytical performance of the microwave plasma. The MPT is different from the other microwave plasma designs and instead actually resembles the ICP configuration. It is composed of three concentric metal tubes. The outer tube is constructed from brass and the other two tubes from copper. The plasma forms between the intermediate and central tubes near the top of the torch. The plasma gas, which can be either helium or argon, is introduced through the intermediate tube. The energy is coupled to the plasma by a cylindrical antenna which surrounds the intermediate tube. This produces a high microwave field at the top of the torch. The sample is introduced into the central channel of the plasma through the central tube, thereby promoting an increase in the analytical performance [73]. The emission signal can be viewed either from the side or end-on. The MPT is robust and thus has a high tolerance to water vapor and molecular species, contrary to the MIP. It can handle up to 14 mg/L of water vapor without extinguishing [74]. There is minimal perturbation of this plasma by foreign material [72]. The MPT is easy to tune, is resistant to detuning, and has not demonstrated memory effects. However, it is easily disturbed by air convection and therefore must be contained. The MPT with ultrasonic nebulization sample introduction has obtained low ppb detection limits [72]. The MPT has also been used as an element selective detector for GC and SFC [73]. The MPT has even been applied as the atomizer for the determination of Hg by fluorescence [75].

Another proposed solution to the problems encountered with the MIP was the kilowatt-plus microwave induced plasma (KiP-MIP) developed by Cull and Carnahan [76]. This plasma is capable of operating at powers in the kilowatt range. This high power of operation serves to increase the plasma volume, and thus the residence time of the analyte in the plasma allowing for improved desolvation, atomization, and excitation. This plasma has been observed to reach a length of 5-6 cm and a diameter of 7-8 mm [77]. The KiP-MIP is simply a modified Beenakker cavity [76]. The KiP-MIP is still being investigated although preliminary use has demonstrated ppm detection limits for the halogens [76] as well as for Ca and Zr [34].

CHAPTER 2
CAPACITIVELY COUPLED MICROWAVE PLASMAS

History

Microwave plasmas were first discovered by physicists and engineers with the development of radar equipment [78]. However, they were believed to be a nuisance since they caused problems in the design of radar transmitting and receiving switches. It was not until the work of Cobine and Wilbur [79] in 1951 that the usefulness of microwave plasmas was realized. They examined plasmas produced as an "electronic torch" used for melting refractory materials. The setup they described employed a 1000 MHz magnetron for sustaining microwaves at 1 kW of power. The magnetron was coupled to a coaxial line that terminated in the torch. The plasma was produced in a variety of different gases on the tip of a rod made from copper, brass, silver, tungsten, or molybdenum. They observed that a plasma formed from CO_2, N_2, or air could melt a tungsten rod (mp = 3370 °C). An argon plasma could not ignite paper held perpendicular to the flame. They found helium to be a "cooler" plasma as well. They attributed this to the fact that neither argon nor helium dissociates into any other species, while the polyatomic gases generate heat from the association of molecules. Grigorovici and Cristescu [80] later studied the electrical, optical, and thermal temperatures of such a discharge. They went on to model the mechanism for the formation of this high frequency discharge.

The first application of the CMP as an excitation source was reported in 1963. Mavrodineanu and Hughes [81] used a 2450 MHz magnetron to generate a helium and hydrogen mixed plasma at 2 kW of power. The plasma was produced on top of a central electrode which was held in position by a torch and coupled to a waveguide. They analyzed both solutions and solids. Solid samples were placed in the crater of a graphite electrode and vaporized. One sample of interest was tin-lead solder. Liquid samples were nebulized into the plasma. The temperature of the discharge was estimated between 2900 and 3300 K by its ability to melt molybdenum but not tantalum or tungsten.

Jecht and Kessler [82] also developed a CMP system. This one used a molybdenum water-cooled electrode. They examined plasmas produced at 2400 MHz for air, nitrogen, and helium. They also investigated the excitation mechanism of the plasmas. This CMP was later applied to the analysis of real samples, such as limestone and dolomite [83]. Concentrations of Ca, Mg, Al, and Fe were measured.

Yamamoto and Murayama [84] introduced solutions into a CMP by nebulization. They produced an argon plasma utilizing a water-cooled aluminum electrode. The sample was introduced tangentially to the electrode. They measured the detection limits for several elements, such as Al, Zn, and Ca, in the ppm range. They observed this plasma to have an excitation temperature of 8150 K. Murayama extended this work to the investigation of inter-element effects of Na on the excitation of eight elements [85] and the rare earths [86]. Goto *et al.* [87] continued work with nebulized samples into a nitrogen CMP. They explored the effects of experimental parameters, including current, flow rate, and acid concentration. Also in Japan, Kitagawa and Takeuchi [88,89] performed spectroscopic studies and compared the microwave plasma to the chemical flame. At this time, the CMP was even applied to the analysis of steels [90]. Work achieved by these various research efforts led to the commercialization of CMP equipment for emission spectrometry by (1) Hitachi of Japan, designated ultra high frequency (UHF) plasma, (2) Applied Research Laboratories of Switzerland, and (3) Erbe-Elektromedizin of the Federal Republic of Germany [91].

Recent Developments

Recent developments with the CMP have focussed on the electrode design with much of this work being accomplished by Winefordner and coworkers. Hanamura *et al.* [50] improved upon the electrode design used for prior elemental analyses. They developed a Pt clad tungsten electrode which was more versatile with respect to input power, gas flow rate, and gas type. It was not as susceptible to melting as was the aluminum electrode. They determined a limit of detection for Hg of 2 ng with 5.4 % relative standard deviation (RSD). Work with this new electrode was extended to several materials. The elements C, H, N, O, and Hg were measured in orchard leaves and tuna fish directly using a device based upon differential vaporization of the species [48]. The analysis of trace water levels in solids was also achieved with an evolved gas apparatus by the detection of elemental H and O [92]. In addition, elemental H and O analyses were performed on titanium metal [93].

Previously, CMP systems included a solid electrode. Patel *et al.* [94] improved upon this arrangement with the development of a tubular electrode. This electrode permitted the direct introduction of the sample through the center of the plasma. This tantalum electrode was incorporated with hydride generation for the examination of organotin species [94] and with nebulization [95]. The tubular electrode proved beneficial as it allowed for efficient sample introduction and increased the concentration of the analyte reaching the plasma. This same electrode design was later used in the development of the CMP as a element selective detector for GC [60,61]. The capillary column was introduced into the CMP through the tubular electrode.

Hwang and coworkers [49] refined the electrode design further. They constructed an electrode from graphite instead of metal. This enabled the CMP to be operated at powers up to 1600 W with minimal deterioration of the electrode. Detection limits in the ppb range were observed for several elements with this design.

Ali *et al.* [96] and Ali [97] developed a graphite cup electrode for discrete sampling. A microvolume of solution was placed in the cup and the plasma forms on top of the electrode. Therefore, the sample was directly vaporized into the plasma for atomization and excitation. The cup had a 20 μL capacity. With a helium/nitrogen plasma, pg detection limits with better than 12 % relative standard deviation could be measured. In addition, this same graphite cup allowed for the direct analysis of solids without prior dissolution [57,97]. A wide variety of elements were detected in small samples of coal fly ash and tomato leaves using a 20/80 mixture of nitrogen and helium respectively, as the plasma support gas.

Ali and Winefordner [98] developed an electrode fabricated from tungsten wire. This filament electrode provided a higher rate of sample vaporization because of its smaller mass. Filament electrodes were also inexpensive, simple to construct, and free from molecular carbon species interferences. Picogram limits of detection were achieved as the sample is more exposed to the plasma heat. The effects of gas flow rate, atomization power, and electrode position were studied along with the determination of spectroscopic temperatures [99]. It was discovered that the filament electrode produced a fairly constant signal over a wide range of conditions.

Masamba and coworkers [100] and Masamba and Winefordner [101] investigated the introduction of hydrogen into a helium CMP. The influence of power, observation position, the rate of solution uptake, and carrier gas flow rate were explored. Also, rotational and excitation temperatures along with electron number densities were measured. Direct introduction of steels was later performed [58]. This demonstrated that solid samples could be examined *in situ* with little sample preparation.

Spencer [51] designed a tungsten electrode used for pneumatic nebulization. This electrode was applied to the analysis of Si in an oil matrix. A detection limit of 0.3 ppb was determined when a kerosene matrix containing Si was nebulized through the center of the tubular tungsten electrode. Spencer [51] also constructed a 30 μL tungsten cup electrode to be used for thermal vaporization sample introduction. In this case, 900 pg of Si in kerosene could be detected. This tungsten cup electrode and several variations are currently employed in some present CMP work. Additionally, Spencer *et al.* [102] characterized a high flow rate plasma (> 7 L/min), known as a cylindrical plasma.

Spectroscopic temperatures and electron number densities were measured and compared for both organic and aqueous solutions. The cylindrical plasma was used for the Si analyses in the above mentioned instances.

Wensing *et al.* [64,65] developed a method for the determination of Pb in whole blood using a CMP. This was the first successful application of the CMP with discrete sampling to a complicated matrix. The method was capable of Pb detection in under 5 minutes without the need for dilution or the addition of matrix modifiers. A tungsten filament electrode was used for the measurement of Pb at 35 pg with 15 % relative standard deviation. This CMP system can be readily automated.

Diagnostics

Temperatures and electron number densities may be determined to gain an improved understanding of plasmas. These assessments are of interest as they provide information about fundamental gas-kinetic interactions and energy transfer events occurring in the plasma. Over the years, many researchers have performed extensive diagnostics studies on the CMP in a variety of different gases with various electrode designs. Murayama [85,103] found that an Ar-CMP operated with an aluminum water-cooled electrode had an excitation temperature (T_{exc}) which varied over the range of 6500 to 8000 K with power. The electron number density (n_e) was on the order of 10^{14} cm^{-3}. Also, the temperature and degree of ionization were lower in the outer region of the plasma. Fallgatter *et al.* [104] discovered that a 100 W Ar-CMP with and without water introduction had a rotational temperature (T_{rot}) of 2440 K and 1440 K respectively. Also, the excitation temperature was similar to those reported by Murayama. With water introduced into the plasma, the T_{exc} was 8520 K and without added water it was 7990 K. In addition, the electron number density was also on the order of 10^{14} cm^{-3} with a maximum value at the plasma center. Zhang *et al.* [105] performed diagnostic studies on a CMP formed with air. An excitation temperature was determined to be 4700 K at 6.3 L/min air flow when operated at moderate power. Zhang *et al.* also observed that the emission intensity would decrease with increased air flow but would increase with increased power. It was even noted that the background would increase at low flow. Kirsch *et al.* [106] studied the spectroscopic properties of various gases with a CMP that employed a Pt clad tungsten electrode. The temperatures measured were comparable with an ICP. Also, trace metal detection was enhanced when using an Ar-CMP while trace nonmetal detection was enhanced when using a He-CMP. Although no great differences were observed between the two plasmas, it was decided that pure plasmas produced superior emission signals over mixed gas plasmas.

Recently, Masamba *et al.* [100] performed a thorough investigation of the diagnostic measurements of a He-CMP to which H_2 had been added. The reader is referred to Masamba's dissertation [107] for the extensive details but a brief overview is provided here. He reported a T_{rot} of 1800 to 3000 K, a T_{exc} of 2000 to 5000 K, and an n_e of 4-9 x 10^{14} cm^{-3}. He observed that with a graphite cup electrode, this plasma had approximately constant temperature and n_e with changing horizontal position. Meanwhile, these parameters showed a decrease with increasing observation height and an increase with increasing power. In addition, the T_{exc} decreased with H_2 addition as a result of a reduction in the excitation energy [101]. The T_{rot}, which represents the actual kinetic temperature of the plasma, increased with H_2 addition in response to the heat of association of atoms which are dissociated by the microwaves [101]. Overall, the parameters appeared to be of similar magnitude to the values estimated in prior studies.

Ali and Winefordner [99] assessed temperatures for a He-CMP with the tungsten filament electrode. They measured the T_{rot} to be 2500 K and the T_{exc} to be 4500 K when operating at 4 L/min. The n_e was also on the order of 10^{14} cm^{-3}. All parameters were found to be relatively independent of power, electrode position, and helium flow rate.

Spencer [51,102] evaluated temperatures and electron number densities for both aqueous and organic solutions aspirated into a He/H_2 mixed gas CMP utilizing a tungsten electrode and a 10 L/min flow rate. He reported that both the temperatures and number densities were not statistically different for the two solution types. The T_{exc} was approximately 3400 K and the T_{rot} was estimated at about 1600 K. He concluded that the T_{exc} of this cylindrical He-CMP was similar to a low flow rate He-CMP, a He-ICP, and a He and an Ar-MIP. However, this plasma had a lower excitation temperature than both an Ar-CMP and ICP. The T_{rot} was similar to a He-MIP, a He-ICP, and an Ar-CMP but lower than an Ar-MIP and ICP. The n_e was greater than that of a He-ICP, equal to that of an Ar-CMP and a He-MIP, and lower than that of an Ar-MIP and ICP.

The He-CMP can be compared to both an ICP and an MIP as well. Abdallah and Mermet [108] found that for a He and an Ar-MIP the T_{exc} was 4500 and 4420 K respectively. The excitation temperatures for a He and an Ar-ICP were 4100 and 4800 K respectively. The T_{rot} were measured to be 3600 K for an Ar-MIP and 2100 K for a

He-MIP. In contrast, Tanabe *et al.* [109] found that for a He-MIP, the T_{exc} was 3400 K while for an Ar-MIP was 4500 K. The rotational temperatures were measured to be 1100 K for an Ar-MIP and 1300 K for a He-MIP. The n_e ranged from 5×10^{13} to 1×10^{14} cm^{-3} for a He-MIP. It seems evident that the temperatures and electron number densities differ to some extent among the various plasma types. However, most studies demonstrate that these values are within the same magnitude. Even though the individual research efforts discovered some degree of variation in the temperature and electron density measurements, most agree that the CMP is not in local thermodynamic equilibrium [53,100,102-104,106] and represents a high temperature flame [102].

Interferences

An understanding of the possible interferences that effect the CMP is vital to trace elemental analysis. Numerous attempts have been made to evaluate these interferences. In early work, it was discovered that the CMP was not homogeneous in temperature and therefore chemical composition, unless Na was added to the plasma [103]. Also, the intensity of an element would increase with Na addition if that element was easily ionizable [85]. However, if the element produced emission from the central core of the plasma, it was minimally affected by Na. In contrast, if the element produced emission from the outer regions of the plasma, such as the metallic elements, it was strongly affected by the presence of Na. Rare earths were observed to have improved detection limits by up to 1000 times when Na was added to the plasma [86]. Unfortunately, high concentrations of sodium have also appeared to cause plasma instability [53].

It has been realized that easily ionizable elements (EIE) impose severe changes on analyte emission signals [53]. The increased introduction of EIEs, such as Na, has proven to induce large changes in the emission intensities of Ca, Cr, Mo, and Zn in an Ar-CMP [53]. In opposition to this, Masamba and Winefordner [101] found that Na had a negligible effect on Ca atomic emission in a He/H_2 mixed gas CMP. In an air plasma, it was observed that signals were enhanced in general with EIE addition [105]. Boumans *et al.* [54] noticed that the CMP would contract when alkali metals were introduced, and in some instances, detection limits would improve.

The effect of various species on Ca emission has also been closely examined. It has been determined that phosphate and aluminum can interfere with both ionic and atomic Ca emission [53]. This was confirmed by Masamba and Winefordner [101] who noticed that Ca emission was depressed with increased phosphate concentrations. Also, the results of Zhang *et al.* [105] verified that Ca emission was reduced in the presence of aluminum.

Boumans and coworkers [54] conducted a comprehensive comparison of the effects of interferences on the CMP and the ICP. They concluded that the ICP was superior to the CMP in resisting interferences. They found that the sensitivity, background noise, emission signals, and detection limits of the CMP were more drastically influenced by the matrix used. Accordingly, most agree that the CMP does suffer from a high degree of interference effects. Comparing the CMP to the ICP, it seems that the CMP is more susceptible to inter-element effects. As a result of the increased chance of interferences, poorer detection limits of trace elements in solution have been reported for the CMP.

Microwave Radiation

Many safety concerns are associated with the use of microwave instrumentation. Exposure to microwaves has been proven to cause a wide variety of health hazards. In minor dosages, subjection to microwave radiation can result in headaches, fatigue, sleepiness, irritability, appetite loss, anxiety, unstable moods, and memory difficulties [110-112]. Meanwhile, prolonged exposure to microwaves can lead to eye cataracts, sterility, blood changes, and heart enlargements or murmurs [110-112]. Thus, it is necessary that safe exposure limits be established, although there exist discrepancies as to what these levels should be [113]. In the United States, the standard safe exposure level is set at 5 mW/cm^2 for 2450 MHz [114] by the American National Standards Institute (ANSI). In Russia, the maximum permissible level is more restrictive as the standard is 0.01 mW/cm^2 for continuous exposure [111].

Due to the apparent health risks related to microwave radiation, it is mandatory that leakage above the indicated safe levels be prevented. Stray radiation from microwave plasmas can be easily contained using wire mesh and/or metal shielding [38,115]. In this research, the CMP was enclosed within an aluminum box with copper screen placed around any openings. Measurement of microwave leakage was tested using an approved leak detector calibrated for 2450 MHz (Narda Microwave Corporation, Hauppauge, NY). The measurement of stray radiation was made at a distance of 5 cm from the source.

Another means of reducing stray radiation from microwave plasmas has been to change the type of carrier gas being used. It has been discovered that radiation leakage varies with the carrier gas used [111]. It appears that leakage will increase as the ionization potential of the gas decreases and the molecular weight of the gas increases [111]. As the ionization potential of the gas decreases, more ions can be formed therefore producing more radiation. Thus, helium, which has the highest ionization potential and is the lightest of all the commonly used inert gases, will result in the smallest amount of microwave leakage [115]. Helium will produce stray radiation that is confined near the vicinity of the magnetron. Other gases, such as Ne, Ar, and Kr, will emit radiation that extends a greater distance into the work area. Addition of a molecular gas to the plasma carrier gas will promote a reduction in microwave leakage as well [111]. This is because molecules help to absorb excess radiation, decreasing the amount available for release.

Sample Introduction

Sample introduction has drawn considerable attention and remains the area where most experimental difficulties are encountered with plasmas. The goal of sample introduction is to provide for the reproducible transfer of a representative portion of the sample to the atomizer with a high efficiency and no adverse interference effects [116]. An ideal sample introduction technique should be highly efficient, have the ability to accept small sample volumes, be tolerant to complex matrices, and be amenable to liquid, solid, and gaseous samples with minimal sample pretreatment [117]. Sample introduction provides the essential link between the plasma and the sample and is therefore the crucial component to the success of a plasma-based system. The choice of sample introduction method depends on the type of sample being analyzed, the levels to be determined, the accuracy and precision required, the amount of material available, the time constraints on the analysis, and any special requirements such as speciation [118]. There are several ways in which the sample can be introduced into the plasma. These include pneumatic nebulization, hydride generation, and thermal vaporization.

Pneumatic Nebulization

Pneumatic nebulization is the most common method of sample introduction into a plasma source [119,120]. In pneumatic nebulization, a capillary tube carries the sample to the spray chamber. A fine aerosol is produced as a result of reduced pressure at the capillary tip induced by concentric gas flow around the capillary. The carrier gas stream transports the fine mist of droplets to the plasma. In the plasma, the sample droplets are desolvated, vaporized, dissociated into atomic vapor, and excited. The requirements for successful nebulization include: a high velocity gas stream, a reasonable pressure drop, maximum interaction between the carrier gas and liquid sample for fine aerosol production, and freedom from blockage [118].

Nebulization is common for routine analysis because it is convenient to operate [120-122]. It provides rapid sample handling at low cost [119,122] and few memory effects [123]. Nebulization does suffer from numerous disadvantages. It has a low transport efficiency. Typically only 2 % of the sample reaches the plasma [116] while the rest is discarded as waste. As a result, the transport efficiency is the criterion commonly used to evaluate nebulization. In addition, nebulization suffers from high sample solution consumption, requiring the use of sample volumes greater than 1 mL [117,124]. Thus, nebulization can not be used in situations where sample sizes are limited. Pneumatic nebulization also has problems with viscous samples or those with a high salt content [120]. This causes clogging and blockage in the nebulizer due to particulates or high dissolved solids. Another fundamental limitation of nebulization is the production of droplets of a wide variety of sizes [118]. The larger drops will not be completely desolvated and can cause plasma instability or extinguish the plasma due to high solvent loading. An intrinsic disadvantage to this sample introduction method is the need for complicated and often times tedious sample preparation of solid samples [125]. This can result in the loss of analyte information, dilution of trace elements below detectable levels, or contamination of the sample. Thus, the nebulizer system has been recognized as the weakest link in ICPs [122]. Therefore, alternative sample introduction systems have been investigated.

One such alternative is the monodisperse dried microparticulate injector (MDMI). This device produces controllable drop sizes on demand [126]. These droplets are injected into a flowing stream of gas, are desolvated to any desired extent in a furnace, and reproducibly carried to the plasma. Thus, transport efficiency is close to 100 % [126] as there is no drain or waste. Currently, the MDMI is being employed to examine fundamental processes within the ICP.

Although pneumatic nebulization has associated with it several inherent disadvantages, it has been used in previous research with CMPs [49,95,101,123].

Nebulization with a CMP has recently been extended to organic samples as well [102, 127] where Cl, F, and Si were determined. Nebulization sample introduction with a CMP is easily achieved due to the robust nature of this plasma which makes it tolerant to molecular species introduction [49]. This is in direct contrast to the MIP which is easily extinguished with continuous sample introduction or if concentrations greater than 500 ppm are used [24]. The low power of operation of the MIP proves difficult in accepting liquid aerosols.

Hydride Generation

Hydride generation has also found some use as a means of sample introduction. It is particularly useful for the determination of As, Bi, Ge, Pb, Sb, Se, Sn, and Te as these elements form volatile hydrides. In this technique, aqueous samples containing the analyte of interest are acidified and treated with a reducing agent to generate the hydride of the analyte. The hydride is then carried out of the reaction vessel into the plasma where it is decomposed to gaseous metal atoms and excited. Hydride generation has improved detection capabilities over nebulization [63]. This is due to the high efficiency of introducing gases into the plasma, which approaches 100 %. Thus, more analyte reaches the plasma resulting in better detection limits. Also, matrix interferences are eliminated since the generated gas is separated from solution. Preconcentration of the sample is possible by trapping the gas and introducing it as a plug into the plasma. Finally, the plasma does not have to desolvate or vaporize the analyte as it is introduced as a gas. This facilitates the use of low powered plasmas. However, this technique suffers from increased complexity of the required instrumentation and time consuming procedures. As a result, hydride generation with a CMP has found little use and has mostly been employed for As detection in aqueous [63] and sewage [62] samples.

Thermal Vaporization

Thermal vaporization (TV) is another viable alternative for sample introduction. Thermal vaporization is the term used whenever thermal, electrothermal (ETV), electrical, or direct vaporization is used to produce the appropriate free species for spectrometric detection [122]. In TV, a discrete amount of sample is deposited inside or on top of an atomizer. The atomizer can be a cup, rod, platform, tube, or wire filament [120]. The atomizer is then heated in three steps [128]. The first step is the drying or desolvation stage. Here sufficient energy is applied to evaporate the solvent from the sample and leave a solid residue. The next stage is the ashing or preatomization step. In this stage, the power is increased to convert any organic material into H_2O and CO_2 and vaporize any volatile inorganic species. The final step is the atomization stage, where the power is increased to vaporize and atomize the sample. The atomic vapor is swept into the plasma for excitation by means of a carrier gas. A transient signal will be produced due to the rapid formation of the atomic vapor [117,128]. In some instances, an additional cleaning step may be performed. Here a higher power is generated to remove any residual sample from the atomizer. The use of a TV device allows for separate optimization of the vaporization and excitation processes [129,130]. Thus, it has been discovered that separating the vaporization/sampling process from the atomization/excitation process can lead to improved overall analytical capability of the system [131-133].

Thermal vaporization has become increasingly important as a method of sample introduction in plasma spectrometry. In fact, several extensive reviews concerning TV into an MIP [11,117,133,134] and an ICP [117,120,122,133] have been published. Thermal vaporization offers many advantages over the alternative sample introduction method, solution nebulization. Detection limits are improved since a larger portion of the sample is transported to the plasma [117,120,128,135-137]. In addition, the possibility of removing certain sample components before vaporization exists through the use of temperature programming [117,128,129,135]. TV is also well suited for the analysis of very small samples [117,118,129,132,135]. Direct analysis of solid samples without the need for pretreatment is feasible as well [117,132,138]. However, TV does suffer from variable or incomplete vaporization, memory effects, possible transport losses, poorer precision, and from the formation of refractory compounds [117,131,135].

Thermal vaporization devices have been used with MIPs [31,45,134]. Due to its small size and low operating power, the MIP has limited ability to vaporize and atomize solid or liquid samples [117,134]. In addition, a change in impedance of the plasma occurs when small amounts of foreign material are introduced. Thus, because of the need for separate vaporization, MIPs have been readily coupled to ETV devices. As a result, the MIP has more energy available for excitation of the analyte producing lower limits of detection than with nebulization introduction [134]. Sample atomizers used with an MIP include a tantalum filament [28,29], a tungsten boat [27], and a graphite furnace

[33]. However, the ETV-MIP-OES system is limited by a narrow range of parameters for stable plasma operation [13,33].

Nixon *et al.* [139] were the first to couple an ETV device to the ICP. Since then, a wide variety of elements have been examined by ETV-ICP. The atomizers typically used in ETV-ICP-OES include filaments [28,121,139], rods [140,141], and tubes [131,142] fabricated from metal or graphite. Typically, ETV devices used with the ICP are modified from a graphite furnace atomic absorption spectrometer (GFAAS) [117]. The samples are dried and vaporized in the ETV and then transported into the ICP for atomization and excitation. Thus, the transport efficiency of the sample to the plasma becomes critical to analytical performance [129,136]. As a result, the effects of sample transport and the use of matrix modifiers have been investigated [117,119,124,143,144]. ETV-ICP-OES is inhibited by a change in the rate of sample transport between the atomizer and the ICP, irreproducible analyte losses during sample transportation, and the tendency towards memory effects [121,131,135,145]. Even with its limitations, ETV-ICP-OES has been applied to the analysis of ceramic powders [131], botanical solids [138], and biological samples [28].

Another method of TV sample introduction into the ICP is direct sample insertion (DSI). Direct sample insertion is a device or technique in which a sample is placed into or onto a probe [125]. The probe is subsequently inserted into plasma. The plasma remains "on" during manipulation of the probe [137]. The probe is raised to within a few mm of the plasma where drying and ashing of the sample occur as a result of thermal heating. The analyte is vaporized and excited upon insertion of the probe into the plasma.

DSI-ICP does not suffer from transport losses or dilution of the sample by carrier gases [122]. It allows for the analysis of discrete samples in the μL or mg range [146]. Disadvantages of DSI-ICP include a shift in the background level following probe insertion and irreproducible positioning of the probe resulting in lower precision [137]. The use of DSI-ICP for analysis has been extensively reviewed [125,137]. Current research involves automation of the introduction assembly [146].

TV in a CMP has also been performed. The sample is deposited into the electrode. A low microwave power, without the use of a plasma, is employed for desolvation by thermal heating. The power is then increased to produce a plasma on the electrode surface for atomization. Therefore, TV-CMP is accomplished *in situ* as the plasma forms directly around the sample [57,96]. Thus, the need for sample preparation and procedural steps, such as matrix modification, essential to ICP-OES [142] and MIP-OES [33,134], is eliminated. This technique can be readily employed for discrete sampling without any sample dilution or losses inherent with ICP-OES [122,131] and MIP-OES [13,33]. Since the plasma in a CMP is formed *in situ,* carrier gases are not required and analyte transport from the TV device is not a limitation. Also, positioning of the electrode does not change between sample determinations, eliminating the positioning errors that may occur with DSI-ICP-OES [137]. Even so, poorer precision, possible contamination from the electrode materials, and changes in the background level with microwave power do pose problems. In addition, it is necessary to reignite the plasma between sample injections, which may contribute to the poorer precision.

CHAPTER 3
INSTRUMENTATION

Introduction

The operation of the CMP is distinct from that of other types of plasmas. A microwave generator, usually a magnetron, is used to produce microwave energy. This energy is then transported from the magnetron through a rectangular waveguide as a standing wave. The microwaves capacitively couple to an electrode which is inserted at the opposite end of the waveguide. A plasma is formed at the surface of this electrode. If high enough power is applied, the surrounding gas will partially ionize and autoignition of the plasma occurs. If low power is used, the plasma is initiated by seeding electrons. This is accomplished by using a tesla coil or touching the electrode tip with an insulated piece of wire.

Instrumental Design

A schematic diagram of the experimental design used in this research is shown in Figure 3-1. The instrumental components are described in Table 3-1. The laboratory-constructed torch is made from two concentric quartz tubes. The central tube has an inner diameter of 4 mm and an outer diameter of 6 mm. This tube is used to hold the electrode in position. The outer tube has a 15.5 mm inner diameter and a 17.5 mm outer diameter.

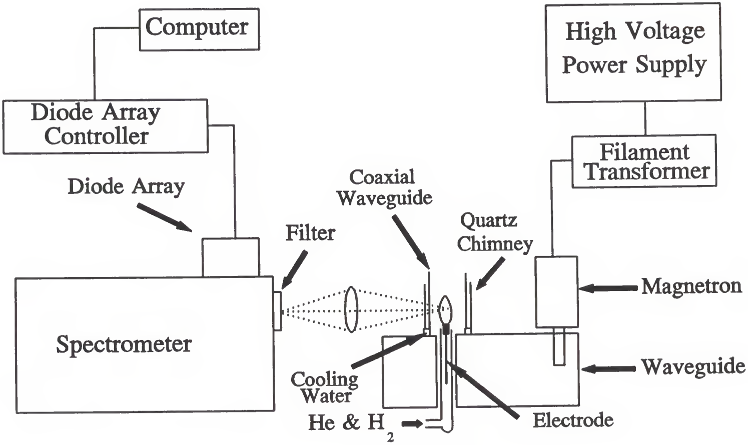

Figure 3-1. Schematic diagram of the experimental design.

Table 3-1
Instrumental components

Components	Manufacturer
High voltage d.c. power supply: Model 805-1A (maximum power output of 1.6 kW)	Hipotronics; Brewster, NY
Magnetron: Model NL10251-2 (frequency 2.45 GHz, maximum output power 1.6 kW)	National Laboratories; Orlando, FL
Silver plated brass waveguide	Laboratory made
Torch: Two concentric quartz tubes	Laboratory made
Spectrometer: Jobin-Yvon HR1000, 1 m, 2400 grooves mm^{-1}, linear dispersion 0.5 nm mm^{-1}	Instruments SA, Inc.; Metuchen, NJ
Photodiode array: OSMA model IRY-1024G	Princeton Instruments; Princeton, NJ
OSMA detector controller	Princeton Instruments
Photodiode array software: Spectrometric Multichannel Analysis, ST 120, Ver. 2.00	Princeton Instruments
Computer: 80286, 8 MHz	PC's Limited; Austin, TX

The outer tube directs the plasma gas flow around the electrode. The entire torch is 187 mm in length. The torch is water-cooled by cooling coils which surround the torch and cover the top of the waveguide. The cooling coils also serve as a support for the brass coaxial waveguide. The coaxial waveguide helps to propagate the microwaves out of the waveguide, towards the top of the electrode for plasma formation. A quartz chimney which is 4 cm in diameter surrounds the coaxial waveguide. It is used to keep air currents from disturbing the plasma. The emission signals are observed from the side into the spectrometer. A series of neutral density filters are used to maintain linearity in the detector response.

Microwave Generators

The magnetron is the most commercially available microwave generator and therefore is the most commonly used. These M-type cross field devices are designed so electrical and magnetic fields are crossed at right angles to each other [147]. Magnetrons are compactly built and consist of two concentric blocks with an evacuated region present between them. The center is the cathode, which when heated, produces thermionic emission of electrons, which are subjected to an electric field. The electrons then should travel in a straight path towards the anode [147]. However, the magnetron also contains a permanent magnet which applies a perpendicular magnetic field, which induces the electrons to move in a curved path [148]. Therefore, the electron movement will depend on both the applied electric and magnetic fields [147]. The proper strength magnetic field, as well as the continual emission of electrons, generates a circulating electron cloud in the evacuated region between the cathode and anode [148]. This electron cloud sweeps past the anode which is composed of a series of resonant cavities. The shock of the passing electron cloud excites the cavities into self-oscillation of their electromagnetic fields with a portion of these fields being coupled to the circulating electron cloud [148]. The electron cloud is accelerated and decelerated by these fields causing bunching to occur. The oscillations of the cavities combine to set up an electric wave between the cathode and anode. A sustained wave at microwave frequency results. The frequency is dictated by the physical dimensions of the resonant cavities cut into the anode [147]. These cavities are spaced around the anode such that the induced resonant fields will enhance the bunching of the electrons allowing a larger portion of the electron kinetic energy to be recovered as microwave signal [148]. Magnetrons have an efficiency of over 80 % and a low cost. However, they suffer from high noise output and from a difficulty in maintaining a stable output frequency [149].

Waveguides

The waveguide is the major component of the CMP. It is used to transmit electromagnetic radiation from the magnetron to the electrode where the plasma is formed. The waveguide can either be a rectangular or cylindrical hollow cavity. However, the rectangular shape is the most common [147,148].

Waveguides are more efficient at transmitting energy at microwave frequencies than conventional transmission lines such as coaxial cables used with MIPs [147]. Conventional transmission lines suffer from ohmic, dielectric, and radiative losses [147].

Ohmic losses, which are considerable at high frequencies, are caused by the currents flowing in resistance to the conductor composing the transmission lines. Dielectric losses are a result of the electric field acting on the molecules of the insulator and thus causing heating from molecular agitation. Radiation losses occur as the emitted wave propagates away from the surface of the conductor of the transmission line. In contrast, waveguides have negligible dielectric losses since they are normally filled with air [148,150]. Also in waveguides, electric and magnetic fields are maintained on the inside walls. Therefore, no power is lost by radiation [147]. Ohmic losses are decreased since the internal walls of the waveguides are constructed from materials which have low resistivities, such as Ag or Au [147]. Furthermore, waveguides have a higher power handling capability, a lower loss per unit length, and a lower cost mechanical structure than coaxial cables [150].

Waveguides are generally used for high power operation. This is because coaxial cables have the tendency to become hot and radiate heat at power levels above 100 W, causing a loss of power [147]. Even so, when microwaves propagate through a waveguide, some power is still lost as heat. These power losses are kept to a minimum and are related to the skin depth or depth of penetration (δ) of the material. The skin depth is defined as the depth at which the current decays to 1/e or 37 % of its value at the surface [148]. The skin depth is depicted by this equation [147]:

$$\delta = \frac{1}{\sqrt{2\pi f \mu \sigma}} \tag{1}$$

where f = frequency (Hz), μ = permeability (Henry/m), and σ = conductivity of the medium (mhos/m). The skin depth is inversely proportional to the frequency of electromagnetic radiation. Thus, at microwave frequencies, which are in the GHz range, the skin depth of the material is in the micrometer range. As a result, the current flows along the surface of the conductor creating an increase in the resistive effect. This is referred to as the "skin effect" since the current becomes concentrated in the outer surface of the material [150]. Materials with small skin depths will have less power lost to heat.

The skin depth is also inversely proportional to the conductivity of the material of the waveguide as shown by equation (1). Consequently, the waveguide is fabricated from highly conductive metals. These include brass, Al, Au, Cu, and Ag [147]. The metals Au, Cu, and Ag are not used often as they are difficult to machine. Also, Ag and Cu corrode easily in air and Au is expensive. Generally, waveguides are manufactured from Al or brass which is often plated with Ag.

Waveguide use imposes certain boundary conditions. These conditions suggest that for the electric field to exist at the surface, it must be orthogonal to the conductor, while the magnetic field must not be orthogonal, but parallel to the surface [147]. Thus, waveguides require that electromagnetic waves propagate in only two modes: transverse electric (TE) or transverse magnetic (TM) [148]. In the TE mode, transverse electric waves are perpendicular to the direction of propagation. In the TM mode, transverse magnetic waves exist normal to the direction of propagation. As a result, the electric field is parallel to the height or "b" dimension of the waveguide while the magnetic field is parallel to the width or "a" dimension [147]. This is illustrated in Figure 3-2 [151].

Each field will have a distinct distribution inside the waveguide. These fields are pictured in Figure 3-3 [151]. The magnetic field propagates along the width, or the "a"

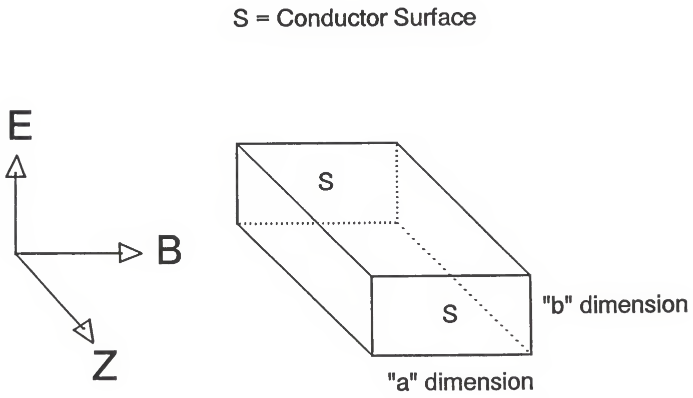

Figure 3-2. Illustration of the boundary conditions required in a waveguide [151]. E is the electric field, B is the magnetic field, and Z is the direction of propagation.

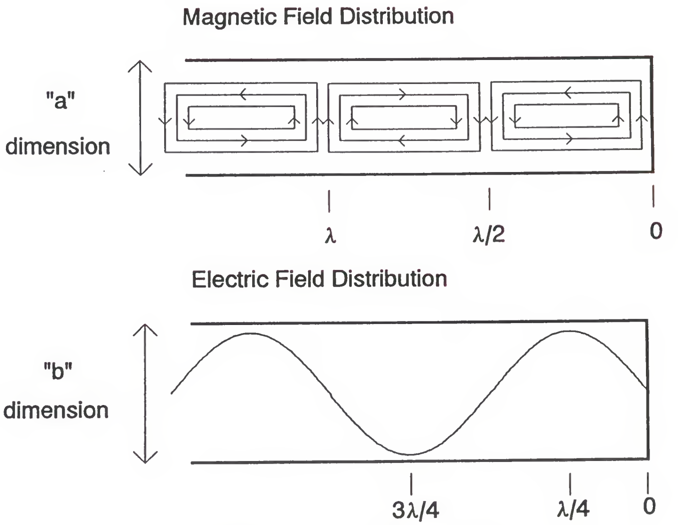

Magnetic Field Distribution

Electric Field Distribution

Figure 3-3. Field distributions inside a waveguide [151].

dimension of the waveguide. It has a maximum field density at $\lambda/2$ from the end of the waveguide and at each repeating $\lambda/2$ interval. In contrast, the electric field propagates along the height or the "b" dimension of the waveguide. The maximum field density in this case is at $\lambda/4$ from the edge of the waveguide and repeats at every odd $\lambda/4$.

The role of the waveguide is to support a standing wave as microwaves are reflected from the walls [147]. The microwaves are emitted from the magnetron probe which is inserted vertically at $\lambda/4$ from the edge of the waveguide [148]. The emitted waves travel $\lambda/4$ distance from the probe to the wall, which results in a 90° phase shift. The wave then undergoes a 180° phase shift as it reflects off the wall. It then travels back the $\lambda/4$ distance, again experiencing a 90° phase change. This results in a total phase change of 360°. Thus, the reflected wave constructively interferes with the outgoing wave so no energy is lost [147]. The energy produced inside the waveguide can then be extracted by the electrode. The electrode is inserted at $\lambda/4$ from the opposite edge of the waveguide to insure efficient coupling with the electric field [107]. A maximum coupling efficiency and a maximum electric field density occur when the magnetron probe and the electrode are placed at a $\lambda/4$ distance from the waveguide edges [97]. Ali [97] found that the optimum depth inside the waveguide for the electrode should be 3 cm. This also corresponds to $\lambda/4$.

Size governs the propagation of the modes inside the waveguide. Hence, the wavelength in the waveguide (λ_g) must be known. In an air-filled waveguide, λ_g is defined as [147]

$$\lambda_g = \frac{\lambda_0}{\sqrt{1 - (f_c / f)^2}} \tag{2}$$

where λ_0 is the wavelength in free space, f is the operating frequency (usually 2450 MHz), and f_c is the cutoff frequency. The wavelength in free space is equal to c / f where c is the speed of light (3×10^8 m/s). The cutoff frequency is the frequency at which no current can flow [150]. It is related to the cutoff wavelength, λ_c, which is the longest wavelength that can be supported by the waveguide and is defined as [147]

$$\lambda_c = 2a \qquad (3).$$

Here a again represents the width of the waveguide. Therefore, the "a" dimension must satisfy the inequality

$$a > \frac{\lambda_c}{2} \tag{4}$$

in order for power to flow [150]. Since a wave travels in any medium at a velocity of $v = f_c \lambda_c$, the cutoff frequency for the waveguide is [150]

$$f_c = \frac{v}{2a} = \frac{c}{2a\sqrt{\mu_r \epsilon_r}} \tag{5}$$

where μ_r is the relative permeability (dimensionless) and ϵ_r is the relative permittivity (dimensionless). The value μ_r is equal to the magnetic permeability of the medium (μ) in Henry/m divided by the free space permeability (μ_0) also in Henry/m. Likewise, ϵ_r is equal to the dielectric permittivity of the medium (ϵ) in Farad/m divided by the free space dielectric permittivity (ϵ_0) also in Farad/m. Accordingly, the waveguide has the properties of a high pass filter since power transmission is only possible when $f > f_c$ or $\lambda < \lambda_c$ [147, 150]. The cutoff frequency is a function of both the dimension of the waveguide and the mode being studied. Therefore, the mode with the lowest cutoff frequency in the waveguide is designated as the dominant mode. In a rectangular waveguide, the dominant mode is TE_{10} [147,148,150]. For TE_{mn}, m and n represent the number of half wavelengths that propagate along the magnetic axis (a dimension) and the electric axis (b dimension) respectively. In the waveguide, other modes may also be present. However, only the dominant mode will propagate and the higher modes will decay rapidly [150].

Electrodes

The development of TV-CMP-AES has focussed on the improvement of the electrode system. The electrode is the component that makes TV-CMP unique over thermal vaporization with an MIP or an ICP. The electrode enables the direct vaporization of the sample by the plasma. It should be chosen carefully however, as it can erode with time and can give spectral interferences. These interferences are due to emission lines produced by the electrode that may overlap or interfere with the analyte emission lines. The electrode must be conductive and should have a high melting point to withstand the plasma temperatures. Ideally, the electrode should be amenable to the analysis of both liquid and solid samples.

The electrode can take on various designs. Ali and coworkers developed the electrode cup system [57,96] using high purity graphite. The graphite cup however exhibited memory effects, the potential for carbide formation with the analyte under examination, and the need for frequent replacement due to plasma etching. Filament electrodes fabricated from tungsten wire were also studied for a variety of elements in aqueous samples [98,99] and Pb determinations in whole blood [64,65]. Recently, a tungsten cup electrode was constructed and used for the analysis of Si in an oil matrix [51]. In this research, the electrode was also a tungsten cup with a capacity in the microliter range. The selection of the electrode material is of considerable importance because it is the major source of sample contamination. Tungsten was chosen because it can withstand operation at high power levels without any deterioration, it produces low background emission, and does not suffer from adverse memory effects [51].

Three distinct electrode cups were used for this work and compared. Figure 3-4 illustrates the different designs studied. The 30 μL capacity cup, which shows the electrode position in the torch, has a 4 mm depth. The 10 μL capacity cups each have a 2 mm depth. All the cups have a 3 mm inner diameter and a 4 mm outer diameter. The 30 μL cup and the 10 μL "thick" bottom cup both have 5 mm heights, while the other 10 μL cup has a 3 mm height. All the cups were fabricated from high purity (99.95 % and 99.96 %) tungsten (ThermoElectron/Tecomet, Wilmington, MA). Each cup was supported by a laboratory-constructed graphite holder (Ultra Carbon Corporation, Bay City, MI) of similar design. As depicted in Figure 3-4, the graphite holder is placed in the inner tube of the two concentric tube torch, the design of which is described

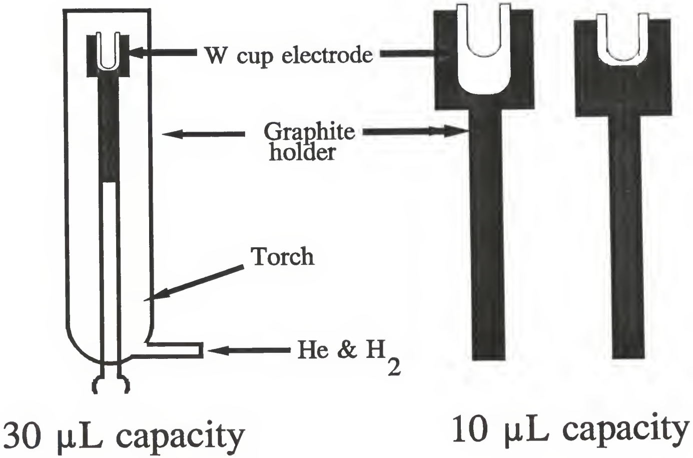

Figure 3-4. Exaggerated view of W cup electrode designs.

elsewhere [51]. As previously indicated, the electrode cup system was placed at a depth of 3 cm inside the waveguide in order to achieve optimal coupling with the microwave field [97].

Plasma Composition

Microwave plasmas have been successfully produced from a variety of different gases, such as nitrogen, helium, argon, and air [50,100,101,105,152,153]. Helium and argon are the preferred plasma gases because they do not give background molecular spectra [18]. The background using a helium MIP is an order of magnitude lower than with an argon MIP [109]. Helium usage is advantageous over that of argon. Helium has a higher ionization energy which makes it an efficient excitation source for emission [154]. Excited helium can also populate higher energy levels of free atoms and ions [7] which makes it useful for analysis of the halogens [31,127] and nonmetals [29,30,155]. In addition, less microwave leakage occurs. This is due to the large ionization energy of helium [111] which promotes a smaller degree of ionization and the release of fewer ions, and therefore less radiation. Helium is not without its problems however. Helium suffers from a high electrical resistivity which causes a lower power transfer efficiency [154]. Also, helium has a high thermal conductivity thereby promoting the dissipation of heat to the outer tube of the torch at a fast rate [156], which increases the chances of torch melting. In order to alleviate this problem, a small amount of molecular gas can be added to the plasma gas [107]. A variety of different molecular gases have been studied [7,51]. These include hydrogen, nitrogen, and oxygen. However, hydrogen was shown to improve the emission signals obtained, as well as the signal-to-noise ratios [100,101]. Hydrogen also helps to create a reducing environment and decreases the chances of oxide formation [51]. For these reasons, the plasma in this work was produced from a mixture of commercial grade helium and hydrogen gas.

The helium plasma can be depicted by a stability diagram. This stability diagram, which is shown in Figure 3-5 [102], demonstrates the dependence of the plasma on both microwave power and plasma gas flow rate. It should be noted that these boundaries are not rigid and will change upon the addition of a molecular gas or by changing the plasma support gas. For helium, a stable plasma is formed from 2-17 L/min gas flow and from 150-1400 W of microwave power.

Based on this diagram, the plasma is divided into four regions. No plasma occurs at all flow rates at powers < 130 W. The filament plasma is bright pink in color. It is very small, thin, extremely unstable, and difficult to focus on the entrance slit of the spectrometer. It also tends to erode the electrode at a fast rate. Therefore, this plasma is not analytically useful. The other two types of plasmas which are of interest are the spherical and cylindrical plasmas.

The spherical plasma, which gets its name from its shape, generally occurs at flow rates < 6 L/min. This plasma is extremely stable. It is pinkish-blue in color. It has a small size which varies slightly with plasma gas flow rate and power. It can have a diameter of 1-1.5 cm and a length of 2-3 cm. At increased flow rate, the spherical plasma will transform into the cylindrical plasma.

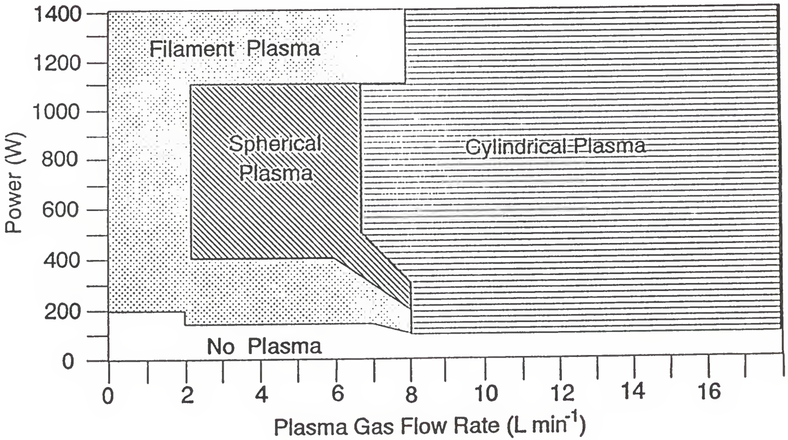

Figure 3-5. Stability diagram for a He-CMP [102].

The cylindrical plasma, also gets its name from its shape. It occurs at all microwave powers at flow rates above 6-7 L/min. It is very bright pink and extremely stable. This plasma has a diameter that is equal to that of the electrode (approximately 0.4 cm). It has a length that ranges from 2 cm at low flow rate to 4.5 cm at high flow rate. The cylindrical plasma differs from the spherical plasma in color, size, and background emission. Both of these plasmas, which have been described in greater detail elsewhere [51,102], are analytically useful and were used for this research.

Detector

The detector used for this work was a photodiode array (PDA). The PDA is composed of 1024 silicon photodiodes (or pixels) arranged in a linear manner covering a 20 nm spectral range when mounted on a 1 m focal length spectrograph. The PDA, which operates in a charge storage mode, has a photodiode center-to-center spacing of 25.4 μm [157]. The incident radiation is collected by the diodes for a specified integration time. The integration time, which ranges from 0.033 s to greater than 2 s, is the interval of time the photons are acquired. Long integration times can lead to overexposure of the PDA. Integration studies were performed in previous work [107] and the results were incorporated here. The PDA has a dynamic range of 2 to 4 orders of magnitude [157]. The dynamic range is limited on the low end by readout noise and on the high end by the saturation level [157]. However, variable integration capabilities can increase the effective dynamic range. The PDA is characterized by several disadvantages. The diodes must be read sequentially as the system does not allow for random access of any diode. In addition, it is necessary to the cool the detector to decrease the dark current which is generated from thermal charge. The PDA is not as sensitive as a photomultiplier tube (PMT). Most importantly, the diode array is too small to achieve both the desired resolution and the desired wavelength coverage for multielement analysis. The wavelength range that can be monitored is determined by the width of the individual diodes and the dispersion of the spectrograph. The PDA software was used to collect and analyze data sequentially from each diode. Additional software programs were written in order to improve the data handling capabilities. The spectrometer is described in Table 3-1. The entrance slit of the spectrometer was set at a height of 3 mm and a width of 20 μm for all experiments.

CHAPTER 4
DETERMINATION OF TRACE ELEMENTS IN SOLUTION

Introduction

A CMP operating at 450 to 1000 W was used for atomic emission spectrometry. The laboratory-constructed system, which was described in previous chapters, contained a tungsten cup electrode capable of holding a volume of up to 30 µL. Microwaves are used to dry the sample, while at higher powers, the plasma is ignited for sample vaporization and excitation. The entire analysis can be carried out in less than 5 minutes. A mixture of helium and hydrogen was used as the plasma gas. A spherical or cylindrical shaped plasma can be formed depending upon the gas flow rate and the microwave power selected. The effects of experimental parameters, such as gas flow rate, atomization power, electrode position, and plasma shape were examined. Detection limits for Ca, Cd, K, Mg, Na, Pb, and Zn were in the pg range for a 10 µL sample; the relative standard deviation (RSD) was less than 10 %. In addition, the accuracy and precision of this technique were investigated.

Experimental

Reagents

Aqueous standards of cadmium (1000 μg/mL), calcium (1000 μg/mL), and zinc (1000 μg/mL) were obtained from Inorganic Ventures Inc. (Toms River, NJ). The aqueous magnesium (1000 μg/mL) and lead (1000 μg/mL in HNO_3) standards were obtained from Fisher Scientific (Fairlawn, NJ). The aqueous potassium (1000 μg/mL in 1 % HCl) atomic standard was obtained from Aldrich Chemical Company (Milwaukee, WI). The sodium standards were made from sodium chloride salt obtained from Fisher Scientific (Fairlawn, NJ). Water from a Milli-Q Plus water system (Millipore Corporation, Bedford, MA) was used to prepare all subsequent dilutions.

Procedure

Aqueous samples of 10 μL volume were deposited with a pipette (Eppendorf, Brinkmann Instruments Inc., Westbury, NY) into the tungsten cup. They were dried by heating at a microwave power of 75 W for 45 s when the 10 μL cups were used. The "thick" bottom 10 μL cup was used for the Mg experiments while the "thin" bottom 10 μL cup was used for the Ca, K, Na, and Pb experiments. For the Cd and Zn analyses with the 30 μL tungsten cup, the drying stage consisted of a microwave power of 90 W for 60 s. After the drying step, the gas flow rates were set to the appropriate levels depending on the plasma shape being studied. The power was then raised rapidly to the optimal atomization power, while simultaneously starting the computer for data acquisition. The emission signal was scanned for 1.0 s intervals over a period of 20 to 30 s depending upon the element being examined. As shown in Figure 3-4, the electrode was submerged 6 mm below the top of the torch in all cases. The emission signal was observed at several mm above the electrode cup. This observation height was optimized for the best signal-to-background ratio. All signals were reported as the mean of 3 measurements with error bars representing one standard deviation from the mean.

Detection Limits

Because of the transient nature of the signal, the scan with the maximum emission intensity for the element of interest was used for analytical purposes. The analytical signal was obtained from the spectrum by measuring the peak height from the sample and subtracting the signal from a blank solution. The computer software automatically accounted for the background correction of the signal. The peak area was also examined, but it did not provide any significant advantage in the detection limits, as will be shown later. The detection limits were determined as 3 times the standard deviation of the blank (blank-limited detection limit) or the background (background-limited detection limit) [158]. The blank standard deviation was calculated from 10 measurements of the blank signal at the wavelength of the analyte under examination. The background standard deviation was calculated from the background signal produced from 10 consecutive diodes near the analyte wavelength. The calibration curves for the elements were performed using conditions chosen from the optimization studies. Each experimental parameter was optimized individually while all other conditions were held constant. A condition was considered optimal if it produced a maximum in the signal-to-background ratio.

Results and Discussion

Drying Stage

The drying stage was a vital part of the thermal vaporization process. It served the purpose of evaporating the solvent from the sample. This was accomplished by heating the electrode using a low microwave power, without the use of a plasma, for a short time. It was found that elimination of this stage produced an initial instability of the plasma causing interference with the atomization process and sputtering of the sample out of the cup electrode. The drying time was related to the solvent being used and also the design of the cup. The drying power produced no significant change in the emission signals for all the elements studied. Figure 4-1 shows the relatively constant effect of drying power on the Cd, Mg, and Zn signals. Figure 4-2 illustrates the drying power relationship to the Pb and Na signals. Although several of the elements studied are considered volatile, there was no resultant loss in emission intensity imposed by the drying stage. Compromised conditions can easily be obtained for mulielement analysis as each element required a similar drying power for its measurement.

Temporal Profiles

The emission signals obtained were transient as depicted by the Cd signal shown in Figure 4-3. However upon investigation, it was realized that the cup design imparted

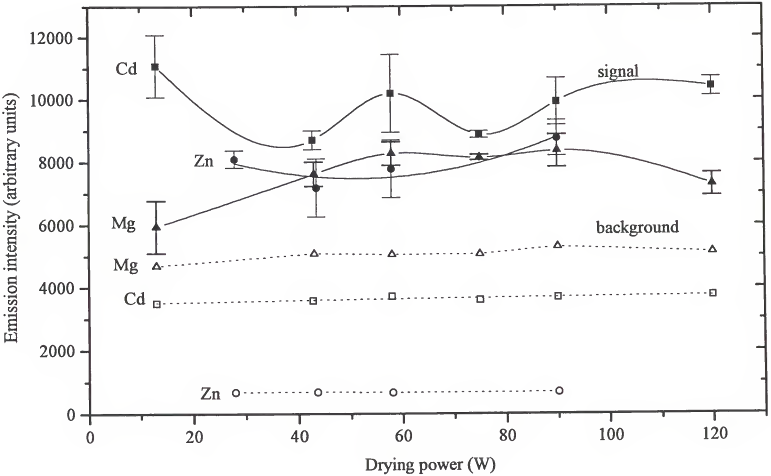

Figure 4-1. Effect of drying power on Cd, Mg, and Zn signals.

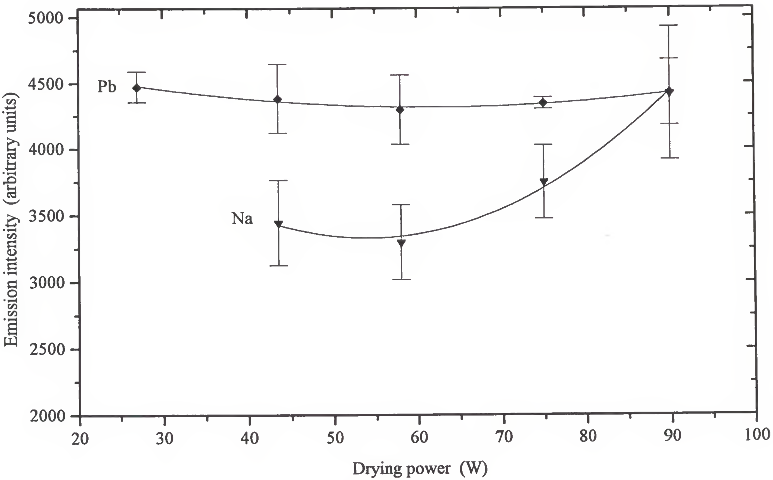

Figure 4-2. Effect of drying power on Pb and Na signals.

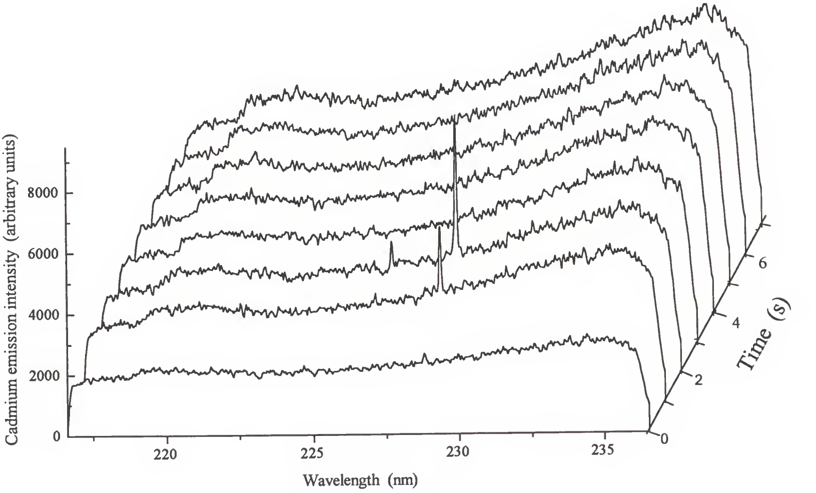

Figure 4-3. Temporal profile of 0.5 ng of Cd at 228.802 nm.

a crucial effect upon the atomization of the analyte. Thus, the temporal profile of the emission signal was highly dependent upon the electrode shape being used. As indicated above, three distinct tungsten cup electrodes (Figure 3-4) were investigated for this work. A cup of 30 μL capacity was employed for the cadmium and zinc experiments, while the 10 μL cups were used for the remainder of the elements. It was found that the deep cup, which possessed a thin bottom surface, allowed for the rapid thermal heating and atomization of the analyte. As a result, the signals obtained were of relatively short duration lasting only 4-5 s for Cd (Figure 4-4) and 6-7 s for Zn (Figure 4-5) with the signal returning to the background level. In contrast, the shallow cup, one of which had a thick bottom surface, seemed to contribute to the uneven heating and heterogeneous atomization of the magnesium sample which was studied in this cup design. To illustrate the influence of the cup wall thickness, samples containing Mg were atomized using both the thin and thick bottom cups under similar operating conditions. As shown in Figure 4-6, the Mg signal in the thin bottom cup was atomized completely and rapidly in comparison to the sample atomized using the thick bottom cup. Therefore, the thickness of the cup wall had a dramatic effect on the ability of the cup to heat then atomize the sample. As a result, a third cup was developed. It was also 10 μL in capacity although it had a thin bottom surface of only 1 mm. This cup was used for the remainder of the elements studied. Even with this improved cup design, the Pb signal lasted for longer than 25 s and complete atomization was questionable. Thus, it was proposed that a more volatile matrix, such as lead chloride, may enhance the atomization of Pb. The results are shown in Figure 4-7. It appears that there was no significant improvement in the

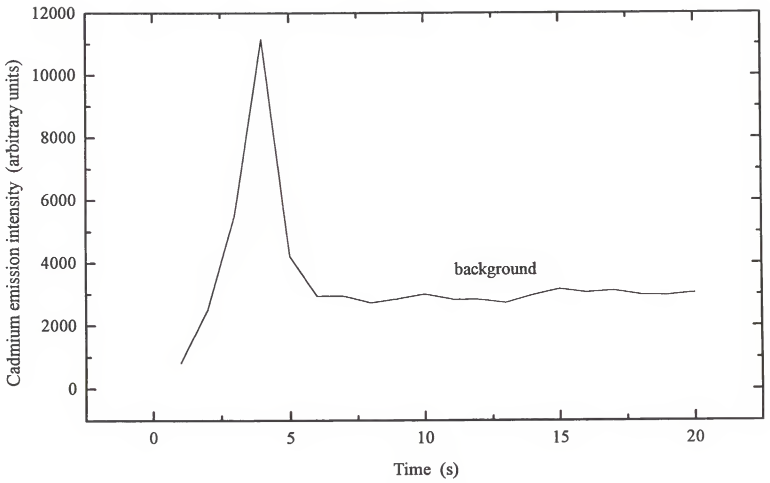

Figure 4-4. Temporal profile of 1 ng of Cd at 228.802 nm using a cylindrical plasma.

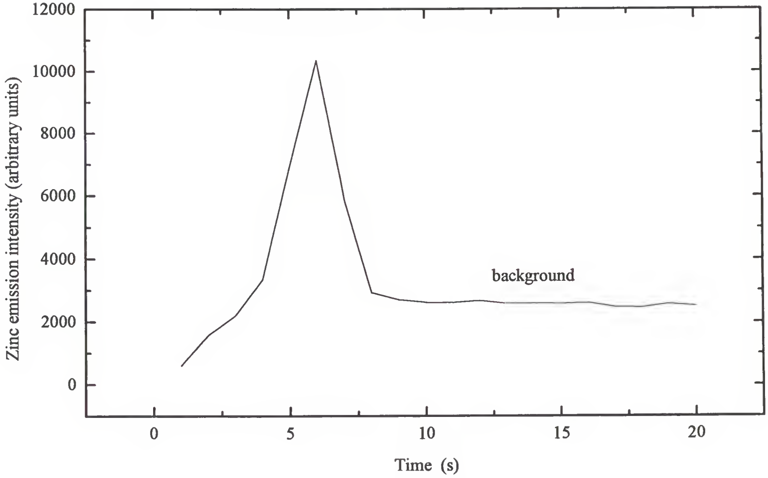

Figure 4-5. Temporal profile of 2 ng of Zn at 213.856 nm using a spherical plasma.

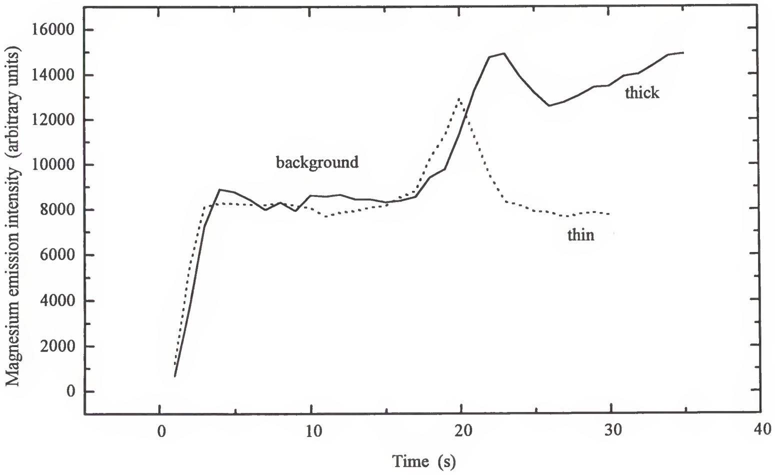

Figure 4-6. Temporal profile for a 0.5 ng sample of Mg at 285.213 nm in each of the thick and thin bottom cups.

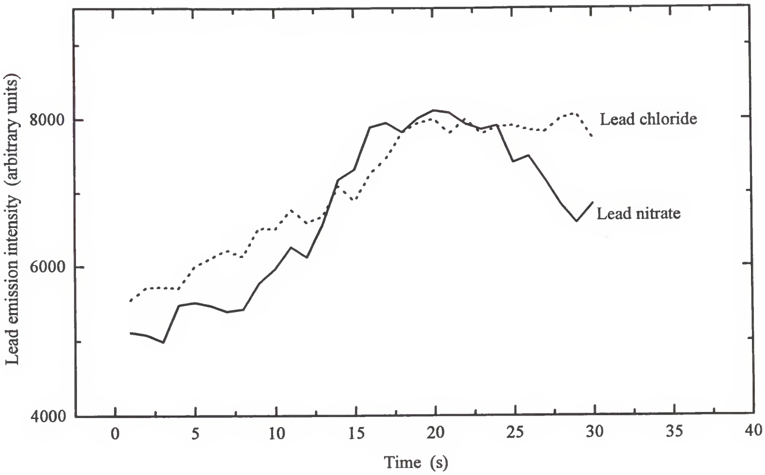

Figure 4-7. Temporal profile of the effect of matrix on 7 ng of Pb at 405.78 nm.

signal profile of Pb as both matrices, lead nitrate and lead chloride, produced similar temporal profiles under identical operating conditions. In addition, the Pb signal due to the lead chloride matrix was still being atomized after 30 s. The utility of the thin bottom 10 μL cup is demonstrated by the temporal profile of Na illustrated in Figure 4-8. The sodium signal was completely atomized with any residual signal being attributed to the blank. Similar results were found for K and Ca. Furthermore, there was no significant change in the temporal profile with plasma shape. Both the cylindrical and spherical plasmas produced similar temporal profiles for all the elements studied.

Vertical Distribution

The vertical emission intensity profiles of Cd and Mg are shown in Figure 4-9, and that of Pb is depicted in Figure 4-10. The observation height is the position above the electrode in the plasma where the signal is observed. A 0 mm observation height corresponds to the electrode surface being even with the center of the entrance slit of the spectrometer. It was found that the observation height is dependent in part on the volatility of the element being analyzed. The optimal observation position occurred close to the cup surface, at 3-4 mm for Mg and 4-5 mm for Cd. This was attributed to the fact that these elements are volatile and thus were completely atomized in the lower region of the plasma. There was also an increase in the background level here due to black body radiation from the cup surface. Similarly, Pb had a maximum emission signal at a 3 mm observation height. It should be mentioned that the Pb signals (Figure 4-10) are reported as the background subtracted peak heights while the Cd and Mg signals (Figure 4-9) are

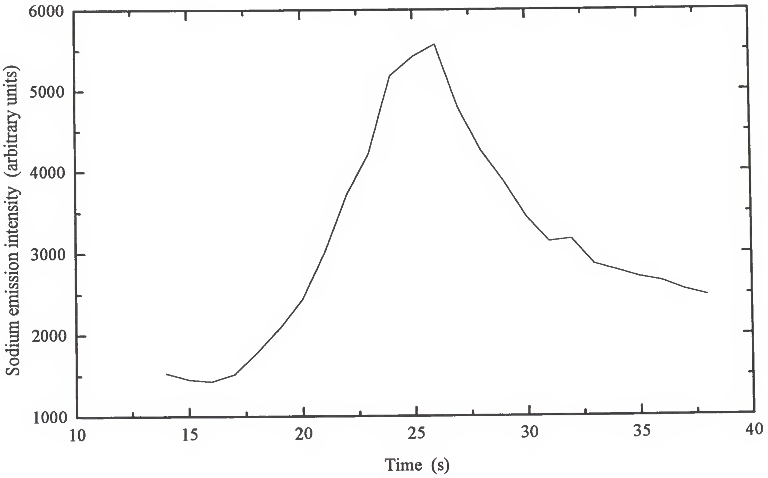

Figure 4-8. Temporal profile of 2 ng of Na at 588.995 nm.

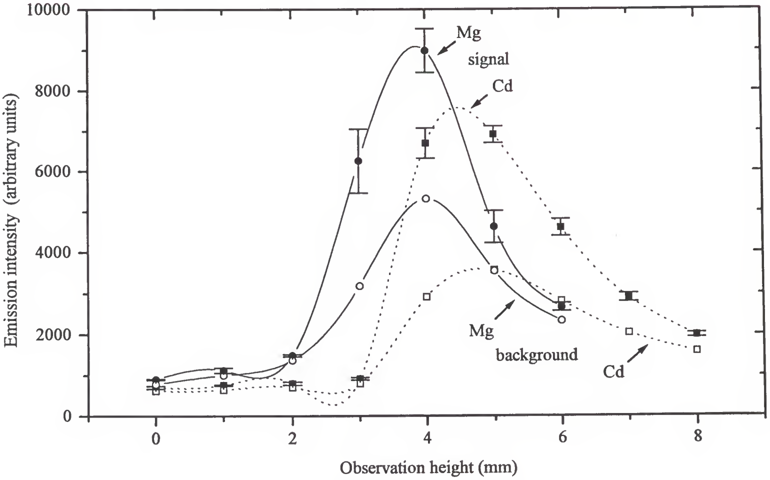

Figure 4-9. Vertical distribution of Cd and Mg signals and backgrounds.

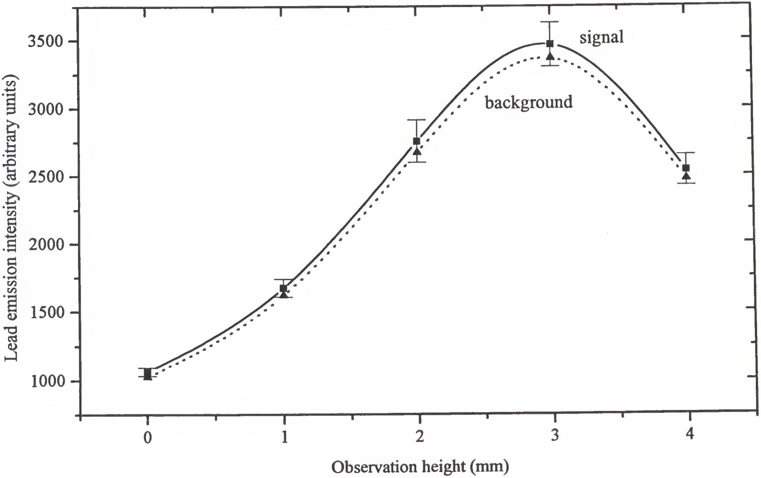

Figure 4-10. Vertical distribution of Pb signal and background.

reported as the peak height plus the background. As a result of these findings, compromised conditions are easily attained for simultaneous multielement analysis since the optimal signals produced overlapped and occurred in a similar region in the plasma for all the elements studied. However, Na was an exception. A Na signal was obtained only at one observation height, 0 mm. All other positions above the cup surface produced a rich spectrum like that displayed in Figure 4-11, making detection of the Na atomic line difficult. It is believed that many of the peaks observed in this spectrum are due to various He lines present in this visible wavelength region. In general, the analyte emission intensity decreased in the higher region of the plasma as a result of diffusion and cooler plasma temperatures [100]. In addition, the spherical and cylindrical plasmas provided similar vertical distributions.

Horizontal Distribution

The horizontal distribution of analyte emission across the plasma, was related to the type of plasma being used, not the element being examined. Thus, the results were similar for all the elements studied. The spherical plasma, which was wider in diameter, produced a uniform emission intensity for the elements over a ± 1 mm displacement to the left and right of the plasma center. The plasma center, which was focussed on the entrance slit, corresponded to a displacement of 0 mm. This relationship is exemplified by a sample of Mg which is shown in Figure 4-12. The cylindrical plasma however, was much narrower, having a diameter equal to that of the cup electrode. This plasma produced a uniform emission signal for all the elements studied over a total width of 1

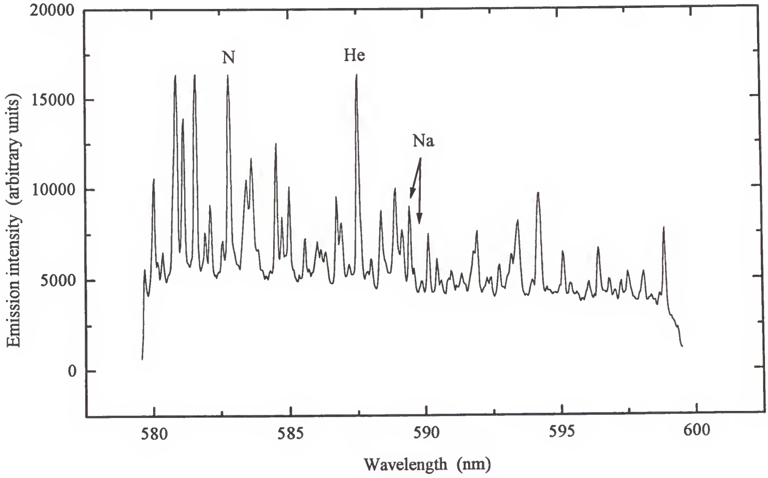

Figure 4-11. Background emission spectrum at 589.0 nm.

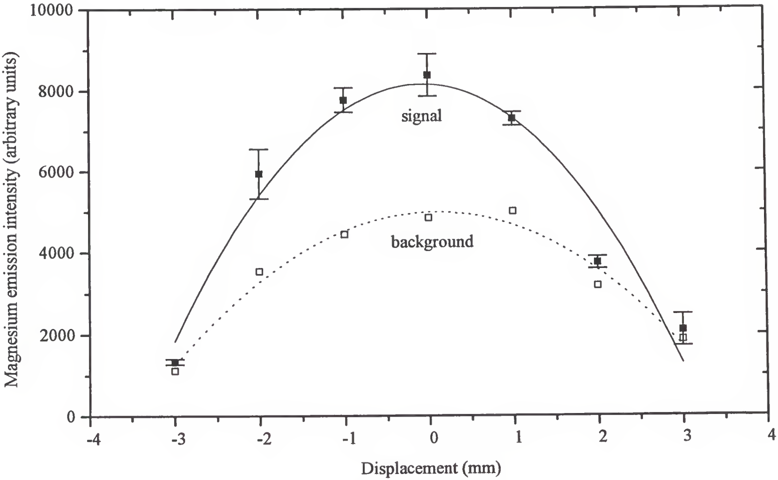

Figure 4-12. Horizontal distribution of Mg signal and background using a spherical plasma.

mm. This is displayed in Figure 4-13 using Cd as an example. The emission intensities were symmetrical across the plasma as long as the plasma was centered on the electrode correctly and the torch was not etched.

Atomization Power

The atomization power varied with each of the elements studied. The reported powers were a measure of the input power to the magnetron. The actual power delivered to the plasma could not be determined. Figure 4-14 shows that for the cylindrical plasma, the Zn emission intensity increased with increasing atomization power to a maximum, after which the signal slowly decreased. In contrast, the spherical plasma generated a relatively constant emission signal for Zn. The lack of change in intensity with power for this plasma shape is probably due to the hotter temperature attained by this plasma [102]. Figure 4-15 illustrates the effect of atomization power on both Pb signal and background. It was found that effective atomization did not occur until at least 1000 W of power was reached. This was believed to be due to the necessity of the cup to reach a temperature of about 1400 °C for the initiation of Pb atomization [159]. As measured by an optical pyrometer, the cup surface was approximately 1400 °C at 1000 W of power. Figure 4-16 illustrates the effect of atomization power on the Cd and Mg signals. For both elements, there was an increase in the emission signal with increasing power until the signal reached a steady state. This trend occurred for both the spherical and cylindrical plasmas. This pattern was produced regardless of the different cup design used for the Cd and Mg experiments. Calcium, potassium, and sodium behaved similarly,

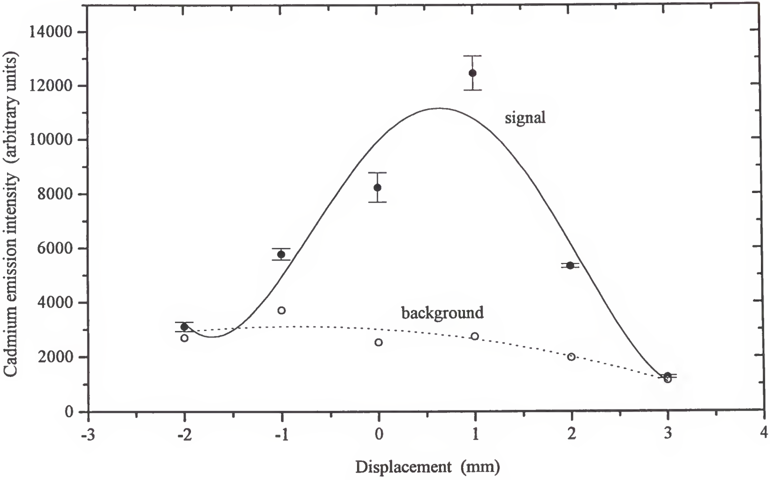

Figure 4-13. Horizontal distribution of Cd signal and background using a cylindrical plasma.

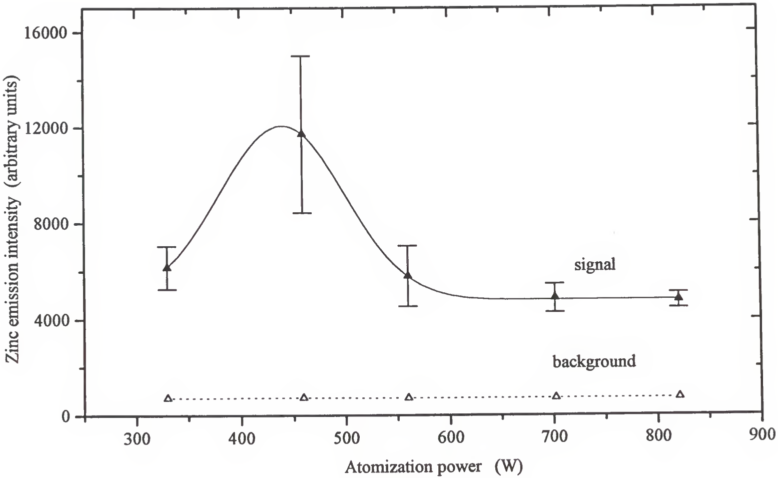

Figure 4-14. Effect of atomization power on Zn signal and background (cylindrical plasma).

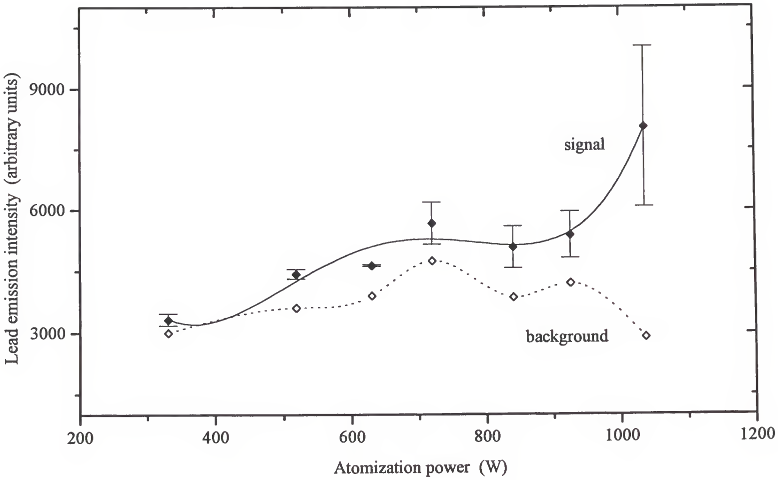

Figure 4-15. Effect of atomization power on Pb signal and background.

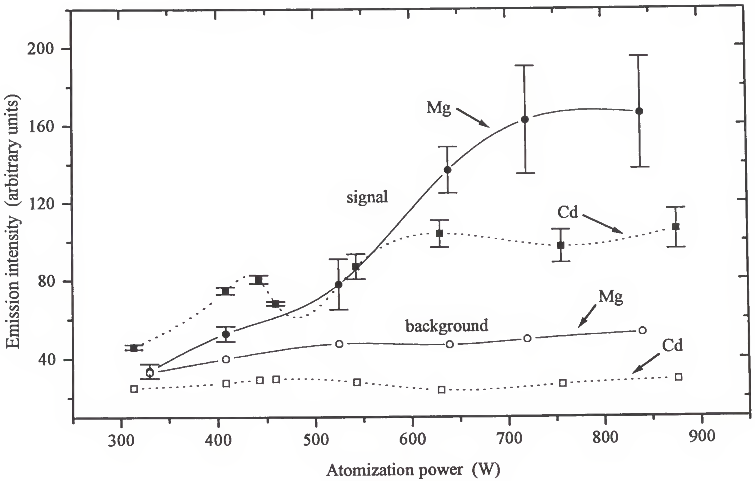

Figure 4-16. Effect of atomization power on Cd and Mg signals and backgrounds.

as shown in Figures 4-17 to 4-19 respectively. However, Ca and K produced the best signal-to-background ratios at powers greater than 800 W, while Na produced a better signal-to-background ratio at about 500-600 W. The volatility of the element under examination was not the only factor to be considered when attempting to explain the influence of atomization power. However, it is important to note that all the analytes can be atomized over a wide power range with a maximum in a similar region. Also, all signals were consistently longer at the lower power levels. Further investigation of the influence of atomization power on the analyte signal needs to be performed before making any definitive conclusions.

Helium Gas Flow Rate

The He flow rate did not prove to have a significant effect on either the Cd, Mg, or Zn signals as demonstrated in Figure 4-20. The behavior was similar for Pb (Figure 4-21) and Na (Figure 4-22). A He gas flow study was not performed for Ca and K since compromised conditions were assumed for the studies of these two elements. For each element studied, each flow rate produced a relatively constant signal within the error of measurement. Recall that the spherical plasma was formed at low helium flow rates while the cylindrical plasma was generated at flow rates greater than 6 to 7 L/min. Thus, both plasma shapes were considered to be suitable for the measurement of these elements.

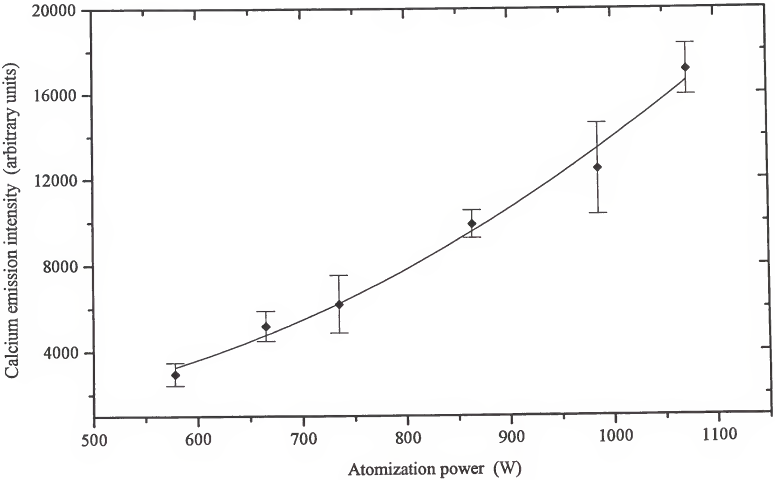

Figure 4-17. Effect of atomization power on Ca signal.

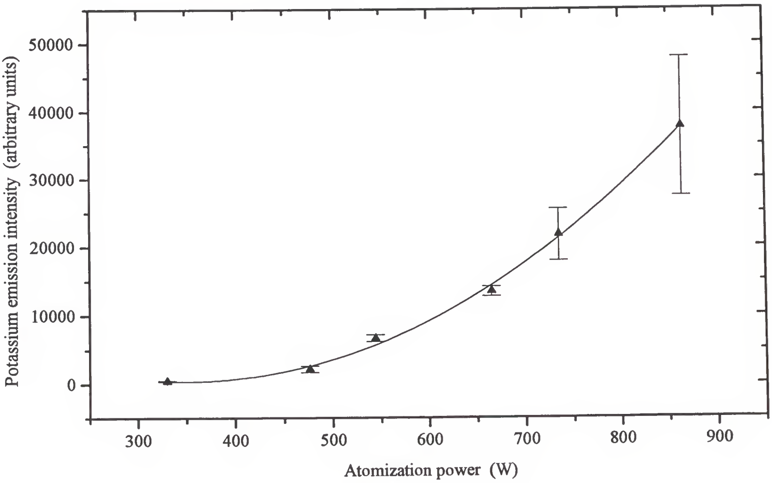

Figure 4-18. Effect of atomization power on K signal.

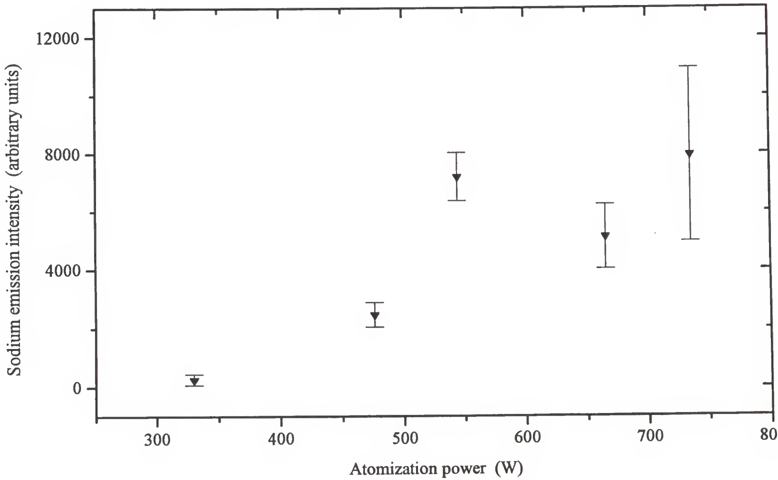

Figure 4-19. Effect of atomization power on Na signal.

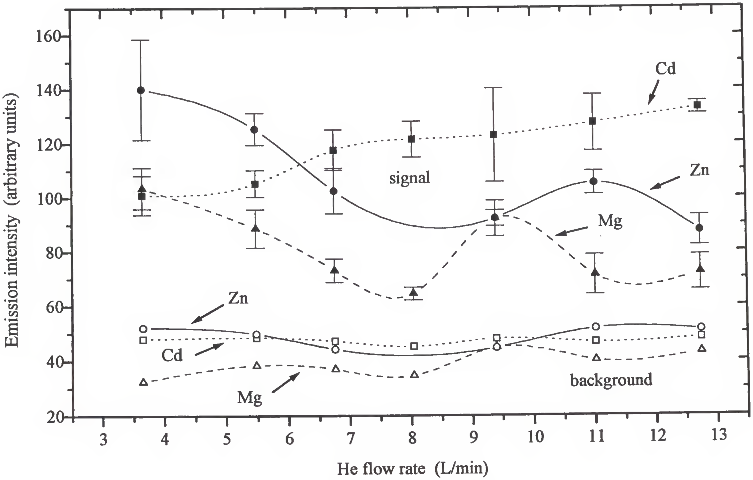

Figure 4-20. Effect of He gas flow rate on Cd, Mg, and Zn signals and backgrounds.

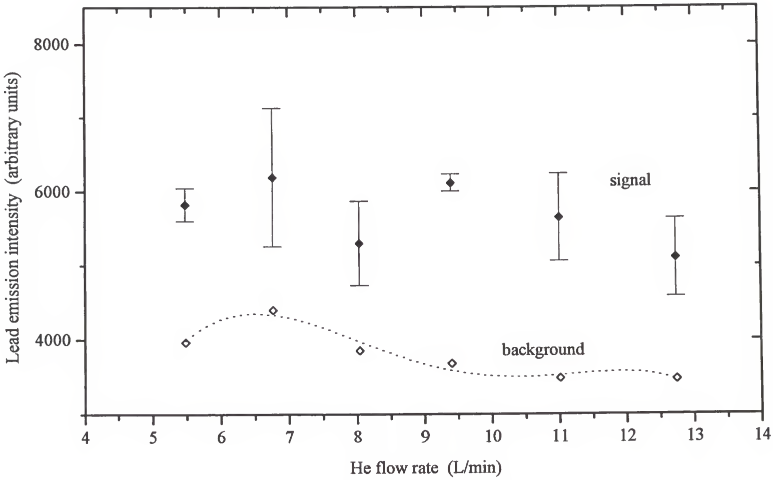

Figure 4-21. Effect of He gas flow rate on Pb signal and background.

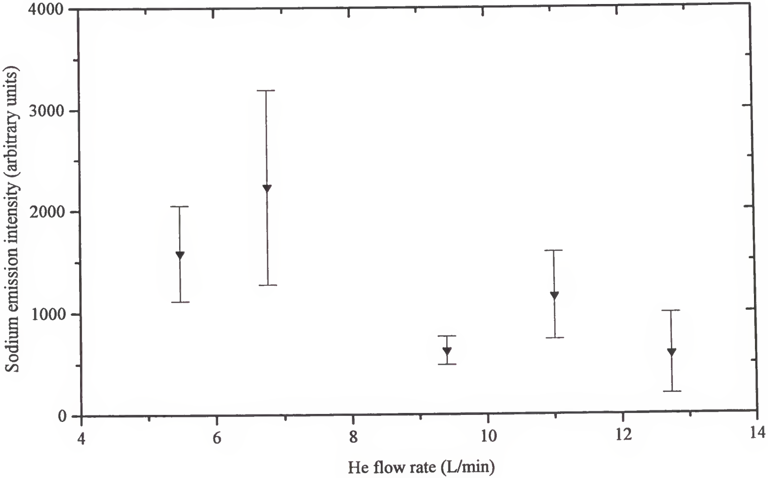

Figure 4-22. Effect of He gas flow rate on Na signal.

Hydrogen Gas Addition

As previously noted, it has been found that hydrogen should be used in conjunction with the plasma support gas [100,101]. This was because of the increased signal-to-noise ratios and decreased oxide formation by creating a reducing environment. As Figure 4-23 shows, H_2 addition does have a significant influence on the emission intensity of Cd, Mg, and Zn. No signal was obtained for Zn without at least a small quantity of H_2 added. However, increased addition of hydrogen did not further influence the Zn emission signal. In the case of Cd, the emission intensity was at a maximum when a small amount of H_2 was introduced. This was probably caused by the decrease in the excitation temperature of the plasma with an increase in hydrogen addition [101]. Also, quenching of the helium excitation mechanism has been shown to occur with molecular gas addition [18]. Similar results to those of Cd were found for Mg except that a larger quantity of H_2 was required for achieving the maximum signal and a much greater enhancement in the emission signals was observed. In the case of Pb, which is shown in Figure 4-24, again, the addition of 500-600 cm^3/min of H_2 was sufficient to produce a reproducible signal which was not further influenced by additional H_2 gas of up to 1.2 L/min. Sodium (Figure 4-25) displayed similar results producing maximum signals at about 700 cm^3/min of hydrogen gas. It should be realized that each element produced a maximum signal within a similar range of added hydrogen, again allowing for the easy attainment of a set of compromised conditions for simultaneous multielement analysis.

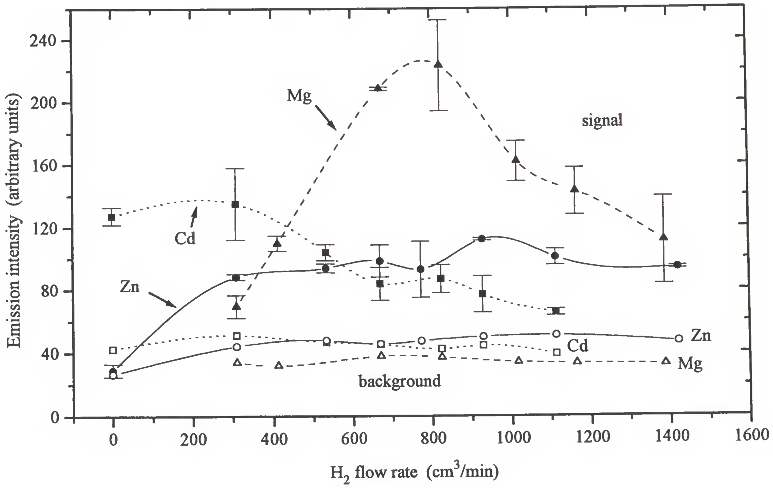

Figure 4-23. Effect of H_2 gas flow rate on Cd, Mg, and Zn signals and backgrounds.

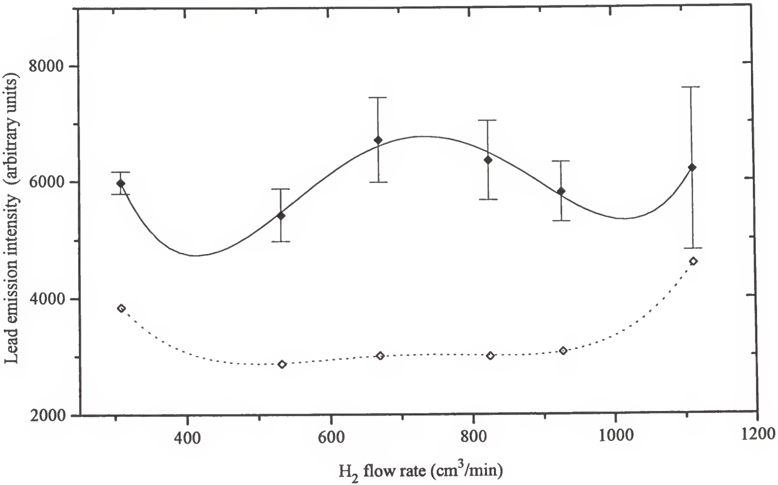

Figure 4-24. Effect of H_2 gas flow rate on Pb signal and background.

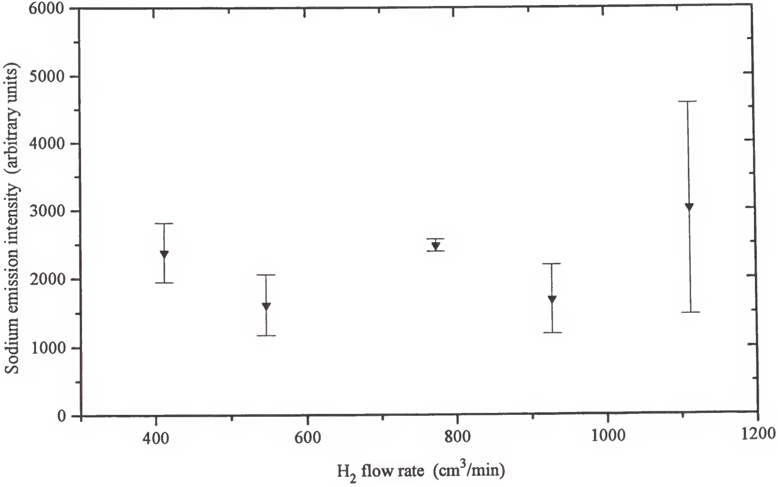

Figure 4-25. Effect of H_2 gas flow rate on Na signal.

Trace Element Measurement

The operating conditions used for evaluating the analytical performance of the TV-CMP-AES system are based upon the studies described above. An optimal condition was defined as one which produced a maximum signal-to-background ratio while all other parameters were held constant. The optimal conditions selected for each element are compiled in Table 4-1 for both the spherical and cylindrical plasmas. It should be mentioned that the experimental conditions used for the Ca and K calibration curves were compromised conditions selected based upon the optimization studies performed for the other elements. The analytical curves for Cd (Figure 4-26) and Zn (Figure 4-27) both had log-log slopes of 1.0 over the region from the detection limit to at least two orders of magnitude higher. Both plasma types provided similar limits of detection (LOD) for each element. The analytical curve for Mg (Figure 4-28) showed pronounced nonlinearity and a log-log slope of 1.2. The higher slope was attributed to the severe memory effects observed in measurements with Mg. The primary cause was believed to be the uneven heating and heterogeneous atomization resulting from the use of the thick bottom cup for this element. Also, it was found that the blank for the Mg studies contained an appreciable concentration of Mg (close to 3 ng/mL as estimated by the calibration curve). In addition, the Mg blank signal was close to 10 times higher than the blank signals obtained for the other elements. Thus, for Mg, the detection limit determined under these laboratory conditions was blank-limited as opposed to the LODs of Cd and Zn which were background-limited. As a result, the LOD for Mg was reported as a measure of the amount of Mg contained within the blank. The analytical curve for lead (Figure 4-29)

Table 4-1
Optimum operating conditions for the cylindrical and spherical plasma

Parameter	Zn	Cd	Mg	Pb	Na	K	Ca
Wavelength (nm)	213.856	228.802	285.213	405.783	588.995	766.490	422.673
Observation height (mm)	4	4	4(5)	3	0	3	3
Displacement (mm)	0	0(1)	0	-2	0	0	0
He flow rate (L/min)	5(9)	5(13)	5(9)	9.4	7	7	7
H_2 flow rate (cm^3/min)	610	460	670	412	772	772	772
Atomization power (W)	476(459)	525(630)	639(851)	1036	544	735	864

* Conditions used for the cylindrical plasma are indicated in parentheses when different from the spherical plasma. Note that the Pb, Na, K, and Ca conditions are for the cylindrical plasma only.

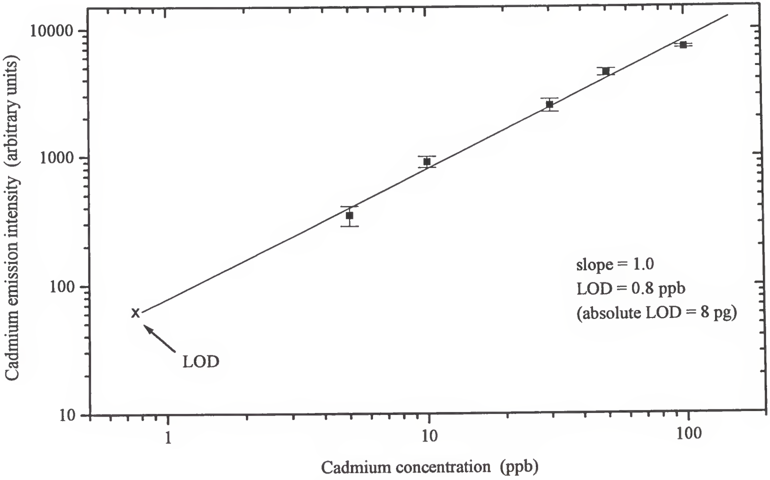

Figure 4-26. Log-log calibration curve for Cd (spherical plasma).

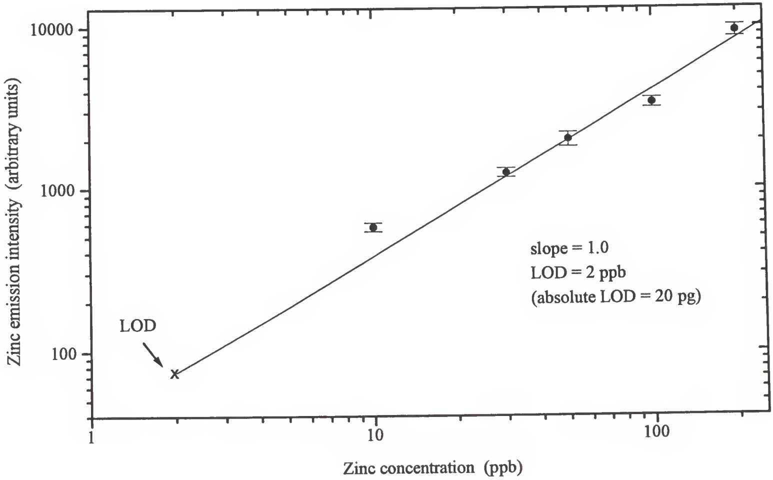

Figure 4-27. Log-log calibration curve for Zn (spherical plasma).

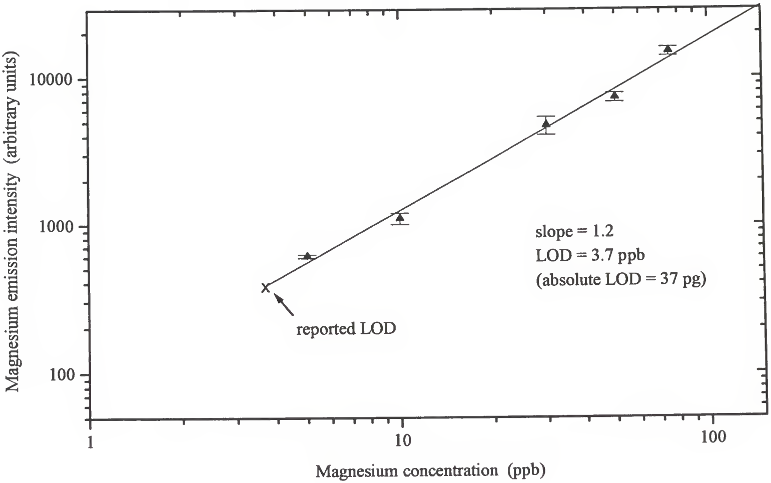

Figure 4-28. Log-log calibration curve for Mg (spherical plasma).

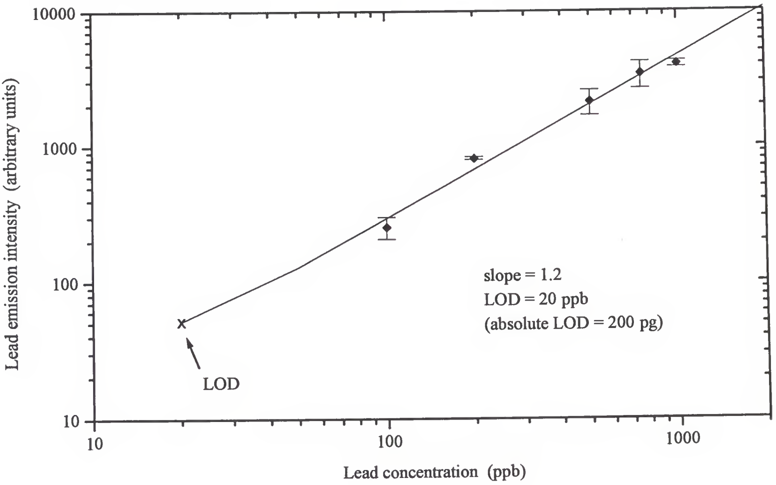

Figure 4-29. Log-log calibration curve for Pb (cylindrical plasma).

exhibited a log-log slope of 1.2, also showing some curvature at the lower concentration. This is thought to be due to the uncertainty of whether the Pb sample was completely atomized. It was noticed that the Pb signals were weak even at higher concentrations as shown in the spectrum of a 5 ng Pb sample (Figure 4-30). The calibration curve for Na also exhibited curvature at the lower concentrations (Figure 4-31) producing a log-log slope of 0.89. It was believed that the LOD for Na, like Mg, was blank-limited. This was due to the high concentrations of Na found to be present in the blank, as well as possible environmental contamination. This could lead to the low value for the slope. Although obtained under compromised conditions, the analytical curves for Ca (Figure 4-32) and K (Figure 4-33) were linear and exhibited log-log slopes of 1.1 and 0.92, respectively. The slopes deviate slightly from 1.0 as a result of possible environmental contamination. The linear dynamic range was found to cover 3 orders of magnitude from the detection limit. In addition, the use of peak area did not produce a significant improvement in the detection limits obtained. Therefore, it was not investigated further. It is believed that some improvement in the LOD and linearity may result from using peak areas for elements whose peak shape changes with time. The detection limits achieved for each element are given in Table 4-2 along with a comparison to those measured in prior work performed in this laboratory using TV-CMP-AES with a graphite cup [96] and also to those obtained by graphite furnace atomic absorption spectrometry (GFAAS) [160], the most widely used technique for elemental analysis of discrete samples. Results obtained by other atomic methods, TV-MIP [31-33,140,161] and TV-ICP [141,144,162], are provided as well.

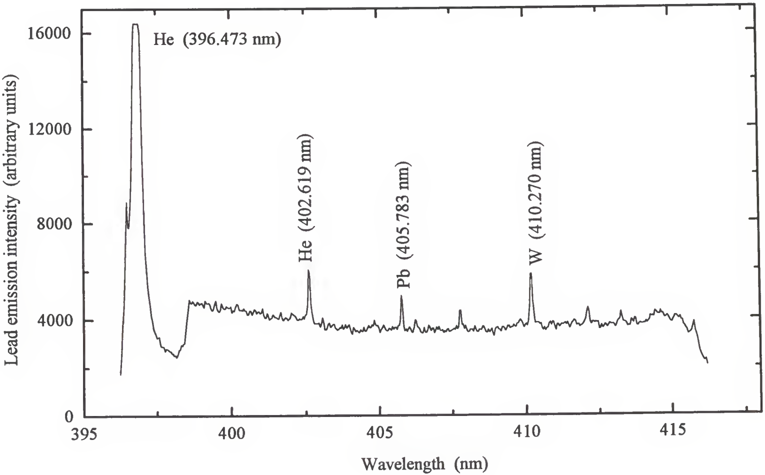

Figure 4-30. Spectrum of a 5 ng sample of Pb.

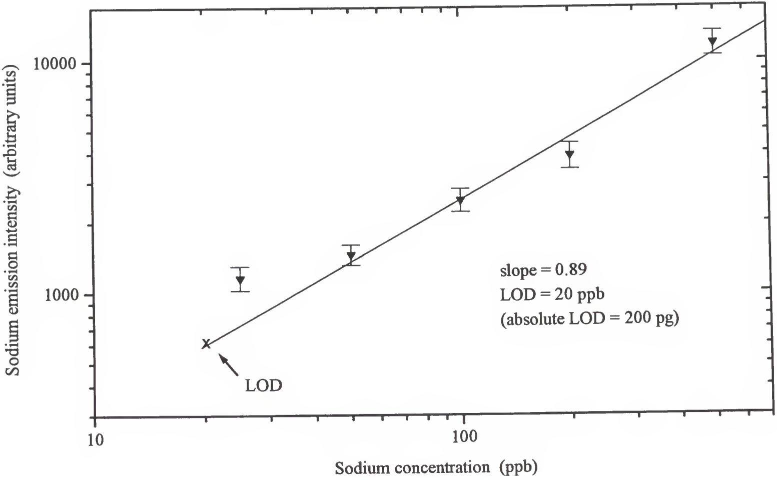

Figure 4-31. Log-log calibration curve for Na.

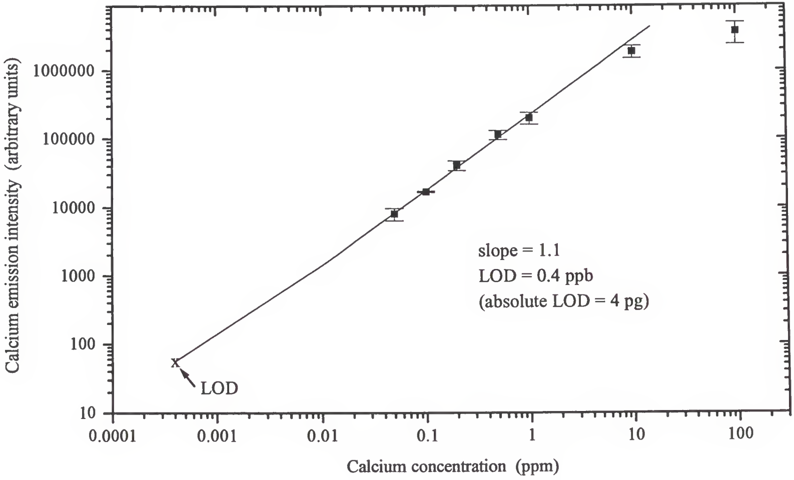

Figure 4-32. Log-log calibration curve for Ca.

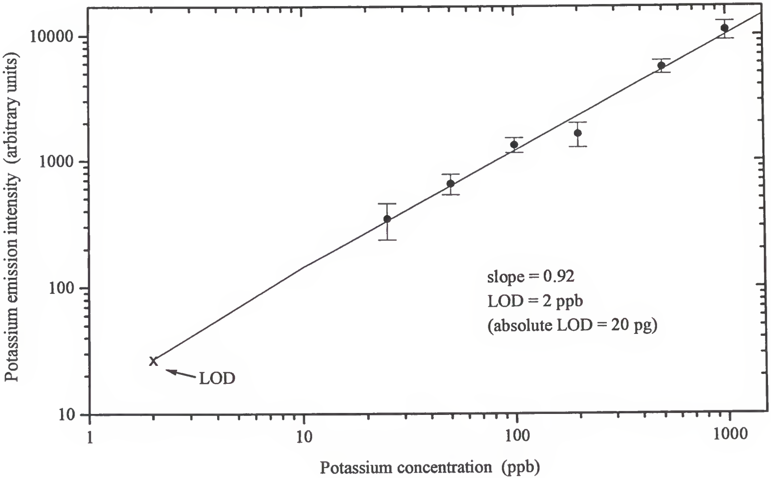

Figure 4-33. Log-log calibration curve for K.

Table 4-2
Comparison of detection limits

Element	This work[†] (pg)	Graph-TV-CMP[96] (pg)	GFAAS[160]* (pg)	TV-MIP (pg)	TV-ICP[141] (pg)
Cd	8	30	0.02	10 [31]	10
Ca	4	---	1	3850[32]	15[162]
K	20	---	0.4	---	1200[144]
Mg	37[‡]	15	0.02	100 [161]	0.1
Na	200	---	0.4	---	400[162]
Pb	200	---	0.7	80[140]	100
Zn	20	65	0.1	150 [33]	3

* Detection limits based on 2σ, resulting in up to 50% relative standard deviation.

† Detection limits based on 3σ of the blank.

‡ This is a blank-limited detection limit and is reported to be the actual concentration of Mg present in the blank.

Tin Analysis

The analysis of Sn was attempted but not completed due to numerous difficulties. The tin standard (1000 μg/mL in 20 % HCl) used was obtained form Inorganic Ventures, Inc. (Toms River, NJ). All subsequent dilutions were prepared in a high percentage of HCl to prevent complexation. The vertical distribution of Sn was the same for that of the other elements studied. The optimal observation height was 3 mm. The helium gas flow rate produced relatively no change in the signal intensity within the error of measurement. Thus both plasma shapes would be suitable for analysis. The hydrogen gas flow rate produced a small maximum in the emission intensity of Sn at approximately 544 cm^3/min. The signal then decreased with increased hydrogen addition, in a similar manner to the other elements investigated.

However, the measurement of Sn was plagued with many problems. The measurements suffered from severe memory effects, weak emission intensities, and poor reproducibilty resulting from Sn being vaporized as a molecular species, probably SnO [159]. This possibilty was confirmed in these experiments by the presence of the strong molecular SnO band heads at 281-290 nm [163]. Thus, it was suspected that the SnO was not being completely atomized resulting in memory effects and poor reproducibility. It has been reported [159] that SnO requires close to 1900 °C in order to be completely atomized in a graphite furnace. However, the cup temperature was measured by an optical pyrometer and found to sustain a temperature up to 1400-1500 °C over the power range used. Thus, it is believed that without modification to the current system design, the analysis of trace quantities of Sn is difficult.

Standard Reference Material

The accuracy and precision of this unique method of trace analysis were investigated. A standard reference material (SRM) of soil was obtained from the National Institute of Standards and Technology (NIST). The soil sample (SRM 2711) was pretreated by an acid digestion procedure recommended by NIST. The soil was digested in a mixture of nitric and hydrofluoric acids. The digested sample was cooled and then additional acid was used to further dissolve the residue. The sample was cooled again and filtered through number 42 filter paper. The filter paper was dissolved and then combined with the original filtrate and diluted to a volume of 100 mL. This procedure was repeated for three separate 1.00 g samples of the soil. These prepared soil samples were subjected to analysis by TV-CMP-AES for the determination of Cd.

The measurement of Cd in the soil was performed using two methods, calibration with aqueous standards and the method of standard additions. A calibration curve of aqueous Cd standards was performed using the operating conditions selected from the previous optimization studies (Table 4-1). The three individually digested soil samples were then measured and the quantity of Cd determined. These results, which are the average of three measurements, are shown in Table 4-3 and are compared with the certified value of 41.70 ± 0.25 μg/g. The measured values for Cd in the soil compare with the certified value to produce an absolute bias of less than 15 %. The average of the Cd concentration in the original soil was 40 ± 7 μg/g. This closely agrees with the certified value and produces an 18 % RSD. In an attempt to improve the precision of this technique, the method of standard additions was investigated. Incremental microvolumes

Table 4-3
Determination of Cd by the calibration method

Sample	Measured concentration (μg/g)	Bias
sample #1	36 ± 11	-14 %
sample #2	37 ± 12 *	-11 %
sample #3	48 ± 10	15 %
average concentration	40 ± 7	-4 %

* this value is the mean of 3 separate concentration determinations of Cd.

of a 10 mg/L solution of Cd were added to the digested soil samples. The same operating conditions were used and the concentration of Cd was determined. The standard additions procedure was repeated on three different occasions and the results are given in Table 4-4. These measured concentrations produced a higher bias than the concentrations determined from the calibration method. The method of standard additions provided a mean concentration of 50 ± 9 μg/g with 18 % RSD. These results suggest that there is a negligible difference in the precision as well as no gain in the accuracy of this technique by performing standard additions on the soil samples. Thus, it appears that calibration using aqueous standards is appropriate for the measurement of Cd in soil.

Conclusions

This novel TV-CMP-AES technique employing a tungsten cup is capable of determining elements at trace levels. Picogram quantities of Ca, Cd, K, Mg, Na, Pb, and Zn were detected with less than 10 % relative standard deviation. Either plasma shape, cylindrical or spherical, was effective for the sensitive detection of these elements. Both plasma types produced similar trends for most of the experimental parameters studied. The optimal plasma conditions for this group of elements in a CMP did not vary widely, and therefore compromised conditions which are required for simultaneous multielement analysis can be easily obtained. The electrode design proved to be a critical factor for this technique in terms of its potential for influencing the atomization and thus temporal behavior of the analyte. It seems that improvement in the cup design would further enhance detection limits for elements, such as Sn, which require high temperatures for

Table 4-4
Determination of Cd by the method of standard additions

Trial	Measured concentration (µg/g)	Bias
1	55 ± 3	31 %
2	56 ± 4	34 %
3	40 ± 0.7	-4 %
average concentration	50 ± 9	20 %

their vaporization. TV-CMP-AES compared quite favorably with analogous methods for microsample trace metal analysis. In addition, the determination of Cd in a standard reference material by this technique demonstrated only a 4 % relative error with 18 % RSD.

CHAPTER 5
DIRECT DETERMINATION OF CADMIUM IN SOLIDS

Introduction

The direct analysis of solids is important for several reasons. Because many samples occur naturally in solid form, pretreatment is usually needed to convert the sample to a liquid for analysis. Dissolution of the solid prior to analysis is time consuming and requires the use of hazardous chemicals. Contamination from the added reagents can occur [164]. Dilution errors and sample transfer losses arising from sample handling steps are possible and can lead to poor detection limits [137]. Also, some digestion procedures may result in loss of some volatile elements [165]. In addition, the resultant solution can contain a high salt content with the potential for clogging nebulizers [57]. The plasma performance as an excitation and atomization source can be degraded from the introduction of the solvent [58]. These problems can be avoided by the direct analysis of solids as this would allow the sample to be analyzed in its natural state [137]. However, direct introduction of solids into plasmas does suffer from some disadvantages. Poorer precision is observed than with solution nebulization techniques [117]. Sample heterogeneity becomes more of a concern due to the small sample sizes required of this method [137]. Furthermore, calibration curves are more difficult to determine as compared to solution analysis where aqueous standards are used directly [138]. Even so, direct analysis of solids offers a means of rapidly quantifying the elemental content of a sample before it is subjected to extensive pretreatment.

Several methods have been used for the direct introduction of solids into an ICP. These include direct sample insertion [125,137,146], electrothermal vaporization [131,132,138], arcs [166], sparks [167], laser ablation [137], and slurry nebulization [168]. However, these techniques have some difficulties. In DSI-ICP, background shifts can occur upon probe insertion, as well as imprecise sample insertion [137]. ETV-ICP suffers from sample losses in.transport of the analyte to the plasma [131]. Arcs and sparks require the samples to be conductive. Thus, matrix additives are sometimes necessary [137]. Laser ablation is limited by the nonavailability of suitable solid standards for calibration [137]. These problems can be alleviated by performing direct solid introduction into a CMP. The CMP allows for the analysis of an analyte *in situ* as the plasma forms directly around the sample.

Until recently, no work had been reported on methods of direct solid sampling without employing some means of analyte vapor transport for microwave plasmas. Ali and coworkers [57] developed a method for the rapid screening of solids using a CMP. The solid powder samples were deposited into a graphite cup electrode and then the electrode was heated to initiate vaporization and atomization of the analyte. This method was evaluated using samples of tomato leaves (SRM 1573a) and coal fly ash (SRM 1633a). Limits of detection were observed in the nanogram range.

Masamba *et al.* [58] used this same technique for the direct analysis of steel samples. Metal samples are conducting, easily machined into different shapes, resistant to sputtering, and relatively homogeneous. For these reasons, metals are amenable to direct analysis. The steel samples were machined into cylinders which could fit snugly into the top of a hollow graphite holder. Power was supplied to the holder to create a plasma for vaporization and atomization of the analyte. Detection of constituents in steel was possible from less than 1 µg/g to the percent range.

In this work, a CMP with a tungsten cup was used for the analysis of Cd. Samples of graphite powder, to which Cd had been added, and a variety of standard reference materials were evaluated. A mixture of helium and hydrogen was used as the plasma gas. The effects of experimental parameters were examined. The detection limit for solid Cd was in the picogram range. The results were compared to those previously obtained for Cd in solution. The accuracy and precision of this method of direct analysis were also investigated.

Experimental

Sample Preparation

The Cd solid standards used for analysis were prepared from cadmium chloride salt obtained from Fisher Scientific (Fairlawn, NJ). The salt was added to a 10 g quantity of high purity graphite powder (grade SP2X, lot 721, Union Carbide Corporation, New York, NY) and thoroughly mixed in plastic vials using a ball mill. This solid standard was quantitatively diluted with additional spectroscopic grade graphite powder to prepare the remaining concentrations. It should be mentioned that is was necessary to use coarse graphite powder for the standards as fine powder posed atomization difficulties.

The SRMs studied in this work were obtained from NIST. These solid samples included coal fly ash (1633a), tomato leaves (1573a), Montana soil (2711), bovine liver (1577b), and oyster tissue (1566a). No pretreatment or dilution steps were performed on these samples prior to analysis.

Procedure

The solid samples were deposited into the tungsten cup using a micropipettor (Drummond model 225, The Drummond Scientific Co., Broomall, PA) with glass capillary tips which was originally designed for liquid introduction. The pipettor was set to 1 μL and the end of the capillary was submerged into the solid sample. The pipettor was repeatedly moved back and forth until the tip was filled. Any sample adhering to the outside walls of the capillary was wiped off before deposition into the W cup. The amount of sample dispensed was determined by calibration. The calibration was performed by weighing 20 loads of the graphite standard with a microbalance. It was determined that for a 1 μL load, 0.6 mg of Cd solid in graphite was introduced with 8 % RSD.

Once deposited into the electrode cup, the sample was subjected to a preatomization step which used a low powered plasma to heat the sample. Preatomization was performed at a microwave power of 124 W for 20 s. After this step, the gas flow rates were set to the appropriate levels. The power was then rapidly increased to the atomization power, while simultaneously starting the computer for data acquisition. The emission signal was integrated for 1.0 s intervals for a 20 s time period. The electrode was again submerged 6 mm below the top of the torch as in earlier studies. The emission signal was observed at 5 mm above the electrode cup. All experimental parameters were optimized for the best signal-to-background ratios.

After each sample was analyzed, it was necessary to clean the electrode cup. This was accomplished using a laboratory-constructed "vacuum cleaner". A Pasteur pipette was connected to a side-arm flask with a rubber hose. The top of the flask was attached to a ceiling vent. The pipette was placed inside the W cup and the suction from the vent was used to remove any residue. This method proved quite satisfactory for sample removal as it was quick and easy to use.

Detection Limits

As previously indicated, peak heights were used in the analysis of the data. The peak height was obtained from the one scan of the 20 that were recorded which exhibited a maximum emission intensity. The peak height from this spectrum was subtracted from the signal obtained from a blank sample. The blank was graphite powder which had also been subjected to mixing with a ball mill. The signals were already background-corrected by the computer software. The calibration curve was performed using the optimal experimental conditions determined for solid Cd. The optimization studies for each parameter were performed individually while all other experimental conditions were held constant. The optimal conditions were defined as those which produced a maximum signal-to-background ratio. The detection limit was determined as 3 times the standard deviation in the blank [158]. The blank standard deviation was calculated from 10 measurements of the blank signal at the wavelength of Cd used, 228.802 nm. All signals are reported as the mean of 3 measurements with error bars representing one standard deviation from the mean.

Results and Discussion

Preatomization Stage

The preatomization stage was necessary for the analysis of the solid Cd samples by thermal vaporization introduction into the CMP. It served the purpose of heating the sample using a low powered plasma. It was found that elimination of this step produced an initial instability of the plasma which led to atomization difficulties. Also, the sample would sputter out of the electrode contributing to irreproducible signals. However, it was found that preatomization at high powers resulted in signal losses of Cd as shown in Figure 5-1. These losses were attributed to the volatile nature of this analyte. Similar results were found by previous researchers [51,57]. It was determined that a preatomization power of 124 W would suffice for solid Cd measurements.

Optimization of the duration of the preatomization stage was also necessary. The preatomization time is the difference between the time the plasma is ignited and the time when the power is increased for atomization. It was found that the Cd signal was relatively constant with increasing preatomization time up to 60 s (Figure 5-2). Again this was attributed to the volatile nature of the analyte.

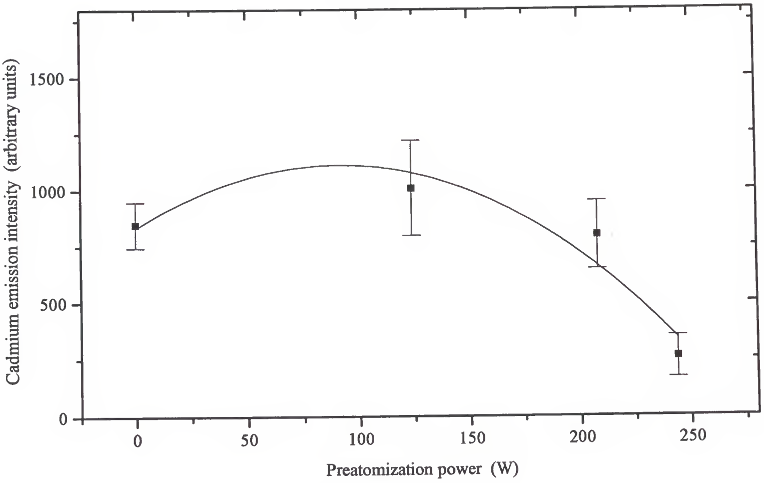

Figure 5-1. Effect of preatomization power on solid Cd signal.

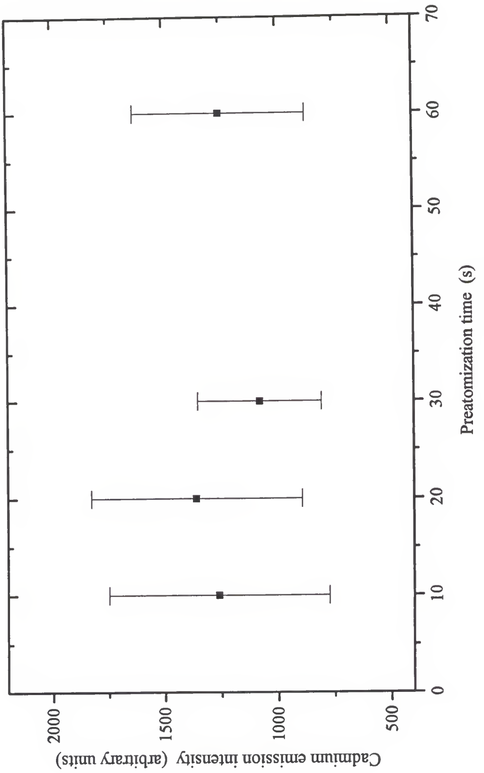

Figure 5-2. Effect of preatomization time on solid Cd signal.

Temporal Profile

The emission signals obtained were transient which is an inherent characteristic of the thermal vaporization technique. The temporal profile of 180 pg of Cd in graphite powder is displayed in Figure 5-3. The signal was obtained using the thin bottom 10 µL cup design. Recall that the electrode cup design was found to be critical to the atomization of the analyte and thereby influenced the temporal profile. For solid Cd, the signal lasted approximately 3 s in duration. These results were similar to those observed for aqueous Cd.

Electrode Position

The vertical distribution of the solid Cd emission is shown in Figure 5-4. The maximum signal-to-background ratio, and therefore optimal signal, was observed to occur at 5-6 mm observation height. This was attributed to the volatile nature of Cd and thus it was atomized in the lower region of the plasma. Similar to aqueous Cd, the background level increased in this region as well. In addition, the emission intensity began to decrease at observation heights greater than 7 mm.

The horizontal distribution of the solid Cd emission across the plasma was also examined. The cylindrical plasma used for the measurements produced a uniform emission intensity for solid Cd over a width of 1 mm (Figure 5-5). These results are similar to those obtained for cylindrical plasmas with aqueous analytes. The asymmetry of the distribution was caused by periodic fluctuations of the plasma.

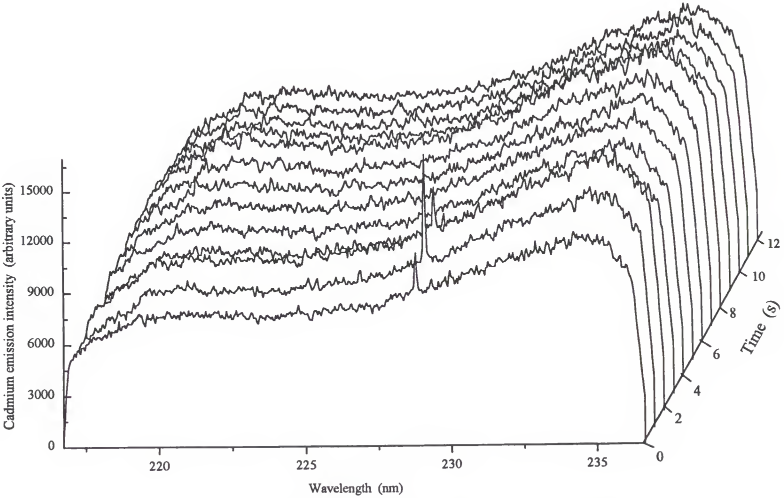

Figure 5-3. Temporal profile of 180 pg of Cd in graphite powder at 228.802 nm.

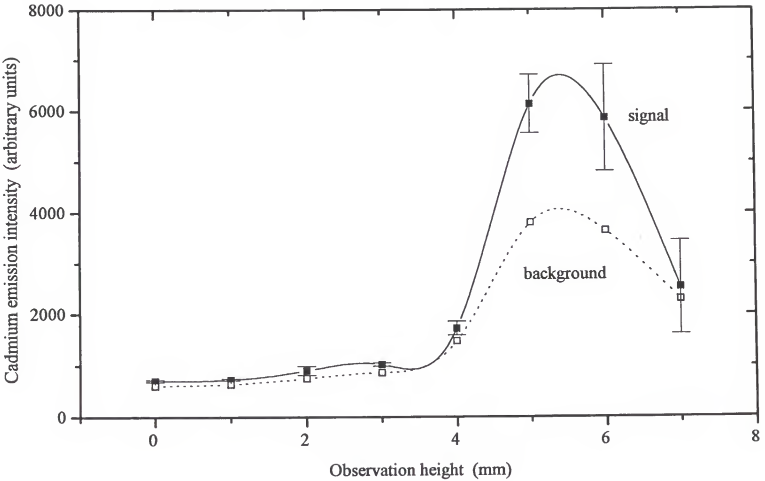

Figure 5-4. Vertical distribution of solid Cd signal and background.

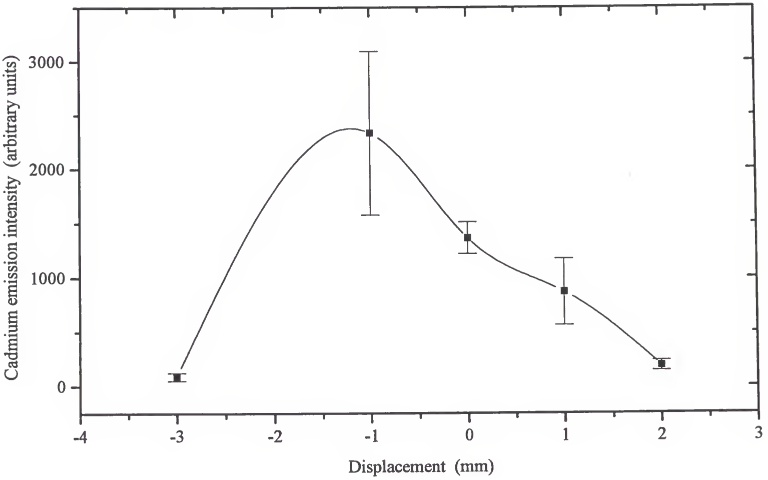

Figure 5-5. Horizontal distribution of solid Cd signal.

Atomization Power

The effect of atomization power on solid Cd emission intensity is shown in Figure 5-6. It was found that the emission intensity increased with increasing atomization power to a maximum. This maximum occurred when 800 W of power was supplied. Further increase in the atomization power led to a decrease in the intensity. These observations differ from those reported for aqueous Cd. The higher atomization power required here is probably due to the solid nature of the matrix.

Plasma Gas Flow Rate

The He flow rate did not have a significant effect on the solid Cd signal as depicted in Figure 5-7. However, the emission intensity did experience a two-fold increase at 7 L/min. The reason for this increase is unknown at this time. Further investigation of solids with a CMP needs to be performed before definite conclusions can be made. The plasma was observed to be cylindrical in shape at this flow rate. These findings are similar to those produced for aqueous Cd.

Similar to the analysis of solutions, hydrogen was added to the plasma gas for the determination of Cd in solids. Figure 5-8 shows that H_2 addition does have a significant effect on the emission intensity of solid Cd. The emission intensity was observed to be at a maximum, and therefore optimum, when a small amount of H_2 was introduced. The signal decreased upon increased hydrogen addition. As with the solution analyses, this effect was attributed to the decrease in the excitation temperature of the plasma with an increase in hydrogen addition [101].

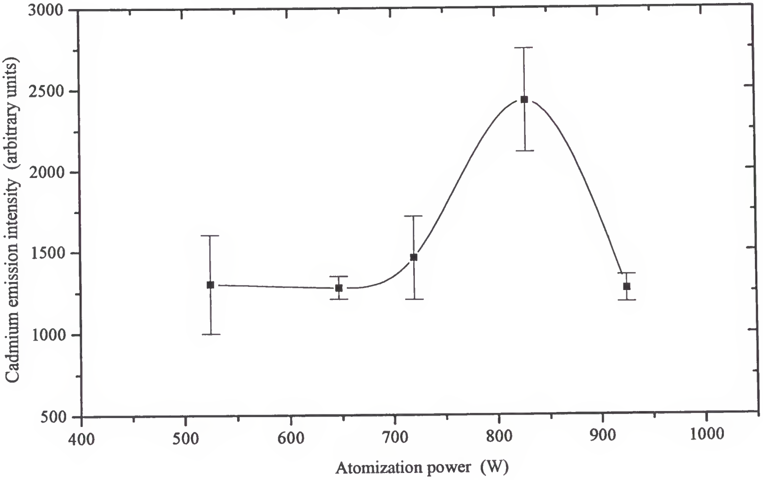

Figure 5-6. Effect of atomization power on solid Cd signal.

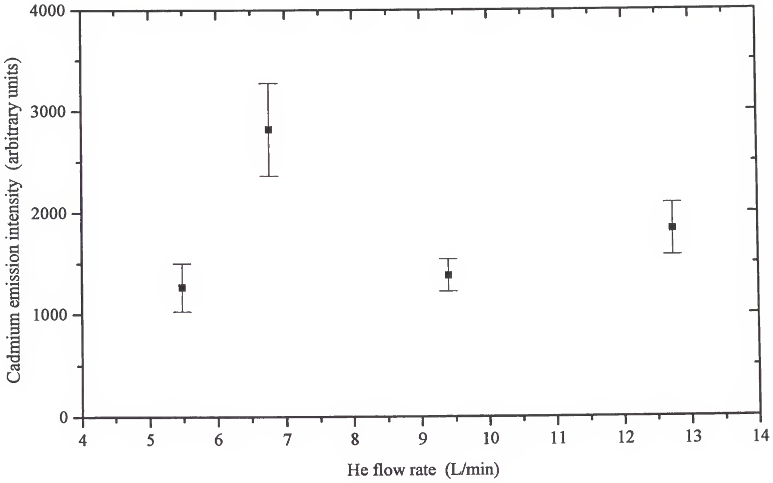

Figure 5-7. Effect of He gas flow rate on solid Cd signal.

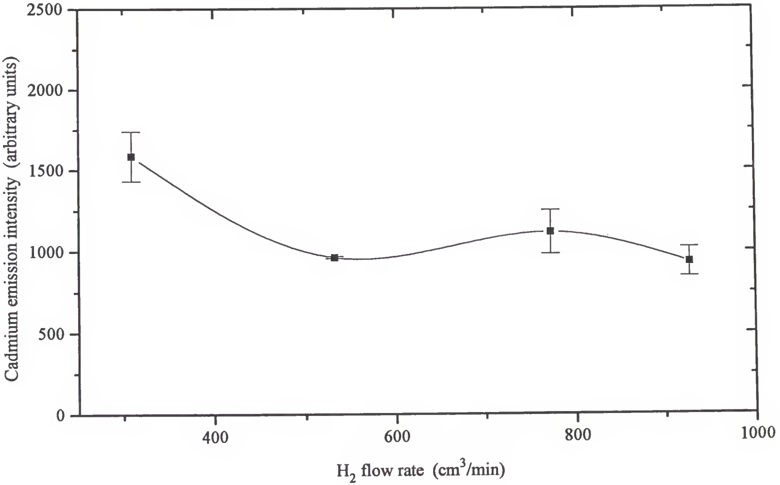

Figure 5-8. Effect of H_2 gas flow rate on solid Cd signal.

Trace Cd Determination

The operating conditions used for evaluating the analytical performance of TV-CMP-AES for solid Cd are based upon the optimization studies just described. The optimal conditions were selected as those which produced a maximum signal-to-background ratio while all other parameters were held constant. These conditions are provided in Table 5-1 and are compared to those selected for aqueous Cd. The conditions for both matrices were similar with the main difference being the atomization power required for analysis. The higher power necessary for the solid analyses is probably due to the nature of the matrix. The analytical curve for solid Cd (Figure 5-9) was linear and had a log-log slope of 1.0 over the region from the detection limit to at least 2 orders of magnitude higher. The detection limit obtained for solid Cd was 40 pg. This detection limit is also compared with those obtained for solid Cd by analogous methods [57,162] in Table 5-2.

When comparing the results obtained for Cd in both an aqueous and a solid matrix, many similarities are realized (Table 5-1). As previously mentioned, many of the operating conditions chosen to be optimal for Cd measurement closely agree. Likewise, the trends observed for most of the experimental parameters correspond. However, it was still discovered that the determination of Cd was not independent of the matrix studied. This is demonstrated by Figure 5-10 which shows a three-fold difference in the slopes of the calibration curves obtained for these matrices. This difference is largely a result of the dissimilar trend in the atomization power required for analysis. The solid matrix required a higher power for Cd measurement and above this power the emission intensity

Table 5-1
Comparison of optimal conditions selected for solid and aqueous Cd

Parameter	Solid	Aqueous
Wavelength (nm)	228.802	228.802
Observation height (mm)	5	4
Displacement (mm)	0	0
He flow rate (L/min)	7	5
H_2 flow rate (cm^3/min)	380	460
Preatomization/drying power (W)	124	90
Preatomization/drying time (s)	20	45
Atomization power (W)	828	525-630

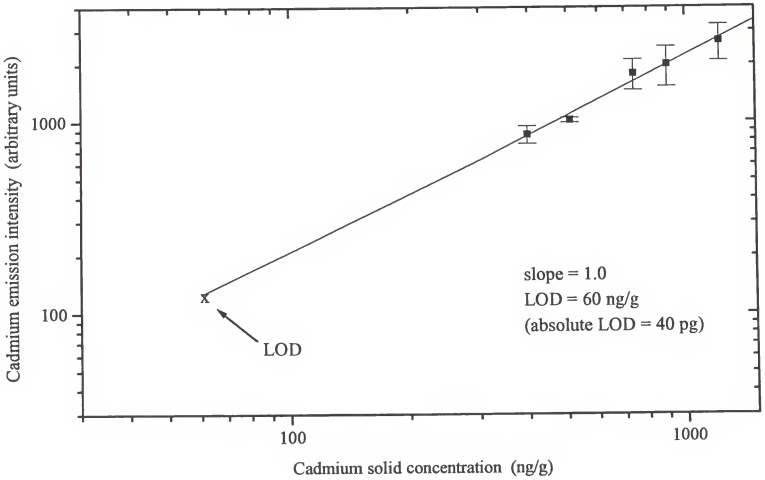

Figure 5-9. Log-log calibration curve for solid Cd.

Table 5-2
Comparison of detection limits for Cd

Technique	LOD (pg)
This work (solid)	40
This work (aqueous)	8
Graphite cup TV-CMP [57]	300
ETV-ICP [162]	50

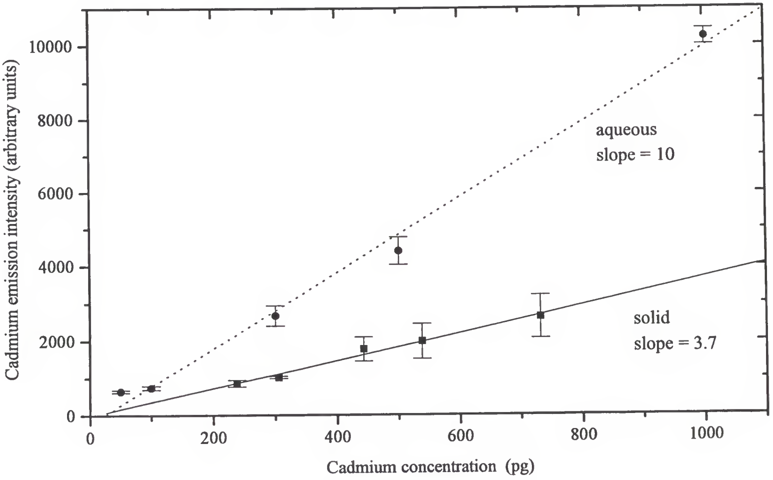

Figure 5-10. Comparison of Cd calibration curves in a solid and an aqueous matrix.

decreased. In an aqueous matrix, the atomization power increased to a maximum and then reached a steady state. Further studies of the behavior of solids in a CMP should be investigated before any more conclusions can be drawn.

Standard Reference Materials

The accuracy and precision of the method developed for the determination of Cd in solids using a CMP were examined. Analyses were performed using a variety of SRMs obtained from NIST without any prior sample preparation. The operating conditions used were those listed in Table 5-1. The results observed for Cd measurement are displayed in Table 5-3 as they compare to the certified concentrations provided by NIST. The listed concentration ranges are one standard deviation of the mean of three measurements. These values were obtained based upon the calibration of Cd in graphite powder. The observed concentrations closely agree with the certified values for each of the SRMs Montana soil, tomato leaves, and bovine liver showing less than 20 % bias. The results obtained for oyster tissue and coal fly ash produced large discrepancies from the accepted concentrations. The exact reason for this is not known at this time, but the inhomogeneity of the solid samples and the use of calibration by a different solid matrix may have contributed to the large bias. The accuracy may possibly be improved by performing the calibration by the method of standard additions, thus eliminating any errors caused by matrix effects. Even so, the precision of the measurements was less than 20 % in most instances.

Table 5-3
Determination of Cd in solid SRMs

Sample	SRM	Measured concentration (μg/g)	Certified concentration (μg/g)	Bias
Montana soil	2711	38 ± 11	41.70 ± 0.25	-9 %
Tomato leaves	1573a	1.4 ± 0.4	1.52 ± 0.04	-8 %
Bovine liver	1577b	0.6 ± 0.3	0.50 ± 0.03	20 %
Oyster tissue	1566a	1 ± 0.5	4.15	-76 %
Coal fly ash	1633a	2 ± 0.6	1.00	90 %

Conclusions

The method developed for the determination of Cd in solid samples using TV-CMP-AES is capable of measurement at trace levels. A detection limit of 40 pg was possible with less than 30 % RSD. Experimental conditions were found to agree closely with those obtained for the analysis of Cd in aqueous solution. The main difference in operating conditions between these two matrices was the atomization power, which at this time, makes the current method matrix dependent. Even so, this technique provided reasonable accuracy when applied to solid standard reference materials and compared favorably with other atomic methods of analysis. In addition, this preliminary investigation demonstrates the promise of TV-CMP for the direct analysis of solid samples.

CHAPTER 6
SIMULTANEOUS MULTIELEMENT ANALYSIS

Introduction

The time and cost of single element analysis can be quite prohibitive. Therefore, simultaneous multielement analysis (SMA) is preferred as it saves time and reduces sample consumption. Atomic emission spectrometry has proven to be the method of choice for SMA in all sample types [1]. It has the potential for rapid analyses of most elemental constituents and inherently has a high multielement capability [128]. As a result, atomic absorption methods, which are fundamentally single-element techniques, have lost their attractiveness [128] and are not readily used for SMA.

Ideally, techniques employed for simultaneous multielement analysis should satisfy a wide variety of requirements [3]. They should be applicable to all elements with detection at major, minor, trace, and ultratrace levels without changing the operating conditions. These methods should not experience inter-element interference effects. Also, they should be able to handle microsamples and be able to achieve acceptable precision and accuracy. Techniques used for SMA should be capable of analysis of liquids, solids, and gases with minimal preliminary sample preparation. In addition, they should be portable, nondestructive, and rapid. Finally, it would be ideal if these methods were commercially available and amenable to process control. As indicated previously in chapter 1, AES methods come close to fulfilling a large majority of these ideal requirements. As a result, AES has become the standard for SMA [169].

SMA is usually approached by considering the various parameters that affect the optimization of each element to be studied. The optimal parameters for each element can be compromised in exchange for a common set of operating conditions that will provide the best possible limits of detection for all the elements, an extended linear dynamic range, and freedom from interferences [170]. Although these compromised conditions may result in some losses in detection power for individual elements, there is a gain in the number of elements that can be determined simultaneously.

Because of the usefulness of SMA, it has been extensively investigated. SMA has been incorporated into elemental analyses involving both MIP and ICP emission techniques. Fricke *et al.* demonstrated the potential of SMA with an MIP using a carbon cup sampler and a multichannel spectrometer [140]. Mulligan and coworkers performed SMA using hydride generation with several different MIP cavities and obtained ppb detection limits [171]. A helium MIP using ETV sample introduction was used for the SMA of Cd, Fe, Au, Pb, and Mn reaching pg levels of detection [172]. Also, SMA has been used for the analysis of solids with a helium MIP obtaining an accuracy of 10 % [173]. Compromised conditions were first realized for SMA with an ICP source by Boumans and de Boer [174]. This research balanced the detection power and interferences of 32 elements and obtained better than 1 ppb detection limits for 27 of these elements with high precision. SMA of microsamples has been accomplished with

ETV-ICP [142] and with direct sample insertion ICP [175]. Uchida *et al.* employed SMA with ICP-AES for the analyses of both whole blood and serum [176].

Over the years, SMA has even been extended to atomic absorption techniques. Tong and Chin studied GFAAS using a PDA and several multielement hollow cathode lamps [177]. Harnly and coworkers [178] developed a simultaneous multielement atomic absorption continuum source (SIMAAC) spectrometer capable of detection of up to 16 elements simultaneously with either flame or furnace atomization. SIMAAC combines a high intensity continuum source, a high resolution echelle polychromator containing numerous PMTs, wavelength modulation, and a high speed computer data acquisition system in order to achieve LODs comparable to line source AAS. However, this approach suffered from poor detection at wavelengths below 280 nm and from the use of complex computer programs [179]. Smith and Harnly applied SMA to GFAAS with a continuum source using a linear photodiode array detector [180]. This design offered improved signal-to-noise ratios over the PMTs, used previously, at wavelengths below 280 nm. In addition, SMA by GFAAS has also been accomplished using an echelle spectrometer in conjunction with line sources [169]. This allowed for the detection of up to 4 elements simultaneously at pg levels.

Although SMA has been readily examined with various techniques, it has yet to be applied to a CMP emission source. Thus, this research provides the first documented examination of SMA performed using a CMP-AES system. As shown in previous chapters, compromised conditions for a variety of elements can easily be realized using the CMP as an atomic emission source. The work to follow will focus on the evaluation of the suitability of the CMP to simultaneous multielement analysis.

Instrumentation

As the popularity of SMA increases, it is necessary to develop instrumentation that is compatible with this type of analysis. Traditionally, AES is performed using a slew scan instrument [157]. However, the slew scan instrument, which can only observe one wavelength at a time, has a speed disadvantage when a number of elements are to be determined [181]. Although a photomultiplier tube is also commonly used with AES, it is inherently a single-channeled detector [182]. In order to monitor several lines simultaneously, a PMT needs to be dedicated to each spectral line. Unfortunately, this configuration is not very flexible, since the movement of the PMTs to alternative wavelengths is not easily implemented. Thus, multichannel detectors are more convenient for SMA. The PDA detector may be used for SMA, but it suffers from the limitation of a small spectral range imposed by the number of diodes contained in the array. Therefore, while possessing high spectral resolution, the narrow wavelength coverage of the PDA is not sufficient for the determination of a large number of elements simultaneously [181]. Consequently, two-dimensional detectors appear to be ideal for SMA. This is because they possess formats large enough to supply the number of resolution elements required for AES, as well as a sensitivity and dynamic range equal to that of a PMT [183]. In addition, an echelle spectrometer with its two-dimensional pattern, is a suitable match for this type of detector [184]. Recently, Pilon *et al.*

developed a charge-injection device (CID)/echelle spectrometer for SMA using an ICP source [181]. In this case, 15 elements were determined using 31 spectral lines to achieve ppb detection limits. Since the CID/echelle spectrometer will allow for the simultaneous acquisition of all spectral information over a wide wavelength range with adequate resolution [182], it was selected and subsequently used as the detector for SMA with the CMP in this research.

Charge-injection Devices

The CID is a solid-state silicon detector with a two-dimensional array structure of pixels. Each pixel consists of a series of metal oxide semiconductor (MOS) capacitors [185]. A MOS capacitor is composed of several key elements: a conductive gate electrode, an insulator, an epitaxy, and a substrate. The insulator, which contains a layer of both silicon dioxide and silicon nitride, separates the electrodes from the n-doped Si region referred to as the epitaxy [186]. The epitaxy is the photoactive portion of the CID. The p-type substrate, which lies beneath the epitaxy, serves as the common electrical contact. It aids in collecting the charge and also in conducting the charge away when it is cleared from the pixel. Two gate electrodes are used in the pixel configuration [185]; one to collect the charge (collection gate) and the other to sense the amount of charge that is collected (sense gate). Each gate is made from highly doped polycrystalline silicon. A metal contact is attached to the gate in order to connect it to an external source of electrical potential. Each electrode is insulated from the other with oxide. The sense gates are usually strapped with a narrow aluminum stripe in order to decrease resistance

[186]. The intersection of a collection gate with a sense gate defines a pixel [186]. Each pixel is surrounded by highly doped oxide in order to prevent charge migration. A cross sectional view of the MOS capacitor structure within a pixel contained inside a CID device is illustrated in Figure 6-1.

The operation of a CID is based on the migration of charge. Each of the gate electrodes in a pixel are initially negatively biased. However, the collection gate has approximately double the applied potential than that of the sense gate [186]. Once the electrodes are biased, a charge inversion is created under the collection gate at the insulator interface which mainly favors the storage of "holes" or positive charge carriers. The impingement of photons onto the pixel will cause electron and hole formation. The "holes" will migrate and accumulate within this inversion region. The positive charge collected is proportional to the amount of light striking the pixel [183]. In order to read the accumulated charge, the potential to the sense gate is disconnected and then measured. The charge is now shifted to the sense gate by altering the potential applied at the collection gate. The movement of the charge to the sense gate results in a proportional change in the sense gate potential [185]. The sense gate potential is again measured. This measurement is subtracted from the original value to obtain the total potential change which may then be related to the quantity of collected charge. Once measured, the charge can be restored by returning the collection gate to its negative value. The charge may also be cleared from the pixel by biasing both gates near ground potential. The charge will then spread into the p-type substrate where it is conducted away.

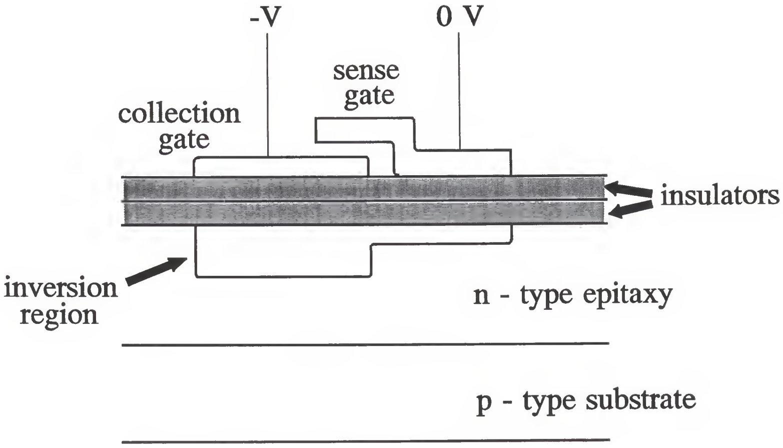

Figure 6-1. Cross sectional view of a MOS capacitor structure in a pixel.

CIDs have many unique features. The CID is found to exhibit a negligible dark current when appropriately cooled [183]. It has precise background correction capabilities [187]. The CID device is also highly resistant to the phenomenon of charge blooming [183,184,186,187]. Blooming occurs when excess charge spills into adjacent pixels, and thereby obscures the true measure of the spectral lines of interest. This can lead to the distortion of a weak, as well as an intense spectral feature since the charge spillage can not be quantitated. A high quantum efficiency, particularly within the ultraviolet region, is also characteristic of a CID device [184]. In addition, CIDs tend to have wide dynamic ranges that may span as many as 8 orders of magnitude [187]. The dynamic range is large due to the random access integration (RAI) feature inherent only to a CID [185,187]. This capability permits the detector to randomly access, and, thus, measure any pixel without disturbing the continual accumulation of charge. RAI involves the variation of the exposure time allowed for charge collection by an individual pixel that is associated with a specific spectral line. Each pixel dedicated to a spectral line is exposed until a predetermined threshold value for the signal-to-noise ratio is reached. Therefore, weak lines can be integrated for long periods, while intense lines undergo short integration during the course of a single exposure to the source. This process is continued until all the spectral lines of interest have been detected within an allotted exposure time to the source. Due to this intrinsic ability, subarrays of the CID may be used for detection, resulting in less unnecessary data being acquired [188]. Finally, a CID is capable of nondestructive readout [183,187,188]. This unique feature enables the charge in a particular pixel to be measured multiple times without any resultant signal losses.

This is made possible since the CID design does not require the charge to be removed from the pixel where it is generated during the readout process. This characteristic helps to decrease the noise. However, the CID does suffer from high readout noise [186] and in some instances, the camera speed can inhibit the number of elements that can be determined simultaneously [187]. Also, the CID is not optimally configured for many current spectroscopic systems because of the small size of the detector elements [185].

Echelle Spectrometers

An echelle spectrometer is a perfect match for an array detector such as a CID [184,188]. It makes efficient use of the two-dimensional format of the CID, therefore allowing coverage of the ultraviolet and visible spectral regions with high resolution. An echelle spectrometer is primarily composed of two essential features. It contains a prism and an echelle grating. The quartz prism, which is the refractive element, serves as a cross disperser in order to separate grating orders [184]. The echelle grating, which is blazed at all wavelengths [169], is designed to disperse light to a large extent in order to obtain high resolution [189]. This grating makes use of an increase in the blaze angle and the order, rather than a large number of grooves and a long focal length, which is typical of other gratings [190]. Thus, by using blaze angles greater than 45 degrees and higher orders, a higher dispersion and resolution are achieved than with conventional spectrometers. As a result, an echelle spectrometer attains the spectral resolution desired for AES.

An echelle spectrometer has several advantages which make it well suited for SMA by atomic emission spectrometry. In comparison to conventional spectrometers, the echelle spectrometer has better than one order of magnitude higher resolution, as well as dispersion, without sacrificing optical speed [190]. The echelle spectrometer is capable of use over a wide spectral range. Lower limits of detection and greater selectivity in AES result due to the decrease in spectral background [190]. Therefore, an echelle spectrometer allows discrimination of the spectral line from the background making it highly compatible with the high temperature and high background characteristics of plasma sources [190]. However, the echelle spectrometer does suffer from low light throughput or luminosity due to its limited slit height [190]. Also, high levels of stray light pose difficulties by contributing to a reduction in the linear dynamic range [189]. In order to alleviate this disadvantage, the echelle spectrometer has been combined with a CID. Perhaps the greatest advantage of this detection system is that it has the flexibility to rapidly choose and simultaneously monitor many regions of the spectrum [187]. Thus, the CID/echelle spectrometer is becoming a powerful detection system for SMA.

Recently, a commercial CID/echelle spectrometer has been developed by Thermo Jarrell Ash (TJA) [181]. The basic design of this detection instrument is illustrated in Figure 6-2. In this configuration, the optical range extends from 170 to 800 nm with improved light-gathering efficiency over other designs of its kind. Also, the quantum efficiency in the ultraviolet is enhanced by the application of a wavelength-conversion phosphor [188]. This optical system operates with only a single pass through the prism to the echelle grating. The light, once dispersed, is focussed on the CID array detector

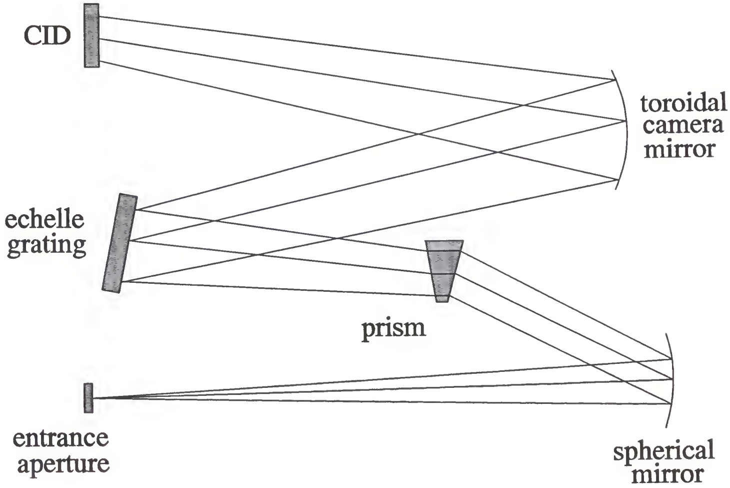

Figure 6-2. Design of a TJA CID/echelle spectrometer.

with a toroidal camera mirror. This particular optical arrangement decreases the amount of stray light by reducing the number of surfaces, and thus improves the light throughput of the spectrometer [181].

Experimental

Sample Preparation

Both solid and liquid samples were examined by SMA using the CMP emission source. A small gold chip of unknown purity was used for the solid analyses. Aqueous standards of cadmium (1003 μg/mL) and zinc (1000 μg/mL) were obtained from Inorganic Ventures Inc. (Toms River, NJ). The aqueous magnesium (1000 μg/mL) and lead (1000 μg/mL) standards were obtained from Fisher Scientific (Fairlawn, NJ). Water from a Milli-Q Plus water system (Millipore Corporation, Bedford, MA) was used to prepare all subsequent dilutions and mixtures. The 29 element standard mixture was obtained from SPEX Industries Inc. (Edison, NJ) and was diluted in 5 % nitric acid. It was composed of 10 μg/mL of each of the following: Ag, Al, As, Ba, Be, Bi, Ca, Cd, Co, Cr, Cs, Cu, Fe, Ga, In, K, Li, Mg, Mn, Na, Ni, Pb, Rb, Se, Sr, Tl, V, U, and Zn.

Apparatus

The SMA work in this chapter was performed in the laboratory of Thermo Jarrell Ash in Franklin, MA. The CMP source used was built in our laboratory and shipped to the TJA lab. It was a prototype of the CMP emission source described in the previous chapters. The high voltage power supply and the filament transformer were shipped to MA as well.

The detection system used with the CMP was the CID/echelle spectrometer introduced by Thermo Jarrell Ash referred to as the IRIS. This f/10 spectrometer has a focal length of 381 mm. The entrance aperture is a 50 μm square. The prism is fabricated from fused silica and is positioned at 17.5 degrees. The echelle grating contains 52.6 grooves/mm with a blaze angle of 61.6 degrees. The IRIS has a reciprocal linear dispersion of 0.14 nm/mm at 200 nm and 0.28 nm/mm at 400 nm. The spectral range used for these experiments was 170 to 330 nm. The CID is comprised of a 512 x 512 array of 25 μm square pixels. The CID is operated at -87 °C.

Procedure

The procedure used for the SMA work was similar to that described previously with several modifications. The detection system was calibrated for accurate peak identification using an internal Hg lamp. Another Hg pen lamp was placed in the tungsten cup position in order to check the vertical and horizontal alignment of the electrode. Carbon was used as an internal standard for monitoring the emission signal intensities and plasma behavior. Any changes observed in the 247.856 nm C line served as a crude indication of optimization difficulties. All measurements were taken during a single 60 s exposure to the CMP source employing the RAI feature. This feature allowed the individual elements to be measured at an appropriate integration time within this one exposure. A set of compromised conditions was selected for all measurements based upon the previous work and is listed in Table 6-1. Any deviations from these conditions are noted where appropriate. The 10 μL capacity cup with the thin bottom surface was used for this work. This is the same electrode that was employed for the Pb, Sn, Na, K, Ca, and solid Cd experiments.

Data Analysis

The data was acquired using ThermoSPEC software which was supplied with the TJA IRIS. This software is also capable of identifying the elemental lines of the analytes of interest. It comes equipped with a mapping library of all the representative lines for each of the elements which was calibrated prior to instrument installation. However, it can only display the emission lines for 7 elements at a time. The data was further handled by M. Bonner Denton's group of the Department of Chemistry at the University of Arizona in Tuscon. They utilized an in-house program which allowed the data read from the CID to be converted into a format amenable for plotting. All plots were subsequently generated using Spyglass Transform software.

Results and Discussion

The CMP was set up prior to my arrival at the TJA laboratory so as to closely model the system used in the Winefordner laboratory in Florida. It was interfaced to the CID/echelle spectrometer manufactured by TJA. The experimental parameters were appropriately optimized to the set of compromised conditions listed in Table 6-1. The electrode was carefully aligned with a Hg pen lamp to the desired position. The achromat

Table 6-1
Compromised conditions for simultaneous multielement analysis

Parameter	Condition Used
Wavelength (nm)	170-330
Sample size (μL)	10
Exposure time (s)	60
Depth of electrode in torch (mm)	6
Observation height (mm)	4
Displacement (mm)	0
Drying time (s)	45
Drying power (W)	75
Atomization power (W)	999
He flow rate (L/min)	7
H_2 flow rate (cm^3/min)	546

located directly behind the entrance slit of the detector was precisely rotated until the signal intensity for the 247.856 nm C atomic line was at a maximum. It was discovered that this line served as a useful indication of the plasma behavior, electrode positioning, and electrode deterioration. Any fluctuation in the C signal suggested the plasma was not centered correctly on the electrode or that the electrode was worn and needed replacement. Therefore, it was closely monitored throughout the course of the studies to follow.

Upon completion of the initial alignment, several elements were examined. Cd, Mg, Pb, and Zn were individually analyzed at 10 mg/L concentrations to demonstrate the feasibility of the marriage of the CMP with the CID/echelle spectrometer. The 214.438, 226.502, and 228.802 nm emission lines of Cd were successfully detected at 665 W. Zinc was atomized at 600 W and the major emission lines of 202.548, 206.200, and 213.856 nm were observed. At an operating power of 700 W, the 279.553, 280.270, and 285.213 nm lines confirmed the detection of Mg. In fact, Pb was detected as well by the presence of the 220.353, 280.199, and 283.306 nm emission lines. It should be mentioned that the most intense line of Pb, 405.783 nm, could not be utilized in these experiments as this line was outside the spectral range currently employed by the CID detector. Also, it was discovered that the coaxial waveguide produced interferences at the high powers needed for the analysis of Pb, and consequently, the power selected for SMA. Since, the coaxial waveguide , which surrounds the torch (Figure 3-1), was made from brass, it was believed to contribute emission from Zn, Cu, and possibly Pb constituents. In some cases, these elements have emission lines which overlap or which are not easily resolved from the elements being studied. Thus, it is recommended that in the future this component be constructed from one pure metal, such as Al, Ag, or Cu, so as not to interfere with the analytes of interest.

Upon further investigation into these elements, it was realized that there was little or no background emission detected. There was no evidence of any He or H_2 emission lines within this spectral range in any of the spectra recorded. Only the presence of C was detected and this proved to be quite helpful as previously mentioned. Preliminary signal-to-noise ratios were determined for Cd, Mg, Pb, and Zn at a concentration of 10 mg/L using a representative peak for each element. These estimated values are provided in Table 6-2. The peaks for each of these elements were quite narrow in shape and well separated from the background. Examples of these peaks, which correspond to a strong emission line for each element, are presented in Figures 6-3 through 6-6.

Based on these initial experiments, some figures of merit for these elements could be predicted. The limits of detection for both Cd and Zn were roughly estimated at 70 and 90 pg respectively. In addition, it was observed that the signals obtained for these elements were reproducible. A linear dynamic range can not be reported at this time, as linearity studies were not extensively performed. Although, it may be noted that over the small concentration range evaluated, Mg demonstrated satisfactory correlation with a correlation coefficient of 0.99. A preliminary calibration curve is depicted in Figure 6-7.

Time gated studies were also performed. The elements of interest were investigated in order to determine the optimal integration times required for analysis. It was found that by changing the integration time allotted for a particular element within

Table 6-2
Estimated signal-to-noise ratios

Element	Wavelength (nm)	Signal	Noise	S/N
Cd	228.802	96.0	2.757	34.82
Mg	279.553	110.0	2.807	39.19
Pb	283.306	82.0	2.173	37.74
Zn	213.856	687.0	1.90	361.6

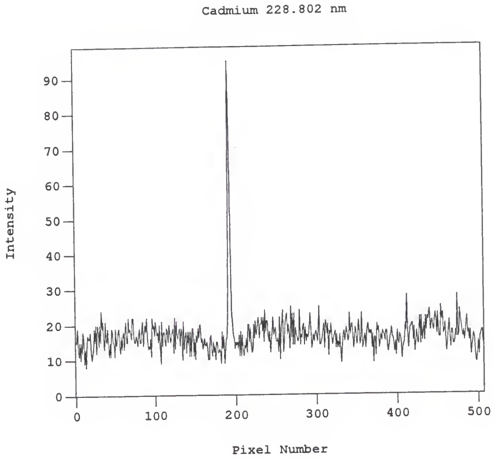

Figure 6-3. Representative peak of 10 mg/L Cd.

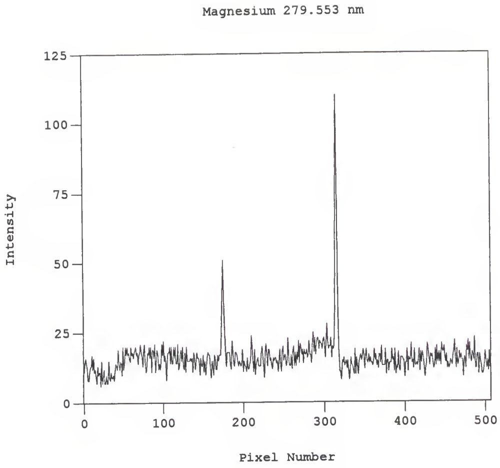

Figure 6-4. Representative peak of 10 mg/L Mg.

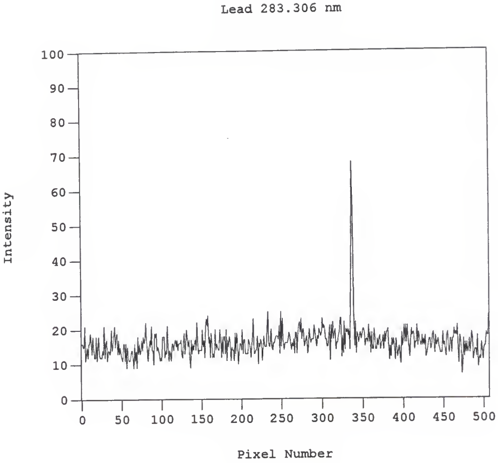

Figure 6-5. Representative peak of 10 mg/L Pb.

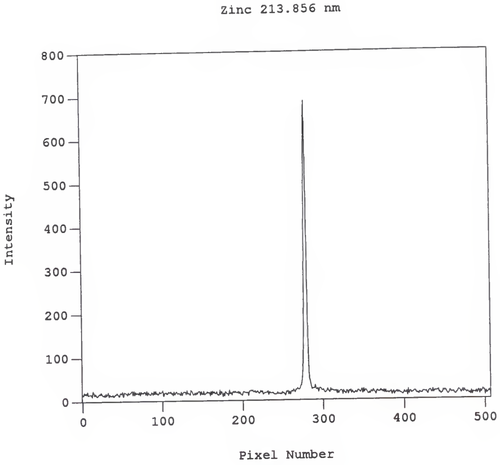

Figure 6-6. Representative peak of 10 mg/L Zn.

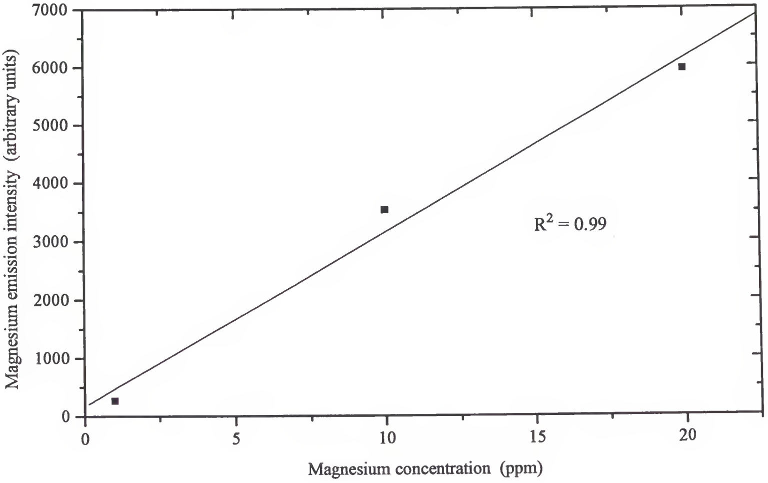

Figure 6-7. Preliminary calibration curve for Mg using the TJA spectrometer.

a single exposure to the CMP source, the emission intensities also changed. Thus, it was possible to alter the integration time for the elements individually, so as to maximize the emission signals produced for each analyte. This would allow for the best possible transient signal to be obtained from each element. Hence, the elements that do not require long integration times will not suffer a loss in intensity due to overexposure. However, it was discovered that contrary to previous results, all the elements studied were completely atomized and excited within 15 s at 999 W of power. It was believed that this may have been the result of subtle differences between the CMP used here and the original CMP used for the developmental research conducted in Florida.

Once all the preparatory studies had been completed, the suitability of the CMP for SMA was evaluated. Both a multielement solid and liquid sample were introduced into the CMP for their subsequent detection. A small gold chip of undetermined weight was placed in the tungsten cup for analysis. The results are displayed in the form of the CID image produced by the TJA spectrometer in Figure 6-8. The intensity of each pixel is depicted by its brightness on the plot. Each peak of a given element is represented by a small array of adjacent pixels. Actual intensity values are available for the irradiated pixels. The software allowed for the identification of all the elemental lines within the displayed data by color coded boxes. Therefore, the existence of the element in the sample is indicated when its corresponding boxes are illuminated. In the case of the Au chip, it was observed that Au, Ag, and Cu were present. This was confirmed by the detection of the 201.200, 242.795, and 267.595 nm lines of Au, the 328.068 and 338.289 nm lines of Ag, and the numerous emission lines of Cu. It should be mentioned that not

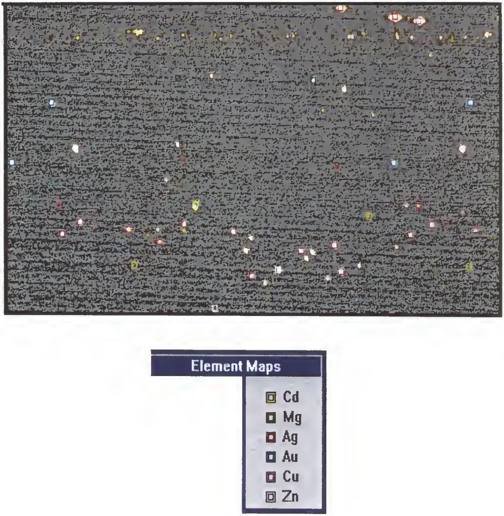

Figure 6-8. CID image of a Au chip.

every line of each of the elements was detected. This is a result of the quantity of the analyte present in the sample, as well as the compromised conditions that were used. Therefore, some of the weaker emission lines may not have been observed. In addition, Cd, Mg, and Zn were detected in the Au chip. However, this is believed to be residual signal from previous high concentration injections of these elements. A 29 element standard solution was also examined and the resultant CID image is illustrated in Figure 6-9. Eleven elements were detected within the spectral range employed. These included Ag, As, Cd, trace amounts of Cr, Cu, trace quantities of Fe, Mg, Mn, Pb, Se, and Zn. It should be noted that not all the elements that were detected are indicated in the image since the software only allowed a maximum of 7 elements to be mapped simultaneously. Also, only some of the elemental lines are displayed as they could not all fit on a single screen with the TJA software.

Conclusions

The feasibility of the marriage of the CMP source with the CID/echelle spectrometer has been demonstrated. It was found that this technique was capable of the detection of a wide variety of elements. Minimal background emission was observed. The signal-to-noise ratios were estimated and appeared to be quite high. All peaks had a narrow shape and were easily resolved from the background. Preliminary approximations of the limits of detection for Cd and Zn were 70 and 90 pg respectively with very minor optimization during a 3 day time period. This corresponds well with the 8 pg detection limit for Cd and the 20 pg detection limit for Zn obtained previously after

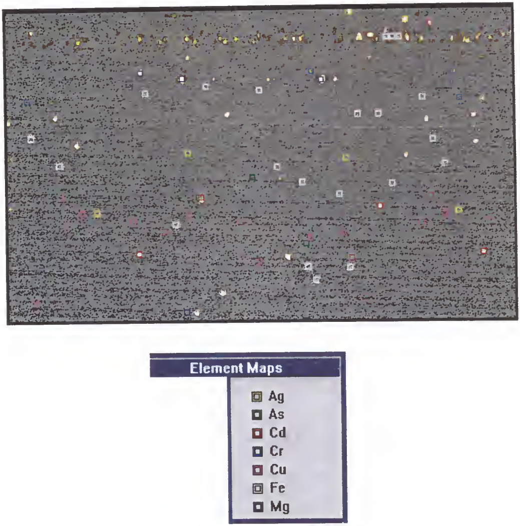

Figure 6-9. CID image of a 29 element aqueous standard.

an extensive optimization period was conducted. These initial experiments also indicate linearity for Mg over the concentration range studied. Finally, it was established that SMA is in fact possible with a CMP source when employing a CID/echelle spectrometer for detection. These initial results show promise that the CMP is capable of simultaneous multielement analysis of both solid and liquid samples.

CHAPTER 7
CONCLUSIONS AND FUTURE WORK

This dissertation has described a method for the determination of metals in trace quantities using a capacitively coupled microwave plasma atomic emission spectrometer. A mixture of helium and hydrogen was used as the plasma gas. Both a spherical and cylindrical shaped plasma were formed depending on the gas flow rate and microwave power selected. A tungsten cup electrode capable of holding a volume of up to 30 μL was employed. It was found that the electrode design was critical to this technique in terms of influencing the atomization, and therefore, the temporal profile of the analytes. Several modifications to the electrode design were thus investigated. It was discovered that a shallow cup of a 10 μL capacity would be suitable. In addition, careful attention should be given to the dimensions of the cup wall thickness. The experimental parameters, such as gas flow rate, electrode position, and atomization power were also studied. Both plasma shapes produced similar trends for most of the parameters for each of the elements Ca, Cd, K, Mg, Na, Pb, and Zn. The behavior of the atomization power was the only parameter which varied significantly amongst the elements studied. This novel method proved capable of measuring these elements for three orders of magnitude down to the picogram level with better than 10 % RSD. Furthermore, the detection limits observed favorably compared to analogous techniques of trace metal analysis. The accuracy of this method was examined using standard reference materials. TV-CMP-AES was found to agree closely with the certified value of Cd in Montana soil.

This technique was extended to the analysis of solid samples as well. TV-CMP-AES is advantageous for the direct analysis of solids without any prior sample pretreatment. Solid standards of Cd in graphite powder were examined by this method and the results were compared with those obtained for Cd in aqueous solution. The conditions selected as optimal (those producing a maximum in the signal-to-background ratio while all other parameters are held constant) for Cd determination were similar in both the matrices studied. However, a comparison of the analytical curves for these two matrices demonstrated that, with the current method, Cd measurement was not independent of matrix. Even so, the detection limit of solid Cd was 40 pg which agreed with results reported in the literature for similar techniques. The accuracy of this method of direct solid analysis was studied using a variety of solid SRMs. Preliminary results showed close agreement for most of the samples. Improvement in Cd measurement may occur by performing the method of standard additions. Thus, TV-CMP-AES showed promise for the discrete sampling of both solutions and solids with minimal sample pretreatment.

Finally, this technique was evaluated for its applicability as an emission source for simultaneous multielement analysis. A prototype of this instrument was constructed and shipped to Thermo Jarrell Ash Corporation in MA. It was interfaced to a TJA CID/echelle spectrometer to test the suitability of this application. In the short duration that the studies were performed, preliminary results show that a CMP is compatible with this sophisticated detection system. In addition, satisfactory signal-to-noise ratios were obtained and all the peaks were baseline resolved. The detection limits of Cd and Zn were estimated to be 70 and 90 pg respectively. Lastly, simultaneous multielement analysis was able to be performed on both an aqueous standard mixture and a solid Au sample.

Future work with this instrument should include further improvement in the electrode cup design. It was found that the electrode design played a major role in the ability of the TV-CMP-AES system to vaporize and subsequently atomize the analyte of interest. A poor design led to atomization difficulties and memory effects. It is imperative to keep the electrode as a cup system so that both solids and solutions can be analyzed. Possible modifications include but are not limited to: decreasing the capacity of the cup to 5 μL, fabricating the electrode and holder from the same metal, coating the inside of the cup with Pt or tantalum carbide, and changing the inner and outer diameter of the cup. It is believed that any, or all, of these proposed changes may improve the ability of the TV-CMP system to measure nonvolatile or refractory elements by enhancing the ability of the electrode to reach the high temperatures required for their analyses.

Because this technique is still in its infancy, there is the need for continued development of the CMP as a method for discrete sampling. Further analysis of elements which are nonvolatile or refractory is necessary. A closer examination of the direct analysis of solids in various matrices, especially particulates, should prove informative. A thorough determination of possible effects caused by interferences should be investigated. Most importantly, an in depth study of the application of TV-CMP-AES to simultaneous multielement analysis should be performed as initial experiments demonstrated its suitability for this purpose.

Presently, there is little to no literature on the use of the CMP as a source for mass spectrometry or atomic fluorescence spectroscopy. It is believed that the CMP may prove useful in these areas due to its advantages over other emission sources. A very stable plasma is produced in the CMP, which can operate for several hours. Also, the CMP is robust and therefore will not be extinguished or perturbed upon high sample loading. Sample pretreatment and transport are eliminated by using TV sample introduction with a CMP; thus contaminants, such as hazardous reagents or carrier gases, are not introduced and consequently detected. The use of He as the plasma gas should reduce mass spectral interferences which occur with the use of Ar-ICPs or MIPs [47].

Limits of detection may be improved by magnetically enhancing the CMP source. The creation of a magnetic field around the plasma may serve to enhance the observed atomic emission intensity of the analyte of interest. This increase in emission signal follows from an induced increase in the electron temperature and an increase in the electron number density with increasing magnetic field strength [191]. Thus, increasing the emission signals attainable would result in lower limits of detection.

Finally, research into the automation of this system should be explored. This will help to decrease the time of analysis, thereby making this technique more suitable for routine applications. Also, automation can aid in improving the precision of this method. Currently, power stepping is achieved manually and this contributes to problems with reproducibility. If the process of power stepping could be more readily controlled, the precision of TV-CMP could be raised. However, these suggestions posed are just some of the possible ways in which to extend our knowledge of this novel technique. Upon increased evaluation, it is suspected that the utility of this method for the detection of elements in situations where the amount of sample is limited and a complicated matrix exists, such as biological tissues, will be realized.

REFERENCE LIST

1. V. A. Fassel, *Science* **202**, 183 (1978).

2. V. A. Fassel, *Spectrochim. Acta* **40B**, 1281 (1985).

3. V. A. Fassel, *Anal. Chem.* **51**, 1290A (1979).

4. S. Greenfield, H. M. McGeachin and P. B. Smith, *Talanta* **22**, 1 (1975).

5. H. Wu, J. M. Gehlhausen and J. W. Carnahan, *J. Chem. Educ.* **69**, 757 (1992).

6. K. A. Forbes, E. E. Reszke, P. C. Uden and R. M. Barnes, *J. Anal. At. Spectrom.* **6**, 57 (1991).

7. A. Montaser and D. W. Golightly, *Inductively Coupled Plasmas in Analytical Atomic Spectrometry*, second ed.; A. Montaser and D. W. Golightly, Eds.; VCH Publishers, New York (1992).

8. S. Greenfield, H. M. McGeachin and P. B. Smith, *Talanta* **23**, 1 (1976).

9. P. Schramel, *Spectrochim. Acta* **43B**, 881 (1988).

10. D. Beauchemin, J. C. Y. L. Blanc, G. R. Peters and J. M. Craig, *Anal. Chem.* **64**, 442R (1992).

11. B. L. Sharp, S. Chenery, R. Jowitt, S. T. Sparkes and A. Fisher, *J. Anal. At. Spectrom.* **8**, 151R (1993).

12. C. I. M. Beenakker, *Spectrochim. Acta* **31B**, 483 (1976).

13. A. T. Zander and G. M. Hieftje, *Appl. Spec.* **35**, 357 (1981).

14. S. R. Goode and K. W. Baughman, *Appl. Spec.* **38**, 755 (1984).

15. R. M. Barnes and E. E. Reszke, *Anal. Chem.* **62**, 2650 (1990).

16. E. C. Fehsenfeld, K. M. Evenson and H. P. Broida, *Rev. Sci. Instrum.* **36**, 294 (1965).

17. J. P. J. van Dalen, P. A. de Lezenne Coulander and L. de Galan, *Spectrochim. Acta* **33B**, 545 (1978).

18. C. I. M. Beenakker, P. W. J. M. Boumans and P. J. Rommers, *Philips Tech. Rev.* **39**, 65 (1980).

19. R. K. Skogerboe and G. N. Coleman, *Anal. Chem.* **48**, 611A (1976).

20. A. T. Zander, R. K. Williams and G. M. Hieftje, *Anal. Chem.* **49**, 2372 (1977).

21. S. Greenfield, H. M. McGeachin and P. B. Smith, *Talanta* **22**, 553 (1975).

22. J. P. Matousek, B. J. Orr and M. Selby, *Prog. Anal. Atom. Spectrosc.* **7**, 275 (1984).

23. K. G. Michlewicz and J. W. Carnahan, *Anal. Chem.* **58**, 3122 (1986).

24. K. C. Ng and T. J. Garner, *Appl. Spec.* **47**, 241 (1993).

25. S. R. Goode, N. P. Buddin, B. Chambers, K. W. Baughman and J. P. Deavor, *Spectrochim. Acta* **40B**, 317 (1985).

26. J. H. Runnels and J. H. Gibson, *Anal. Chem.* **39**, 1398 (1967).

27. K. Chiba, M. Kurosawa, K. Tanabe and H. Haraguchi, *Chem. Lett.* **1**, 75 (1984).

28. F. L. Fricke, O. Rose and J. A. Caruso, *Talanta* **23**, 317 (1976).

29. K. J. Timmins, *J. Anal. At. Spectrom.* **2**, 251 (1987).

30. D. A. McGregor, K. B. Cull, J. M. Gehlhausen, A. S. Viscomi, M. Wu, L. Zhang and J. W. Carnahan, *Anal. Chem.* **60**, 1089A (1988).

31. M. Wu and J. W. Carnahan, *Appl. Spec.* **44**, 673 (1990).

32. A. Aziz, J. A. C. Broekaert and F. Leis, *Spectrochim. Acta* **37B**, 381 (1982).

33. G. Heltai, J. A. C. Broekaert, P. Burba, F. Leis, P. Tschöpel and G. Tölg, *Spectrochim. Acta* **45B**, 857 (1990).

34. Y. Okamoto, M. Yasuda and S. Murayama, *Jap. J. Appl. Phys.* **29**, L670 (1990).

35. H. Matusiewicz, *Spectrochim. Acta* **47B**, 1221 (1992).

36. H. Matusiewicz and R. E. Sturgeon, *Spectrochim. Acta* **48B**, 515 (1993).

37. W. R. McLean, D. L. Stanton and G. E. Penketh, *Analyst* **98**, 432 (1973).

38. J. P. J. van Dalen, P. A. de Lezenne Coulander and L. de Galan, *Anal. Chim. Acta* **94**, 1 (1977).

39. T. H. Risby and Y. Talmi, *CRC Crit. Rev. Anal. Chem.* **14**, 231 (1984).

40. R. Lobinski, W. M. R. Dirkx, M. Ceulemans and F. C. Adams, *Anal. Chem.* **64**, 159 (1992).

41. S. R. Goode and C. L. Thomas, *J. Anal. At. Spectrom.* **9**, 73 (1994).

42. G. K. Webster and J. W. Carnahan, *Appl. Spec.* **45**, 1285 (1991).

43. A. J. McCormack, S. C. Tong and W. D. Cooke, *Anal. Chem.* **37**, 1470 (1965).

44. S. A. Estes, P. C. Uden and R. M. Barnes, *Anal. Chem.* **53**, 1829 (1981).

45. E. H. Evans, J. A. Caruso and R. D. Satzger, *Appl. Spec.* **45**, 1478 (1991).

46. Y. Okamoto, *J. Anal. At. Spectrom.* **9**, 745 (1994).

47. J. J. Giglio, J. Wang and J. A. Caruso, *Appl. Spec.* **49**, 314 (1995).

48. S. Hanamura, B. W. Smith and J. D. Winefordner, *Anal. Chem.* **55**, 2026 (1983).

49. J. D. Hwang, W. Masamba, B. W. Smith and J. D. Winefordner, *Can. J. Spectrosc.* **33**, 156 (1988).

50. S. Hanamura, B. W. Smith and J. D. Winefordner, *Can. J. Spectrosc.* **29**, 13 (1984).

51. B. M. Spencer, *A cylindrical He capacitively coupled microwave plasma: diagnostics and determination of silicon*, Ph.D. Dissertation, University of Florida (1993).

52. J. Burman and K. Bostrom, *Anal. Chem.* **51**, 516 (1979).

53. G. F. Larson and V. A. Fassel, *Anal. Chem.* **48**, 1161 (1976).

54. P. W. J. M. Boumans, F. J. D. Boer, F. J. Dahmen, H. Hoelzel and A. Meier, *Spectrochim. Acta* **30B**, 449 (1975).

55. J. Dahmen, *ICP Info. Newsl.,* A) **6**, 576 (1981), B) **7**, 441 (1982), C) **9**, 81 (1983), D) **10**, 1 (1984), E) **11**, 71 (1985), F) **12**, 7 (1986), G) **13**, 77 (1987), H) **14**, 195 (1988), I) **15**, 94 (1989), J) **16**, 321 (1990), K) **17**, 267 (1991), L) **18**, 103 (1992).

56. H. Vermaak, O. Kujirai, S. Hanamura and J. D. Winefordner, *Can. J. Spectrosc.* **31**, 95 (1985).

57. A. H. Ali, K. C. Ng and J. D. Winefordner, *J. Anal. At. Spectrom.* **6**, 211 (1991).

58. W. R. L. Masamba, B. W. Smith and J. D. Winefordner, *Appl. Spec.* **46**, 1741 (1992).

59. K. Govindaraju, G. Mevelle and C. Chouard, *Anal. Chem.* **48**, 1325 (1976).

60. H. Uchida, P. A. Johnson and J. D. Winefordner, *J. Anal. At. Spectrom.* **5**, 81 (1990).

61. H. Uchida, A. Berthod and J. D. Winefordner, *Analyst* **115**, 933 (1990).

62. I. Atsuya and K. Akatsuka, *Spectrochim. Acta* **36B**, 747 (1981).

63. D. M. Hueber, W. R. L. Masamba, B. M. Spencer and J. D. Winefordner, *Anal. Chim. Acta* **278**, 279 (1993).

64. M. W. Wensing, B. W. Smith and J. D. Winefordner, *Anal. Chem.* **66**, 531 (1994).

65. M. W. Wensing, D. Liu, B. W. Smith and J. D. Winefordner, *Anal. Chim. Acta* **299**, 1 (1994).

66. M. Moisan, C. Beaudry and P. Leprince, *IEEE Trans. Plasma Sci.* **PS-3**, 55 (1975).

67. M. Selby and G. M. Hieftje, *Spectrochim. Acta* **42B**, 285 (1987).

68. M. Moisan, Z. Zakrzewski, R. Pantel and P. Leprince, *IEEE Trans. Plasma Sci.* **PS-12**, 203 (1984).

69. J. Hubert, M. Moisan and A. Ricard, *Spectrochim. Acta* **33B**, 1 (1979).

70. Y. Duan, X. Du and Q. Jin, *J. Anal. At. Spectrom.* **9**, 629 (1994).

71. U. Richts, J. A. C. Broekaert, P. Tschöpel and G. Tölg, *Talanta* **38**, 863 (1991).

72. Q. Jin, C. Zhu, M. W. Borer and G. M. Hieftje, *Spectrochim. Acta* **46B**, 417 (1991).

73. J. Jin, F. Wang, C. Zhu, D. M. Chambers and G. M. Hieftje, *J. Anal. At. Spectrom.* **5**, 487 (1990).

74. Y. Madrid, M. W. Borer, C. Zhu, Q. Jin and G. M. Hieftje, *Appl. Spec.* **48**, 994 (1994).

75. Y. Duan, X. Kong, H. Zhang, J. Liu and Q. Jin, *J. Anal. At. Spectrom.* **7**, 7 (1992).

76. K. B. Cull and J. W. Carnahan, *Appl. Spec.* **42**, 1061 (1988).

77. M. Wu and J. W. Carnahan, *Appl. Spec.* **46**, 163 (1992).

78. M. A. Biondi, *El. Eng.* **69**, 806 (1950).

79. J. D. Cobine and D. A. Wilbur, *J. Appl. Phys.* **22**, 835 (1951).

80. R. Grigorovici and G. Cristescu, *Optics and Spectrosc.* **6**, 85 (1959).

81. R. Mavrodineanu and R. C. Hughes, *Spectrochim. Acta* **19**, 1309 (1963).

82. U. Jecht and W. Kessler, *Fresenius' J. Anal. Chem.* **198**, 27 (1963).

83. W. Kessler and F. Gerbhardt, *Glastech. Ber.* **40**, 194 (1967).

84. M. Yamamoto and S. Murayama, *Spectrochim. Acta* **23A**, 773 (1967).

85. S. Murayama, H. Matsuno and M. Yamamoto, *Spectrochim. Acta* **23B**, 513 (1968).

86. S. Murayama, *Spectrochim. Acta* **25B**, 191 (1970).

87. H. Goto, K. Hirokawa and M. Suzuki, *Z. Anal. Chem.* **225**, 130 (1967).

88. K. Kitagawa and T. Takeuchi, *Anal. Chim. Acta* **60**, 309 (1972).

89. K. Kitagawa and T. Takeuchi, *Anal. Chim. Acta* **67**, 453 (1973).

90. R. Nakashima, S. Sasaki and S. Shibata, *Anal. Chim. Acta* **70**, 265 (1973).

91. P. W. J. M. Boumans, "Plasma sources other than inductively coupled plasmas," in *Inductively Coupled Plasma Emission Spectroscopy*, first ed.; P. W. J. M. Boumans, Ed.; John Wiley & Sons, New York (1987) part 1, chap. 2.

92. S. Hanamura, B. Kirsch and J. D. Winefordner, *Anal. Chem.* **57**, 9 (1985).

93. S. Hanamura, W. Wang and J. D. Winefordner, *Can. J. Spectrosc.* **30**, 46 (1985).

94. B. M. Patel, E. Heithmar and J. D. Winefordner, *Anal. Chem.* **59**, 2374 (1987).

95. B. M. Patel, J. P. Deavor and J. D. Winefordner, *Talanta* **35**, 641 (1988).

96. A. H. Ali, K. C. Ng and J. D. Winefordner, *Spectrochim. Acta* **46B**, 1207 (1991).

97. A. H. Ali, *Electrode heating sample vaporization in capacitively coupled microwave plasma atomic emission spectrometry*, Ph.D. Dissertation, University of Florida (1991).

98. A. H. Ali and J. D. Winefordner, *Anal. Chim. Acta* **264**, 327 (1992).

99. A. H. Ali and J. D. Winefordner, *Anal. Chim. Acta* **264**, 319 (1992).

100. W. R. L. Masamba, A. H. Ali and J. D. Winefordner, *Spectrochim. Acta* **47B**, 481 (1992).

101. W. R. L. Masamba and J. D. Winefordner, *Spectrochim. Acta* **48B**, 521 (1993).

102. B. M. Spencer, B. W. Smith and J. D. Winefordner, *Appl. Spec.* **48**, 289 (1994).

103. S. Murayama, *J. Appl. Phys.* **39**, 5478 (1968).

104. K. Fallgatter, V. Svoboda and J. D. Winefordner, *Appl. Spec.* **25**, 347 (1971).

105. Y. K. Zhang, S. Hanamura and J. D. Winefordner, *Appl. Spec.* **39**, 226 (1985).

106. B. Kirsch, S. Hanamura and J. D. Winefordner, *Spectrochim. Acta* **39B**, 955 (1984).

107. W. R. L. Masamba, *Diagnostic studies and analytical characteristics of a high power helium/hydrogen capacitively coupled microwave plasma*, Ph.D. Dissertation, University of Florida (1992).

108. M. H. Abdallah and J. M. Mermet, *Spectrochim. Acta* **37B**, 391 (1982).

109. K. Tanabe, H. Haraguchi and K. Fuwa, *Spectrochim. Acta* **38B**, 49 (1983).

110. S. M. Michaelson, *J. Microwave Power* **6**, 259 (1971).

111. J. J. DeCorpo, J. T. Larkins, M. V. McDowell and J. R. Wyatt, *Appl. Spec.* **29**, 85 (1975).

112. J. L. Stanley, H. W. Bentley and M. B. Denton, *Appl. Spec.* **27**, 265 (1973).

113. G. J. Monser, *Microwaves & Rf* **21**, 74 (1982).

114. J. Browne, *Microwaves & Rf* **22**, 121 (1983).

115. D. L. Haas and J. A. Caruso, *Anal. Chem.* **56**, 2014 (1984).

116. R. F. Browner and A. W. Boorn, *Anal. Chem.* **56**, 786A (1984).

117. J. M. Carey and J. A. Caruso, *CRC Crit. Rev. Anal. Chem.* **23**, 397 (1992).

118. R. F. Browner and A. W. Boorn, *Anal. Chem.* **56**, 875A (1984).

119. S. A. Darke, C. J. Pickford and J. F. Tyson, *Anal. Proc.* **26**, 379 (1989).

120. K. C. Ng and J. A. Caruso, *Appl. Spec.* **39**, 719 (1985).

121. A. M. Gunn, D. L. Millard and G. F. Kirkbright, *Analyst* **103**, 1066 (1978).

122. H. Matusiewicz, *J. Anal. At. Spectrom.* **1**, 171 (1986).

123. H. Uchida, W. R. Masamba, T. Uchida, B. W. Smith and J. D. Winefordner, *Appl. Spec.* **43**, 425 (1989).

124. I. Ida, H. Yoshikawa, Y. Ishibashi and N. Gunji, *Anal. Sci.* **5**, 615 (1989).

125. V. Karanassios and G. Horlick, *Spectrochim. Acta Rev.* **13**, 89 (1990).

126. J. W. Olesik and S. E. Hobbs, *Anal. Chem.* **66**, 3371 (1994).

127. B. M. Spencer, A. R. Raghani and J. D. Winefordner, *Appl. Spec.* **48**, 643 (1994).

128. E. Hoffmann, C. Lüdke, H. Scholze, *J. Anal. At. Spectrom.* **9**, 1237 (1994).

129. D. C. Grégoire, M. Lamoureux, C. L. Chakrabarti, S. Al-Maawali and J. P. Byrne, *J. Anal. At. Spectrom.* **7**, 579 (1992).

130. H. Matusiewicz and R. M. Barnes, *Appl. Spec.* **5**, 745 (1984).

131. H. Nickel, Z. Zadgorska and G. Wolff, *Spectrochim Acta* **48B**, 25 (1993).

132. D. R. Hull and G. Horlick, *Spectrochim. Acta* **39B**, 843 (1984).

133. T. Kántor, *Spectrochim. Acta* **38B**, 1483 (1983).

134. H. Matusiewicz, *Spectrochim. Acta Rev.* **13**, 47 (1990).

135. P. Barth and V. Krivan, *J. Anal. At. Spectrom.* **9**, 773 (1994).

136. P. Hulmston and R. C. Hutton, *Spectroscopy* **6**, 35 (1991).

137. C. W. McLeod, M. W. Routh and M. W. Tikkanen, "Introduction of solids into plasmas," in *Inductively Coupled Plasmas in Analytical Atomic Spectrometry*, second ed.; A. Montaser and D. W. Golightly, Eds.; VCH Publishers Inc., New York (1992) chap. 16.

138. V. Karanassios, J. M. Ren and E. D. Salin, *J. Anal. At. Spectrom.* **6**, 527 (1991).

139. D. E. Nixon, V. A. Fassel and R. N. Kniseley, *Anal. Chem.* **46**, 210 (1974).

140. F. L. Fricke, O. Rose Jr. and J. A. Caruso, *Anal. Chem.* **47**, 2018 (1975).

141. K. C. Ng and J. A. Caruso, *Anal. Chim. Acta* **143**, 209 (1982).

142. H. M. Swaidan and G. D. Christian, *Anal. Chem.* **56**, 120 (1984).

143. D. L. Millard, H. C. Shan and G. F. Kirkbright, *Analyst* **105**, 502 (1980).

144. H. Matusiewicz and R. M. Barnes, *Spectrochim. Acta* **40B**, 29 (1985).

145. H. Falk, E. Hoffmann and C. Lüdke, *Spectrochim. Acta* **39B**, 283 (1984).

146. W. T. Chan and G. Horlick, *Appl. Spec.* **44**, 380 (1990).

147. J. J. Carr, *Elements of Microwave Electronics Technology*, Harcourt Brace Jovanovich, Inc., San Diego, CA (1989).

148. W. Sinnema, *Electric Transmission Technology*, second ed.; Prentice Hall, Englewood Cliffs, NJ (1988).

149. A. W. Scott, *Understanding Microwaves*, John Wiley & Sons, Inc., New York (1993).

150. P. A. Rizzi, *Microwave Engineering: Passive Circuits*, Prentice Hall, Englewood Cliffs, NJ (1988).

151. M. W. Wensing, *Evaluation of a capacitively coupled microwave plasma atomic emission spectrometer for the determination of lead in whole blood*, Ph.D. Dissertation, University of Florida (1994).

152. K. G. Michelwicz, J. J. Urh and J. W. Carnahan, *Spectrochim. Acta* **40B**, 493 (1985).

153. R. D. Deutsch and G. M. Hieftje, *Anal. Chem.* **56**, 1923 (1984).

154. S. Chan and A. Montaser, *Spectrochim. Acta* **40B**, 1467 (1985).

155. K. J. Jones and J. W. Carnahan, *Spectrochim. Acta* **47B**, 1229 (1992).

156. J. P. Robin, *Prog. Anal. At. Spectrosc.* **5**, 79 (1982).

157. J. D. Ingle and S. R. Crouch, *Spectrochemical Analysis*, Prentice Hall, Englewood Cliffs, NJ (1988).

158. G. L. Long and J. D. Winefordner, *Anal. Chem.* **55**, 712A (1983).

159. G. F. R. Gilchrist, C. L. Chakrabarti, J. T. F. Ashley and D. M. Hughes, *Anal. Chem.* **64**, 1144 (1992).

160. Thermo Jarrell Ash, *Guide to Analytical Values for TJA Spectrometers*, Author, Franklin, MA (1988).

161. A. Aziz, J. A. C. Broekaert and F. Leis, *Spectrochim. Acta* **37B**, 369 (1982).

162. H. Matusiewicz and R. M. Barnes, *Anal. Chem.* **57**, 406 (1985).

163. R. W. B. Pearse and A. G. Gaydon, *Identification of Molecular Spectra*, John Wiley & Sons, Inc., New York (1976).

164. F. J. Langmyhr, *Analyst* **104**, 993 (1979).

165. M. Abdullah and H. Haraguchi, *Anal. Chem.* **57**, 2059 (1985).

166. P. B. Farnsworth and G. M. Hieftje, *Anal. Chem.* **55**, 1414 (1983).

167. A. Aziz, J. A. C. Broekaert, K. Laqua and F. Leis, *Spectrochim. Acta* **39B**, 1091 (1984).

168. L. Ebdon, M. E. Foulkes and S. Hill, *J. Anal. At. Spectrom.* **5**, 67 (1990).

169. B. Radziuk, G. Rödel, H. Stenz, H. Becker-Ross and S. Florek, *J. Anal. At. Spectrom.* **10**, 127 (1995).

170. S. S. Berman and J. W. McLaren, *Appl. Spec.* **32**, 372 (1978).

171. K. J. Mulligan, M. H. Hahn, J. A. Caruso and F. L. Fricke, *Anal. Chem.* **51**, 1935 (1979).

172. M. Zerezghi, K. J. Mulligan and J. A. Caruso, *Anal. Chim. Acta* **154**, 219 (1983).

173. J. M. Gelhausen and J. W. Carnahan, *Anal. Chem.* **63**, 2430 (1991).

174. P. W. J. M. Boumans and F. J. de Boer, *Spectrochim. Acta* **30B**, 309 (1975).

175. M. Abdullah, K. Fuwa and H. Haraguchi, *Spectrochim. Acta* **39B**, 1129 (1984).

176. H. Uchida, Y. Nojiri, H. Haraguchi and K. Fuwa, *Anal. Chim. Acta* **123**, 57 (1981).

177. S. L. Tong and K. S. Chin, *Spectrochim. Acta* **49B**, 459 (1994).

178. J. M. Harnly, T. C. O'Haver, B. Golden and W. R. Wolf, *Anal. Chem.* **51**, 2007 (1979).

179. J. M. Harnly, *Anal. Chem.* **58**, 933A (1986).

180. C. M. M. Smith and J. M. Harnly, *Spectrochim. Acta* **49B**, 387 (1994).

181. M. J. Pilon, M. B. Denton, R. G. Schleicher, P. M. Moran and S. B. Smith Jr., *Appl. Spec.* **44**, 1613 (1990).

182. R. S. Pomeroy, R. D. Jalkian and M. B. Denton, *Appl. Spec.* **45**, 1120 (1991).

183. R. S. Pomeroy, J. V. Sweedler and M. B. Denton, *Talanta* **37**, 15 (1990).

184. P. M. Epperson, J. V. Sweedler, R. B. Bilhorn, G. R. Sims and M. B. Denton, *Anal. Chem.* **60**, 327A (1988).

185. J. V. Sweedler, R. B. Bilhorn, P. M. Epperson, G. R. Sims and M. B. Denton, *Anal. Chem.* **60**, 282A (1988).

186. G. R. Sims, "Principles of charge-transfer devices," in *Charge-Transfer Devices in Spectroscopy*, J. V. Sweedler, K. L. Ratzlaff and M. B. Denton, Eds.; VCH Publishers Inc., New York (1994) chap. 2.

187. R. B. Bilhorn and M. B. Denton, *Appl. Spec.* **44**, 1538 (1990).

188. R. S. Pomeroy, "CTD detectors in atomic emission spectroscopy," in *Charge-Transfer Devices in Spectroscopy*, J. V. Sweedler, K. L. Ratzlaff and M. B. Denton, Eds.; VCH Publishers Inc., New York (1994) chap. 10.

189. C. A. Bye and A. Scheeline, "Two-dimensional array detectors for plasma diagnostics," in *Charge-Transfer Devices in Spectroscopy*, J. V. Sweedler, K. L. Ratzlaff and M. B. Denton, Eds.; VCH Publishers Inc., New York (1994) chap. 9.

190. P. N. Keliher and C. C. Wohlers, *Anal. Chem.* **48**, 333A (1976).

191. A. Raghani, *Magnetically-enhanced miniature glow discharge sources for atomic emission spectroscopy*, Ph.D. Dissertation, University of Florida (1995).

BIOGRAPHICAL SKETCH

Andrea Pless was born on September 12, 1969, in Great Neck, NY. She was raised in Marlboro, NJ, and graduated from Marlboro High School in 1987. She moved to Gainesville in August 1987 to study chemistry at the University of Florida. At this time, she did undergraduate research in the group of Dr. James D. Winefordner. She earned a Bachelor of Science degree with high honors from the University of Florida in May 1991. She returned to the University of Florida in August 1991 to attend graduate school, where she continued her studies in analytical chemistry under the direction of Dr. Winefordner. In May 1996, she received her PhD in chemistry, with a minor in environmental engineering sciences. She will start her career as a chemist with Air Products and Chemicals, Inc., in Allentown, PA.

I certify that I have read this study and that in my opinion it conforms to acceptable standards of scholarly presentation and is fully adequate, in scope and quality, as a dissertation for the degree of Doctor of Philosophy.

James D. Winefordner

James D. Winefordner, Chair
Graduate Research Professor of Chemistry

I certify that I have read this study and that in my opinion it conforms to acceptable standards of scholarly presentation and is fully adequate, in scope and quality, as a dissertation for the degree of Doctor of Philosophy.

Robert T. Kennedy
Assistant Professor of Chemistry

I certify that I have read this study and that in my opinion it conforms to acceptable standards of scholarly presentation and is fully adequate, in scope and quality, as a dissertation for the degree of Doctor of Philosophy.

William Weltner, Jr.

William Weltner, Jr.
Professor of Chemistry

I certify that I have read this study and that in my opinion it conforms to acceptable standards of scholarly presentation and is fully adequate, in scope and quality, as a dissertation for the degree of Doctor of Philosophy.

David H. Powell
Associate Research Scientist of Chemistry

I certify that I have read this study and that in my opinion it conforms to acceptable standards of scholarly presentation and is fully adequate, in scope and quality, as a dissertation for the degree of Doctor of Philosophy.

Joseph J. Delfino
Professor of Environmental Engineering Sciences

This dissertation was submitted to the Graduate Faculty of the Department of Chemistry in the College of Liberal Arts and Sciences and to the Graduate School and was accepted as partial fulfillment of the requirements for the Degree of Doctor of Philosophy.

May 1996

Dean, Graduate School